(1)

.UM SULFUR DIOXIDE CELL

McDonald, P. Harris, F. Goebel, S. Hossa
ierra, M. Guentert, C. Todino

Yardney
TECHNICAL PRODUCTS INC

Yardney Technical Products Inc
82 Mechanic Street
Pawcatuck, CT 06379

Best
Available
Copy

(1)

ADVANCED RECHARGEABLE LITHIUM SULFUR DIOXIDE CELL

R.C. McDonald, P. Harris, F. Goebel, S. Hossain,
R. Vierra, M. Guentert, C. Todino

NOVEMBER 1991

Final Report for Period
September 1988 - February 1991

Contract: DAAL01-88-C-0849

Prepared for:

Electronics Technology and Devices Laboratory
U.S. Army Laboratory Command
Fort Monmouth NJ 07703-5000

Prepared by:

Yardney Technical Products, Inc.
82 Mechanic Street
Pawcatuck CT 06379

TABLE OF CONTENTS

LIST OF FIGURES

LIST OF TABLES

ABSTRACT

The electrochemical performance and safety of the rechargeable lithium sulfur dioxide (Li/SO_2) system has been investigated in laboratory cells and in high rate D cells. Small cell design and active materials were optimized so that cathode utilization of 1.6Ah/gram of carbon and 0.19Ah/cm^3 of cathode were achieved with 100-200 cycles. Discharge and charge of cells at temperatures down to -30°C was examined as were pulse discharge, storage, high temperature and voltage delay. Analytical techniques were developed for the determination of SO_2 electrolyte phase behavior and for the analysis of lithium dithionate degradation product. Cell venting, shorting and over-heating remain persistent problems as the testing proceeds to the larger spiral wound cell. Cell venting appears to occur mostly on charge or shortly thereafter and is associated with accumulation of reactive side-products. Large cell electrodes are pyrophoric when examined in air after extensive cycling.

INTRODUCTION

The objective of this program was to perform research addressing limitations of Li/SO_2 rechargeable batteries with regard to discharge capacity, low temperature performance, cycle life and abuse resistance. Wound D cells were designed and developed with the improvements investigated. The ultimate program objective is to support technology which will replace the U.S. Army's presently used primary lithium batteries with rechargeable batteries.

EXPERIMENTAL

Two electrolytes were evaluated in this study. $LiAlCl_4 \cdot 3SO_2$ was prepared by addition of Matheson anhydrous SO_2 to anhydrous $AlCl_3$ (Aldrich, Fluka or Kings Mountain) and LiCl (Baker or Foote). The LiCl was first vacuum dried at 110°C. The SO_2 was added in one of two ways: 1) as a gas initially during which time the very exothermic reaction of $AlCl_3$ and SO_2 proceeded to form a liquid $AlCl_3 \cdot 3SO_2$ which in turn slowly dissolved the LiCl. After about 30 percent of the SO_2 was added as a gas, we added the remaining amount as a precondensed liquid. The receiving flask was cooled in an ice-salt bath. 2) the entire quantity of SO_2 was preliquified and added directly to the dry salts in a completely enclosed air tight system. The first method appears to produce better results in a shorter span of time, resulting in a light straw colored solution.

$LiAlCl_4 \cdot 6SO_2$ was prepared as in method 2 above, adding the entire quantity of pre-condensed SO_2 using an air tight transfer system. Excess LiCl (up to 10%) was included in both the $LiAlCl_4 \cdot 3SO_2$ and $LiAlCl_4 \cdot 6SO_2$ electrolyte preparations in order to preclude excess $AlCl_3$.

Electrolyte was stored in air-tight 600ml glass pressure bottles equipped with Fisher and Porter valves to accommodate cell filling.

Two types of experimental cells were used to test cycling performance of the Li/SO_2 system.

1) 25cm^2 laboratory cells containing one double sided flat cathode and two half anodes. Various separators and separator configurations were evaluated as discussed below. Electrolytes were kept in place by two hemicylindrical shields within a D-sized stainless 300 series steel can. Covers with glass-to-metal seals were T.I.G.-welded on and electrolyte was filtered through a hollow tube in the seal. The tube was welded shut after filling to provide a hermetic enclosure. The cans were case positive.

The lithium anodes were made by pressing two layers of lithium foil (.010" each) on each side of a 5 mil perforated nickel foil.

The cell configuration was as follows:

Anode/Separator/Cathode/Separator/Anode
(A) (S) (C) (S) (A)

The positive carbon electrode was positioned in the center and sandwiched between two negative lithium electrodes (Figure 1). In some cell systems, dendrite getter made from a carbon cathode was used (Cells 27 and 28). In this case, the cell configuration was:

A/S/Dendrite Getter/S/C/S/Dendrite Getter/S/A

The cell system was packed in a Tefzel (.002" thick, 60% porous) bag. Typical parameters are shown in Table 1.

2) 300 - 600cm^2 spiral wound electrolyte was contained in stainless 300 series steel cans as above. These cans were

also case positive and contained a stamped vent designed to open at about 250PSIA. Preliminary design specifications are given in Table 2.

Metallic .010" thick lithium from Foote or Lithcoa was used for anode material. The lithium anodes and carbon cathodes were pressed onto either nickel exmet or perforated nickel current collectors. Carbon cathodes (.015"-.027" thick) consisted of either Shawinigan Acetylene Black (Chevron) or Ketjen Black (Akzo) carbon with 8 percent Teflon binder. (These are abbreviated SAB and KB throughout.) For cathodes, the perforated nickel was first coated with a thin Teflon/carbon film to improve the contrast between cathode and substrate. Separators evaluated were .003" microporous Tefzel (Raychem) and non-woven glass paper (Crane or Electrolock).

The positive carbon electrodes were made by mixing proper amounts of carbon, Teflon, alcohol and water to form a dough. The dough was then rolled on glass paper to a thickness of about .015" to .025" and air dried in a dry room. The rolled carbon sheet was then cut out from the paper to a proper dimension of the cathode and pressed on both sides of the Teflon-rich carbon coated perforated nickel foil (.006" thick). The resulting cathode was then dried and cured at 280°C under flowing argon for 20 minutes.

The electrochemical measurements were carried out using a Starbuck 20-station cycler system which is connected to a computer to monitor and store data. The cells were normally discharged and charged at a constant rate of 1 mA/cm^2. Lower and upper voltage limits were typically 2.8 volts and 4.0 volts unless otherwise stated with the initial scan direction being cathodic (discharge) from the respective open circuit potentials. A ten minute open circuit period was allowed between each charge and discharge.

Table 1

Design Specifications of Experimental Li/SO_2 Cell

Cathode:	92:8 W% KB: PTFE rolled, dried and then pressed on Teflon-rich carbon coated perforated Ni foil (6 mil)	
Anode:	10 mil Li foil roll-pressed on each side of 6 mil perforated Ni foil	
Reference:	As anode	
Electrolyte:	$LiAlCl_4 \cdot 6\ SO_2$	
Separator:	Porous glass fiber (Lectromat); Tefzel (Scimat)	
Cathode:	Area	25 cm^2
	Thickness	0.04-0.07 cm
	Weight	0.13-0.35 g
	Capacity	1.00-1.35 Ah/g (Experimental)
Anode:	Area	25 cm^2
	Thickness	0.05 cm
	Weight	0.70 g
	Capacity	2.7 Ah (Theoretical)

TABLE 2

Preliminary Design Specifications of a

Wound "D" Li/SO_2 Cell

Case Dimension:	**1.29" OD, 2.35" Height**
Cathode:	92: 8 W% Ketjen Black: TFE rolled onto Teflon-rich carbon-coated perforated Ni foil (.002" thick)
Dimensions:	20.4" x 2.09" x 0.030"
Weight:	7.95g
Capacity:	8.8 Ah (first cycle)
Anode:	0.005" Li foil rolled onto perforated Ni foil (0.002" thick)
Dimensions:	20.4" x 2.09" x .010"
Weight:	3.53g
Capacity:	13.6 Ah
Electrolyte:	$LiAlCl_4.6SO_2$
Weight:	46g
Volume:	27 ml
Separator:	Glass fiber (Lectrolok) and Tefzel (Scimat)
Dimensions:	20.6" x 2.2" x 0.003" (glass)
Total Active Surface Area: 550 cm^2	

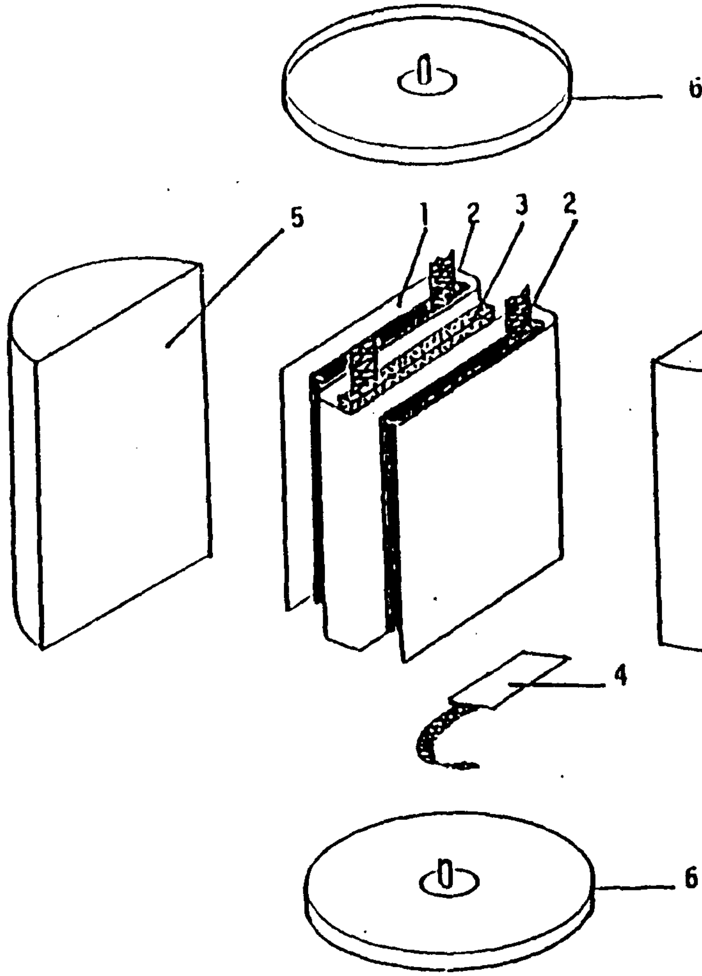

Exploded View of Components

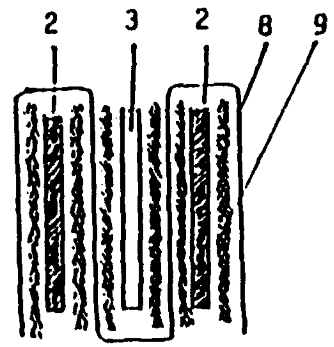

Stack Section

Hermetically Sealed Rechargeable Stack Assembly

1. Separator
2. Anode
3. Cathode
4. Li Reference
5. Teflon Spacer
6. Case Cover
7. Case
8. Tefzel Separator
9. Glass Separator

Figure 1

LABORATORY CELL RESULTS

General Comments Nine groups of $25cm^2$ laboratory cells were built to explore variations in electrode configuration, composition, electrolytes, current density and the limits of voltage on charge and discharge. Cycling was continued until one of three conditions was reached:

1. Cell scheduled for post-mortem chemical/physical analyzer
2. Short or shallow charge and discharge times indicted physical failure
3. Chemical failure leading to short-circuiting, case corrosion or venting from excess pressure.

Table 3 summarizes the results from 56 cells built and tested with comments on configuration and cycling results.

Test Group 1

The first test group consisted of three cells of the type $Li/LiAlCl_4 \cdot 3SO_2$/SAB carbon. The cells were built with a central 2-sided lithium electrode flanked by two single sided cathodes. The separator was microporous Tefzel (Raychem DA6/111, "enhanced conductivity") film folded into an "M" shape and sealed along the edges and bottom to make a flat package with three pockets for the electrodes. After assembling the electrodes, the packages were sealed along the top. Cathodes consisted of SAB with 4% TFE binder, rolled onto glass mat (Crane glass, 0.005") which acts as support as well as providing an electrolyte reservoir next to the carbon electrode. The flat cell packages were placed in demountable cylindrical cells with appropriate spacers and filled with the electrolyte.

Brief (2 minute) discharge pulses at different current densities were imposed on one cell in order to create the

Table 3: Li/SO2 LABORATORY CELL SUMMARY

Test Group	Cell Number	Components	Discharge/Charge Rates (mA/cm²)	Discharge/Charge Limits (Volts)	Cycles Acheived	Cathode Density (g/cc)	Cycle Capacity (Ah/gram carbon) FIRST	LAST	Comments
1	1	Cell package: 0.02" SAB paper on either side of 2x0.010" lithium with center substrate sealed in a separator package of 0.001" enhanced porosity Raychem Tefzel 25cm² test cell. The electrolyte was LiAlCl4·3SO2.	1.0/1.0	2.0/3.9	1		0.99	-	Would not accept charge
	2				1		0.92	-	Cathodes overcompressed
	3				1		0.71	-	Cathodes overcompressed
2	4	Cell package: 0.025" Ketjen black unsupported on either side of 2 x 0.010 lithium sealed in a separator package of 0.001" enhanced porosity Raychem Tefzel. 25cm² test cell with 2 x 0.003 glass paper. The electrolyte was LiAlCl4 .6SO2.	1.0/1.0	2.0/3.9	3		1.31	-	Cathodes overcompressed and computer failure
	5				1		1.17	-	
	6				1		1.11	-	
3	7	Cell package: 0.0025" Ketjen black unsupported on either side of 2 x 0.010" lithium sealed in a separator package of 0.001" enhanced porosity Raychem Tefzel. The 25cm² test cell wih 2 x 0.003 glass paper. The electrolyte was LiAlCl4•3SO2.	1.0/1.0	2.5/3.9	59	.0957	1.05	1.05	Short circuit and vent during
	8				98	.0971	1.04	1.04	Short circuit and vent during
	9				1	.0933	1.08	-	Faulty Test Fixture
4	10	Cell package: 0.025" SAB on paper on either side of 2 x 0.010" lithium sealed in a separator package of 0.001" enhanced porosity Raychem Tefzel. 25cm² test cell. The electrolyte was LiAlCl4•3SO2.	1.0/1.0	2.0/3.9	1	.133	0.98	-	Would not accept charge
	11				1	.132	.91	-	Would not accept charge
	12				1	.159	.97	-	Would not accept charge
5	13	Cell package: 0.022" SAB on paper treated with #15) water, #16) SOCl2 at 240°C and 2 x 0.010in. Li sealed in a separator package of 0.002" Tefzel, 2 x 0.003in. glass separator. 12.5 cm² test cell. The electrolyte was LiAlCl4•3SO2.	2.0/2.0	2.8/3.9	-	.256	-	-	Short during electrolyte fill
	14				-	.273	-	-	Short during electrolyte fill
	15				1	.284	.39	-	Would not accept charge
	16				1	.278	.40	-	Would not accept charge
6	17	Cell package: 0.015" - 0.22" Ketjen black on either side of 2 x 0.010" Li anode sealed in a separator package of 0.002" Tefzel and 2 x 0.003in. glass paper. 25cm² test cell. Li reference electrode in cells 24 and 27. Cell 27 contained carbon getter on both sides of cathode and anode. The electrolyte was LiAlCl4•6SO2.	1.0/1.0	2.8/3.9	53		1.35	0.66	OCV lost but no venting
				2.8/4.0	19	.133	0.88	0.86	
	18			-	-	-	-	-	Short during cover weld
	19			2.8/3.9	79	.118	1.37	0.66	Terminated for analysis
	24			2.8/3.9	68	/120	1.47	0.77	Terminated for analysis
	25			-	-	-	-	-	Short during top weld
	26			-	-	-	-	-	Short after electrolyte fill
	27			2.8/3.9	61		1.20	0.59	Failure at cathode, OCV lost, no venting
				2.8/4.0	14	.108	0.92	0.90	
				2.8/4.1	25		1.07	0.88	
	29			2.8/4.0	106	100	1.17	0.83	Vented on charge after 106 cycles
	30			2.8/3.9	71		1.38	0.66	Cell would not accept charge, no venting
				2.8/4.0	38	.108	1.00	0.83	

Table 3: Li/SO2 LABORATORY CELL SUMMARY (continued)

Test Group	Cell Number	Components	Discharge/Charge Rates (mA/cm²)	Discharge/Charge Limits	Cycles Achelved	Cathode Density (g/cc)	Cycle Capacity (Ah/gram carbon) FIRST	LAST	Comments
	20	Cell package: 0.022" Keljen black on either		-	-	-	-	-	Short after electrolyte fill
	21	side of 2 x 0.010" Li anode sealed in a		2.8/3.9	2	.130	-		Would not accept charge
	22	separator package of 0.002" Tefzel		2.8/3.9	3	.134	-		Would not accept charge
7	23	25cm² test cell. The cathode for Cell 31	1.0/1.0	-	-	-	-	-	Short during cover weld
		was treated with SOCl2 at 240°C. The		2.8/3.9	55		1.64	0.46	
	28	electrolyte was LiAlCl4•3SO2.		2.8/4.0	5	.127	0.65	0.34	PM showed insufficient electrolyte
	31			2.8/3.9	1	.130	0.98		Would not accept charge
	32		1.0/0.5	2.8/4.0	146	.177	0.82	0.34	Terminated after discharge for physical analysis (0°C Test)
	33		1.0/0.5	2.8/4.0	136	.178	0.76	0.30	Termiated after charge for physical analysis (-25°C Test)
	34		5.0/1.0	2.8/4.0	161	.176	1.22	0.39	Terminated after charge for analysis
	35	Cell package: 2 x .010" Li anode on either side	1.0/1.0	2.8/4.0	1	.041	0.19	-	Poor capacity
	36	of 2 x .022: Keljen black cathode "M" fold	2.0/1.0	2.8/4.0	1	.039	.069	-	
	37	Tefzel separator plus glass paper against each	1.0/1.0	2.8/4.0	1	.045	.025	-	
8	38	anode and cathode face. (Cells 35 - 37 used	1.0/1.0	3.0/4.0	169	.167	1.14	0.32	Terminated after discharge for analysis
	39	carbon felt instead of Keljen black cathode.	1.0/1.0	2.8/4.0	111	.188	0.94	0.44	Cell vented on charge
	40	The electrolyte was LiAcl4•6SO2.	2.0/1.0	3.0/4.0	216	.179	1.02	0.26	Terminated after discharge for analysis
	41		2.0/1.0	2.8/4.0	119	.166	1.35	0.49	Cell vented on charge
	42		2.0/2.0	3.0/4.0	102	.188	0.92	0.31	Terminated on charge
			2.0/1.0		151		0.37	0.23	for analysis
	43		2.0/2.0	2.8/4.0	101	.196	1.09	0.29	Vented during charge
	44			2.78/4.0		.093			See text
	45		-	-	-	.122	-	-	Not used
	46		Pulsed		23	.125			
		Cell package: 2 x .010" Li anode on either side		2.75/4.0					
	47	of 2 x .022: Keljen black cathode "M" fold	3.2/1.2	(2.50/- at -30°C)	102	.121	1.50	0.80	-30°C discharge
	48	Tefzel separator plus glass paper against each	-	-	-	.123	-	-	Not used
9	49	anode and cathode face. (Cells 35 - 37 used	-	-	-	.127	-	-	Not used
	50	carbon felt instead of Keljen black cathode.	3.2/1.2	2.75/4.0	3	.117	1.62	1.62	Briefly charged first
	51	The electrolyte was LiAcl4-6SO2.	3.2/1.2	2.75/4.0	101	.117	1.45	0.88	Briefly charged first (-20°C test)
	52		-	-	-	-	-	-	Not used
	53		2.0/1.0	2.8/4.0	57	.149	0.88	0.47	Terminated when low capacity reached
	54		2.0/1.0	2.8/4.0	56	.146	1.01	0.71	Terminated when low capacity reached
	55	LiGaCl4•6SO2	2.0/1.0	2.75/4.0	6	.153	0.61	0.36	Intermittent short
	56	LiGaCl4•6SO2	2.0/1.0	2.75/4.0	34	.149	1.15	0.05	Terminated when low capacity reached

polarization curve shown in Figure 2. Open circuit voltage was approximately 3.2V. The cell was able to discharge at 20 mA/cm^2 with about 350 mV polarization from the OCV (2.85V).

The three cells were then cycled between voltage limits of 2.0V for discharge and 4.2V for charge. Ten hour half cycle time limits were imposed on the cycling regime. The discharge capacity for the first cycle of the three cells was 152, 141, and 109 mAh. The average, 134 ± 22 mAh, corresponds to carbon utilization of 130 ± 20 mAh/cm^3 carbon (Table 4). The first cycle of Cell 1 is shown in Figure 3. The sudden voltage drop during the charge was attributed to physical short circuiting of the cell due to overcompression. On continued cycling two of the cells failed rapidly, the other (Cell 1) continued to cycle at a much reduced capacity. Figure 4 shows the capacity achieved as a function of cycle number. Cycling was continued through the 33rd cycle and then discontinued. It is interesting that when the charge time was reduced, the subsequent discharges were shorter, even though charge capacity was always greater than discharge capacity. this may reflect the inefficiency of the charge reaction and the necessity for overcharge. Examination of the cell components after disassembly indicated that the cathodes had been thoroughly discharged since they were very brittle with discharge products. It was also apparent they had been overcompressed during assembly. The remaining testing utilized reduced compression and more restricted voltage limits for cycling (2.5V for discharge and 3.9V for charge).

<u>Test Group 2</u>

The second test group, Cells 4, 5, and 6, was assembled with unsupported KB cathodes with 8% TFE binder, and activated

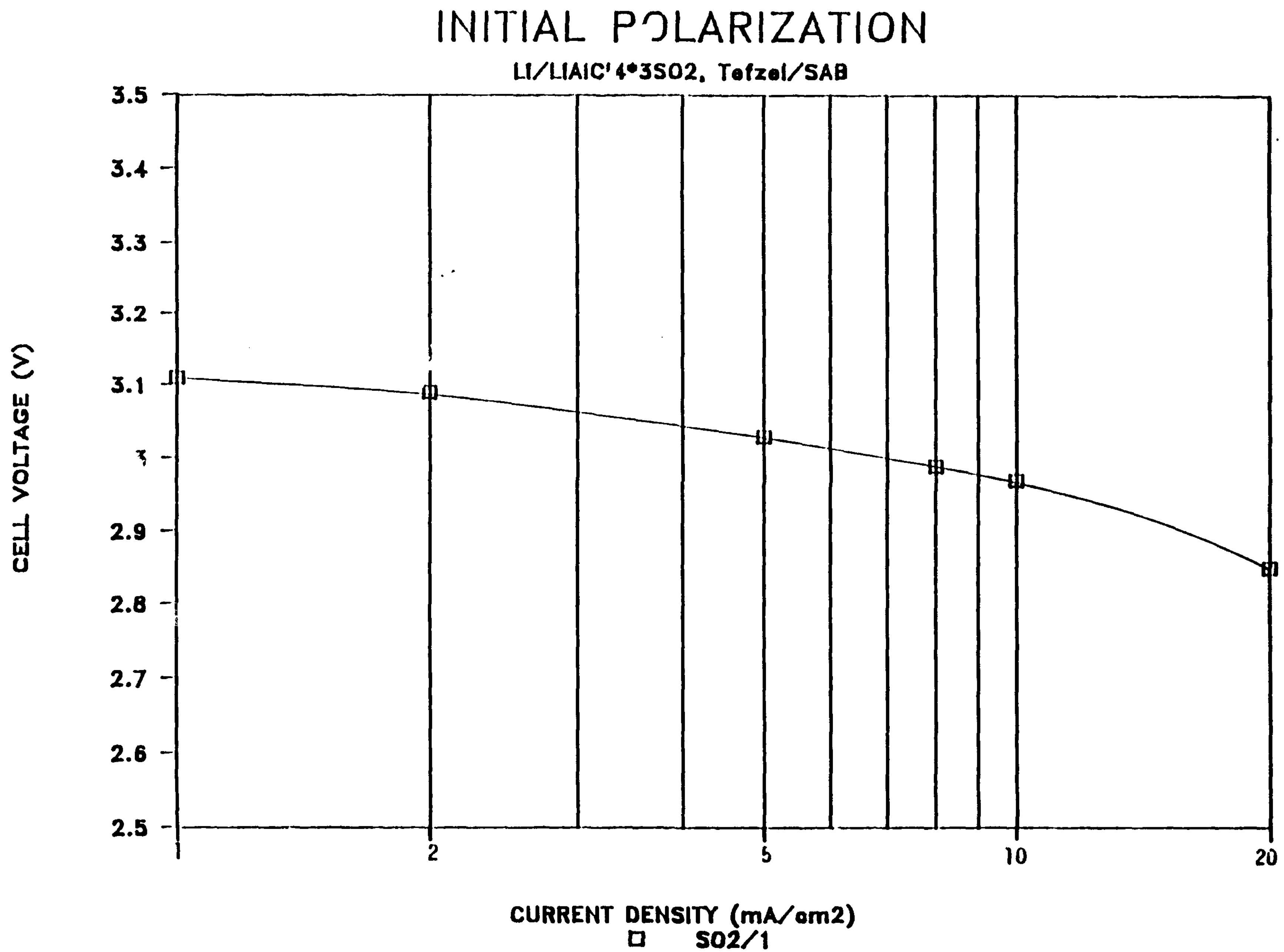

Figure 2: Polarization Curve of Cell 1

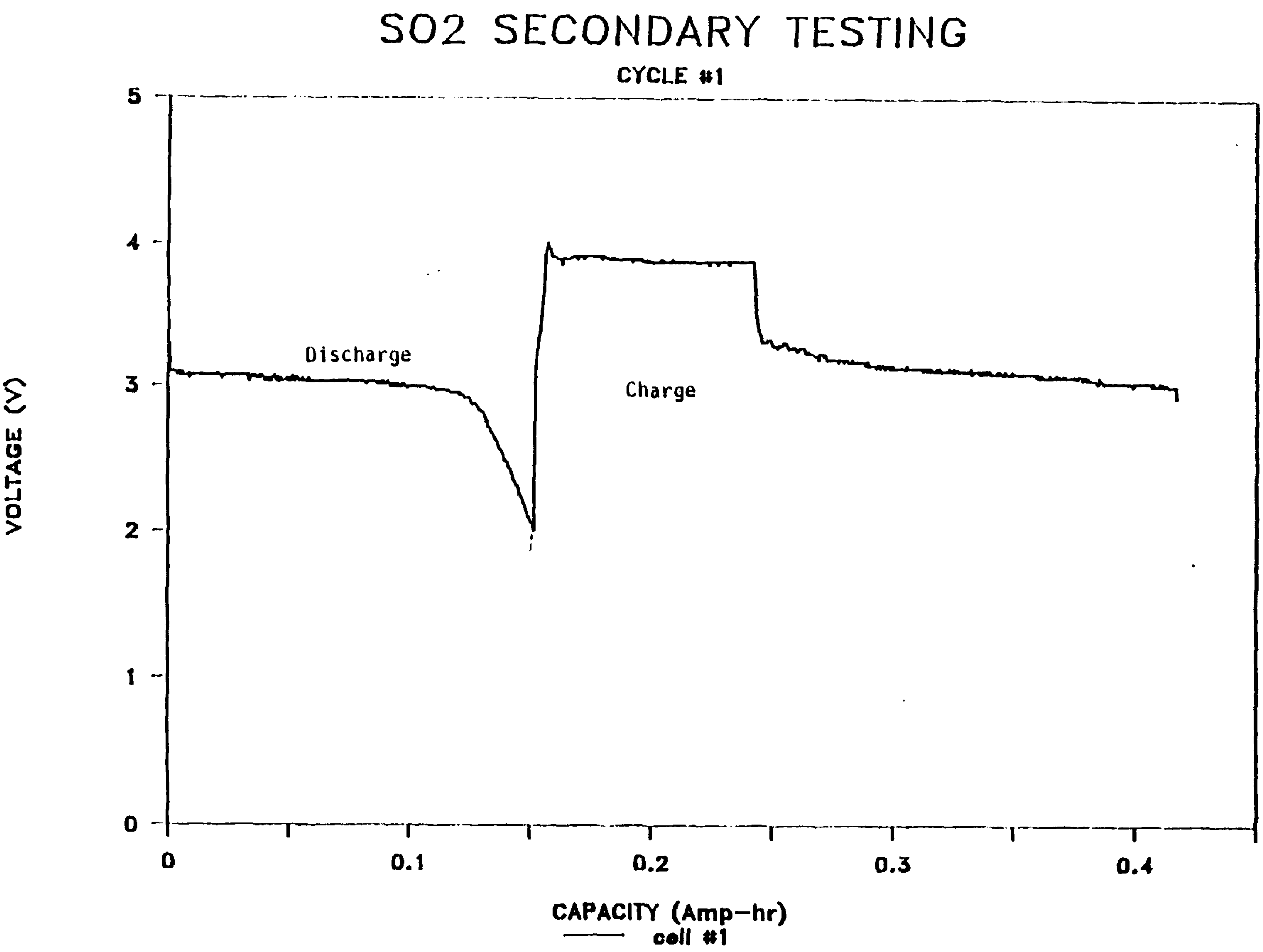

Figure 3: Voltage Profile: Cell 1, Cycle 1

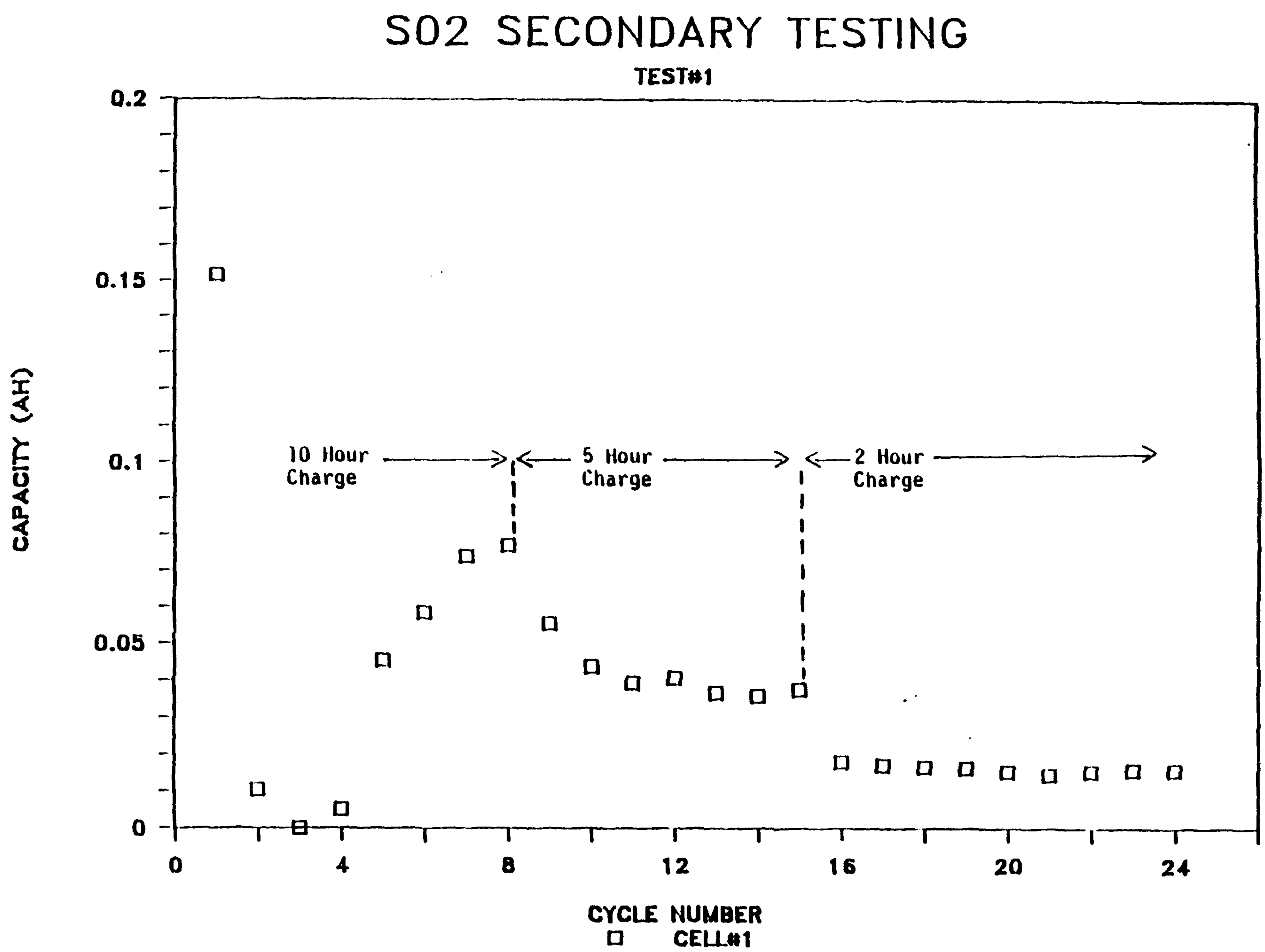

Figure 4: Cycle Capacity of Cell 1

with $LiAlCl_4 \cdot 3SO_2$ electrolyte. Achieved discharge capacities and volumetric cathode capacities are shown in Table 4.

TABLE 4: First Cycle Results - Test Group 2

Cell	Cycle #	Capacity (mAh)	Cathode Utilization (mAh/ml Carbon)
4	1 2 3	225 238 233	190 208 202
5 6	1 1	196 196	175 166

Discharge, 25 mA or 1 mA/cm^2, was limited to 10 hours or to a cutoff of 2.0V; charge also at 1 mA/cm^2 was limited to 10 hours or 3.9V. Within these cycling limits the cells cycled well initially but did not show good reversibility. This can be attributed to the 2.0V discharge cutoff, a voltage low enough to allow irreversible reactions to occur. The volumetric cathode capacity attained (190 ± 20 mAh/ml) is somewhat lower than that reported in the literature, possibly due to overcompression of the cell stack.

Test Group 3

The third cell group, Cells 7, 8, and 9, was built with KB cathodes and 8% TFE binder as had been the second group. These cells were built with no compression beyond the sum of the component thickness. Discharge was limited to 100 mAh/ml carbon (approximately 4 hours) or to a cutoff of 2.5V. Charge limits of 264 minutes (10% overcharge possible) or 3.9V were imposed on the cycle regime.

These cells cycled quite successfully. Cell 7 achieved 59 cycles and Cell 8, 98 cycles before failure by venting. Cell 9 was built in a faulty test fixture which did not permit extended cycling. Cycle life might have been shorter if the cells had been cycled between voltage limits of 3.9V and 2.5V with no time limits. In this case the depth of discharge would have been greater since the Ketjen Black cathodes are expected to give over 200 mAh/ml carbon on the first cycles[1,2,3]. The voltage profiles of Cell 7 for cycles 1, 50 and 59; and of Cell 8 for cycles 1, 50, 80 and 98 are shown in Figures 5-11. Only slight differences could be observed between the first and subsequent cycles of each cell. The average and final voltages during both discharge and charge are constant within 100 mV throughout the cell cycle life. Cell failure in both cases (Figures 7 and 11) was caused by short circuits. The voltage profile as observed on strip chart recordings showed: 1) immediate cell voltage drop at the initiation of the short circuit, 2) voltage rise to the power supply maximum after venting, and 3) voltage drop after the cycler sensed the high charge voltage and placed the cell on open circuit.

Analysis of the cell components indicated that metallic (not carbon) short circuits had caused the venting. The initiation of the thermal runaway reaction appeared to have occurred at a corner of each cell package where compression was greatest because of the added thickness of current collector tabs, and where electrode substrate screens had cut edges and points which could eventually penetrate the Tefzel separator. The edges of the lithium electrode substrate after cycling had developed a soft mud-like consistency. The voltage profile during cell failure is not indicative of dendrite shorting.

From these results it was concluded that cell cycle life could be improved by the use of perforated metal substrates rather than expanded metal screens. Also the use of a double separator system - one microporous Tefzel backed with one non-woven glass fiber separator facing the cathode -

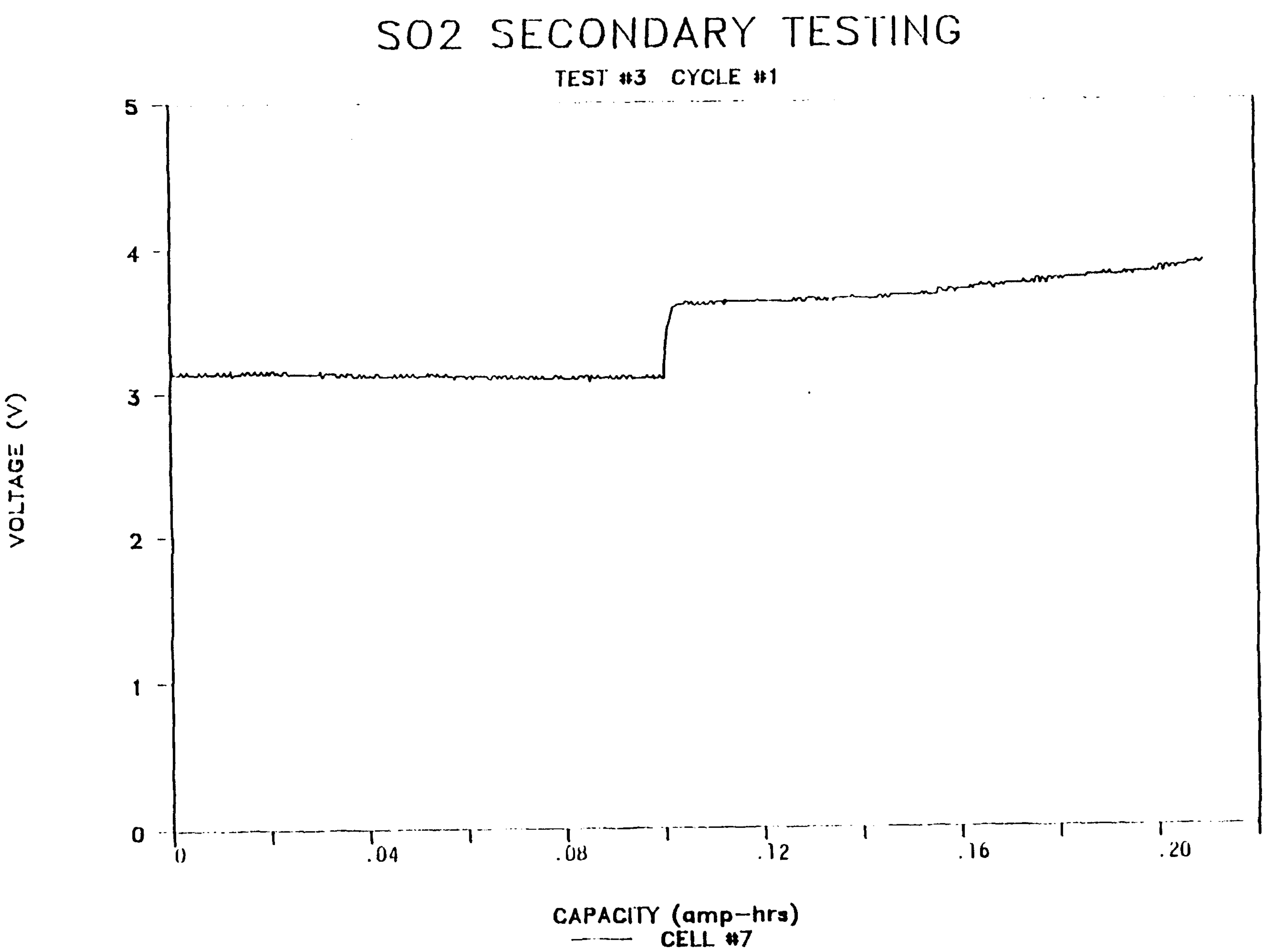

Figure 5: Voltage Profile of Cell 7, Cycle 1

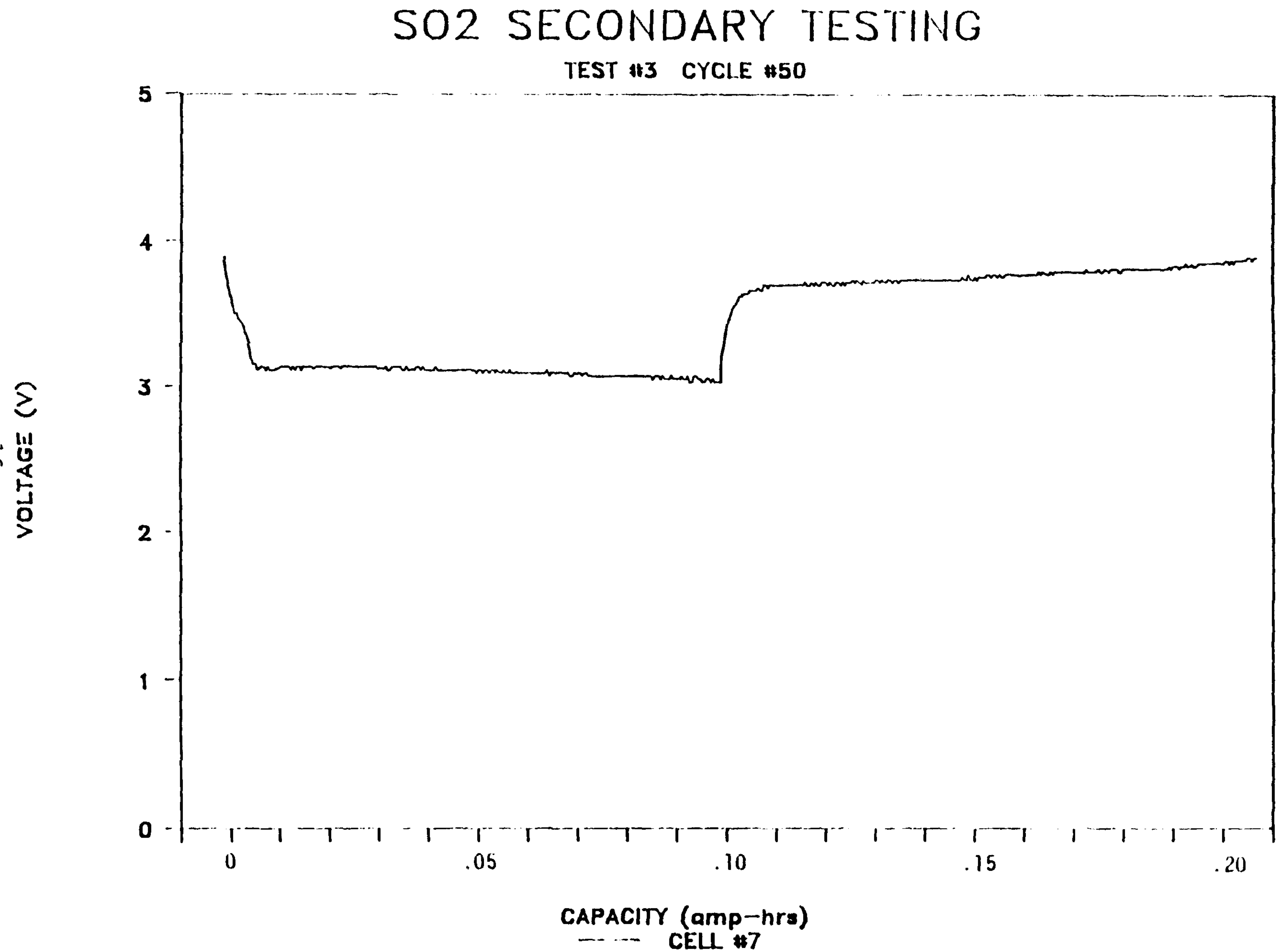

Figure 6: Voltage Profile of Cell 7, Cycle 50

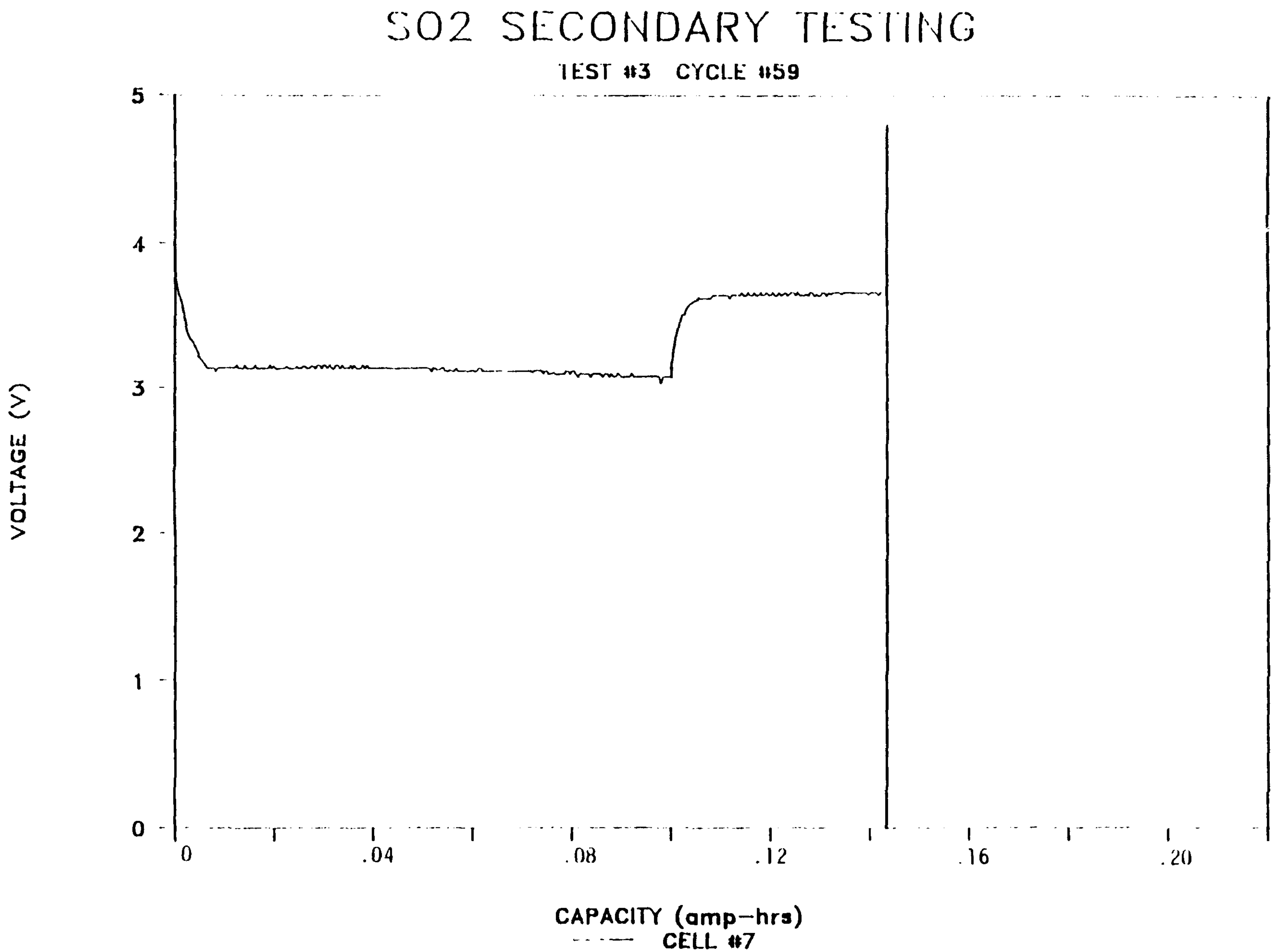

Figure 7: Voltage Profile of Cell 7, Cycle 59

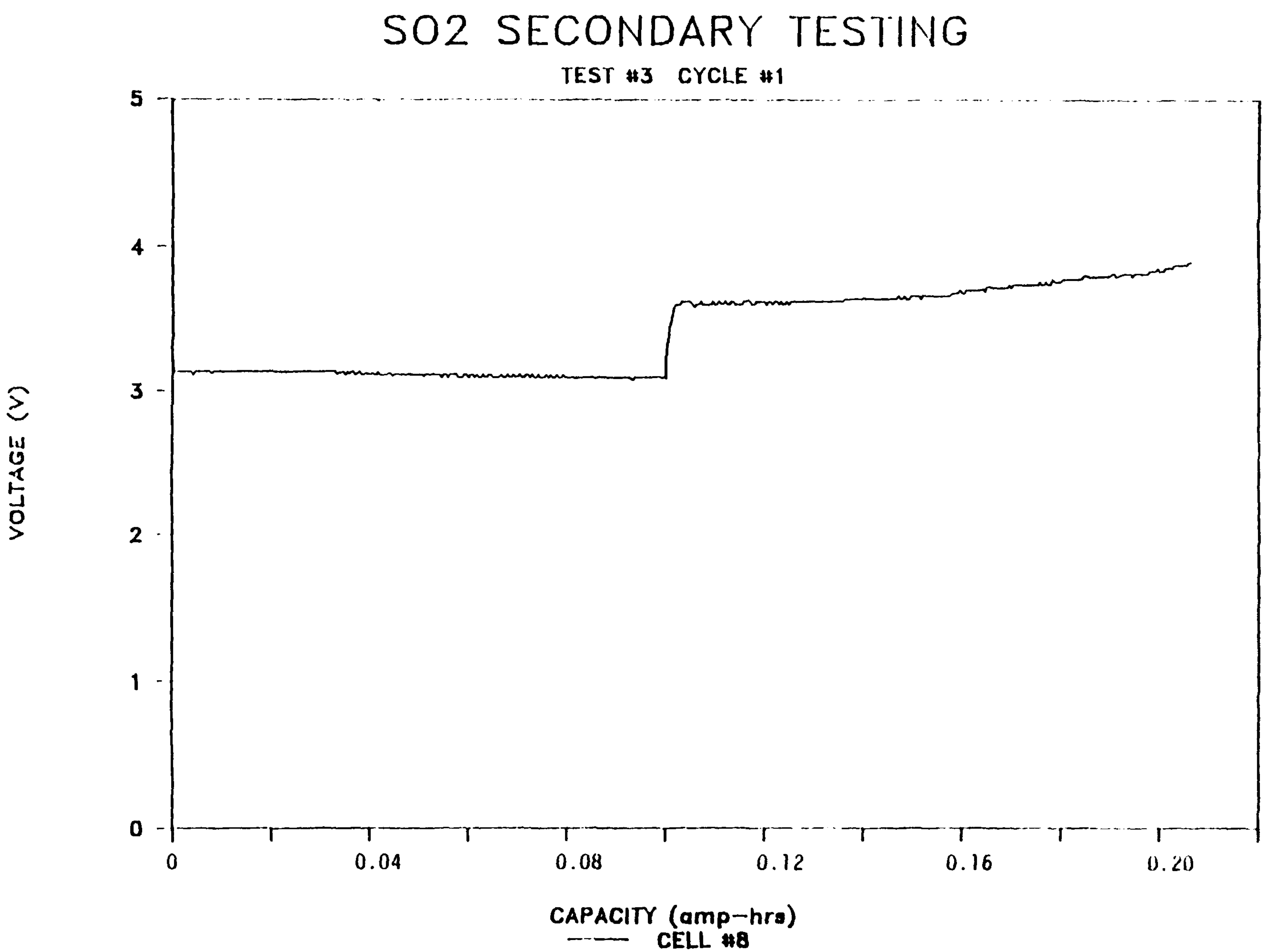

Figure 8: Voltage Profile of Cell 8, Cycle 1

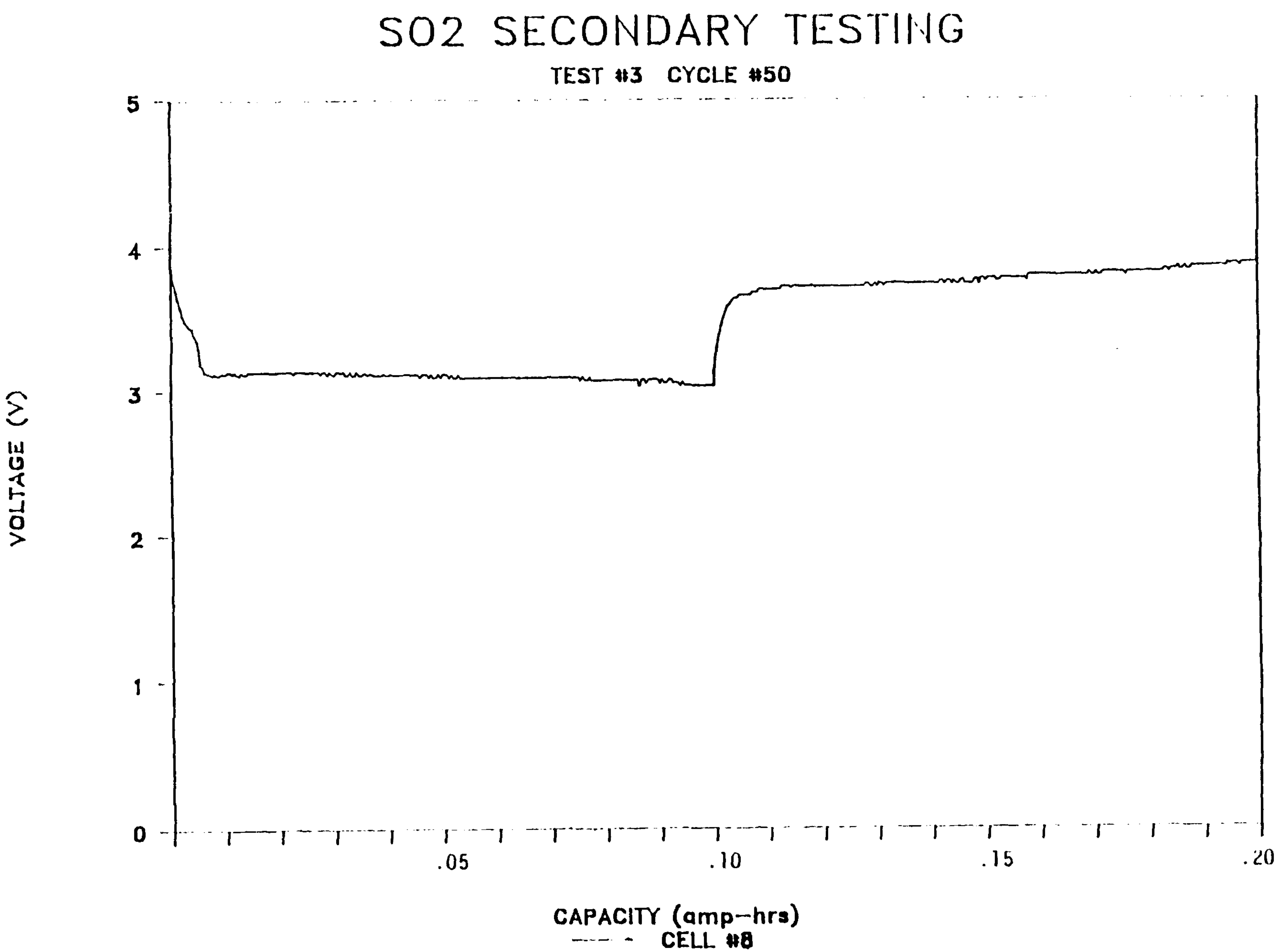

Figure 9: Voltage Profile of Cell 8, Cycle 50

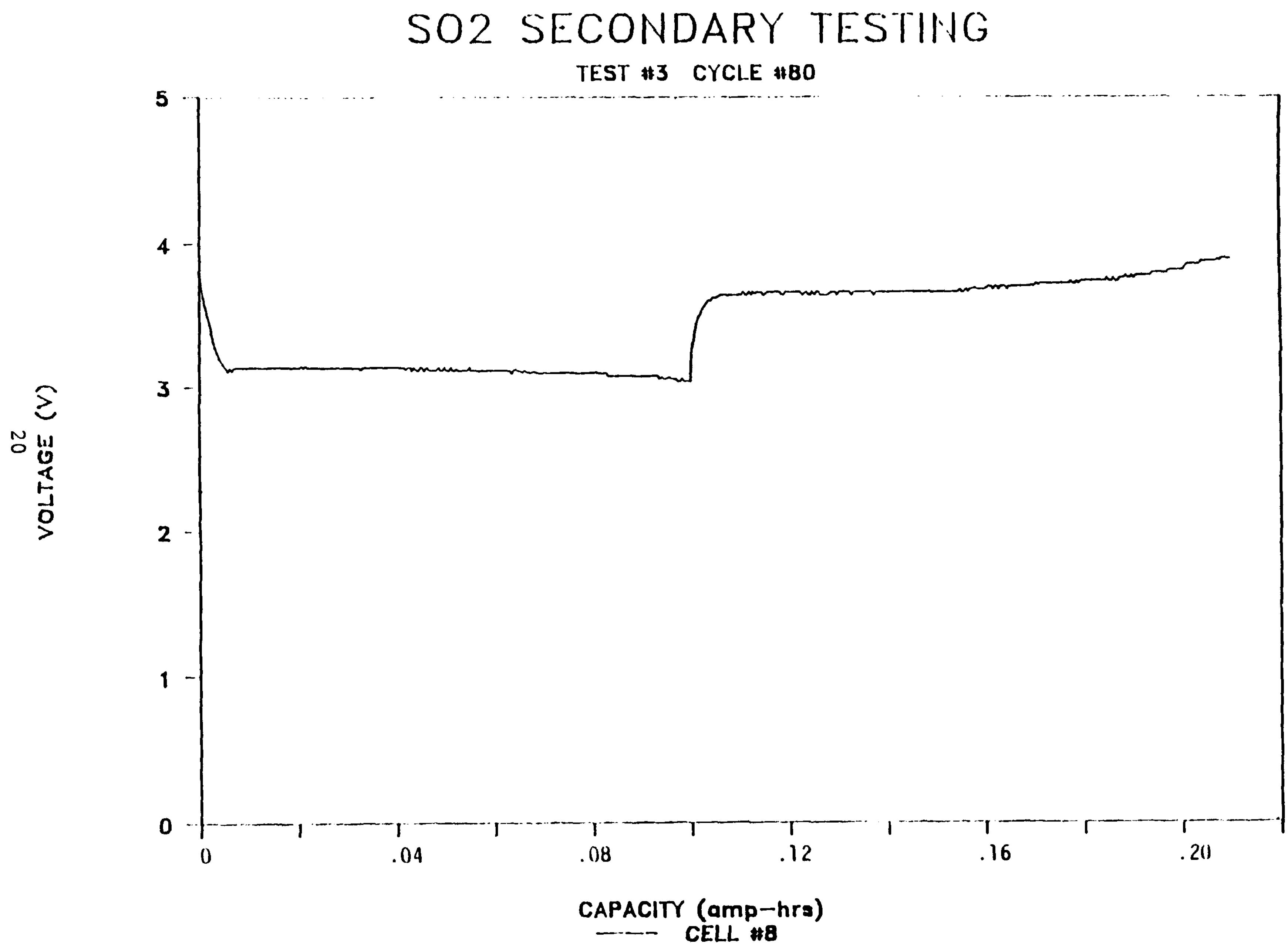

Figure 10: Voltage Profile of Cell 8, Cycle 80

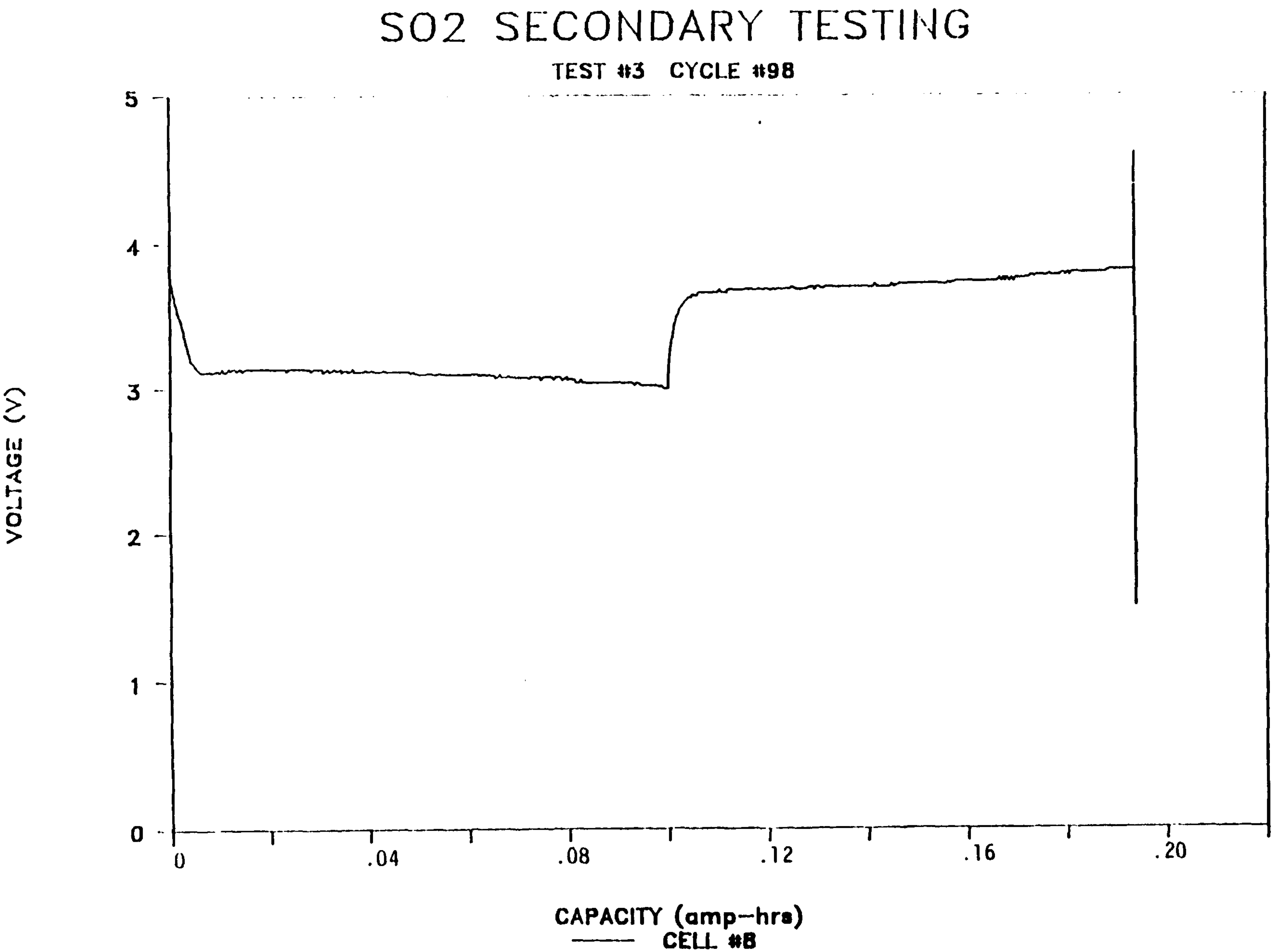

Figure 11: Voltage Profile of Cell 8, Cycle 98

could improve cycle life by providing space for electrode expansion and contraction without submitting the fragile Tefzel to undue stress.

Test Group 4

Test Group 4 was comprised of cells with Shawinigan Black cathodes and activated with $LiAlCl_4 \cdot 6SO_2$ electrolyte. The cells achieved an average capacity of 135 ± 18 mAh/ml carbon. Typical cycles of Cell 12 are shown in Figure 12. Capacity loss after the first cycle was very rapid indicating limited reversibility of the Shawinigan cathode/$LiAlCl_4 \cdot 6SO_2$ system when cycled between 3.9 and 2 8V. After the third cycle the charge limit was increased to 4.0V without improvement of achieved capacity. these results will be compared with heat treated SAB cathodes.

Test Group 5

Test Group 5 was comprised of cells with untreated and surface treated SAB cathodes and activated with $LiAlCl_4 \cdot 3SO_2$ electrolyte. Surface treatments were carried out at 240°C using water (Cell 15) and thionyl chloride (Cell 16). Cathodes were placed in a Parr Bomb, sealed with 3cc of either water of $SOCl_2$ and heated for 8-10 hours. Cells 10, 11 and 12 showed poor cycle life with SAB cathodes in $LiAlCl_4 \cdot 6SO_2$ electrolyte. Similar results were observed by Duracell Group[1] with SAB in small $LIAlCl_4/SO_2$ electrolytes. They, however, obtained a significantly better cathode performance with SAB when $LiGaCl_4$ or $Li_2B_{10}Cl_{10}$ electrolyte was used. This difference in cathode performance of SAB in $LiAlCl_4/SO_2$ and $LiGaCl_4$ or $Li_2B_{10}Cl_{10}$ electrolytes may be associated with the surface properties (e.g. wetability, pore volume, surface area, surface functional groups, etc.) of the carbon. No improved cycling performance was observed with the H_2O treated SAB cathode. The results of $SOCl_2$ treated SAB will be discussed with the results of $SOCl_2$ treated Ketjen Black.

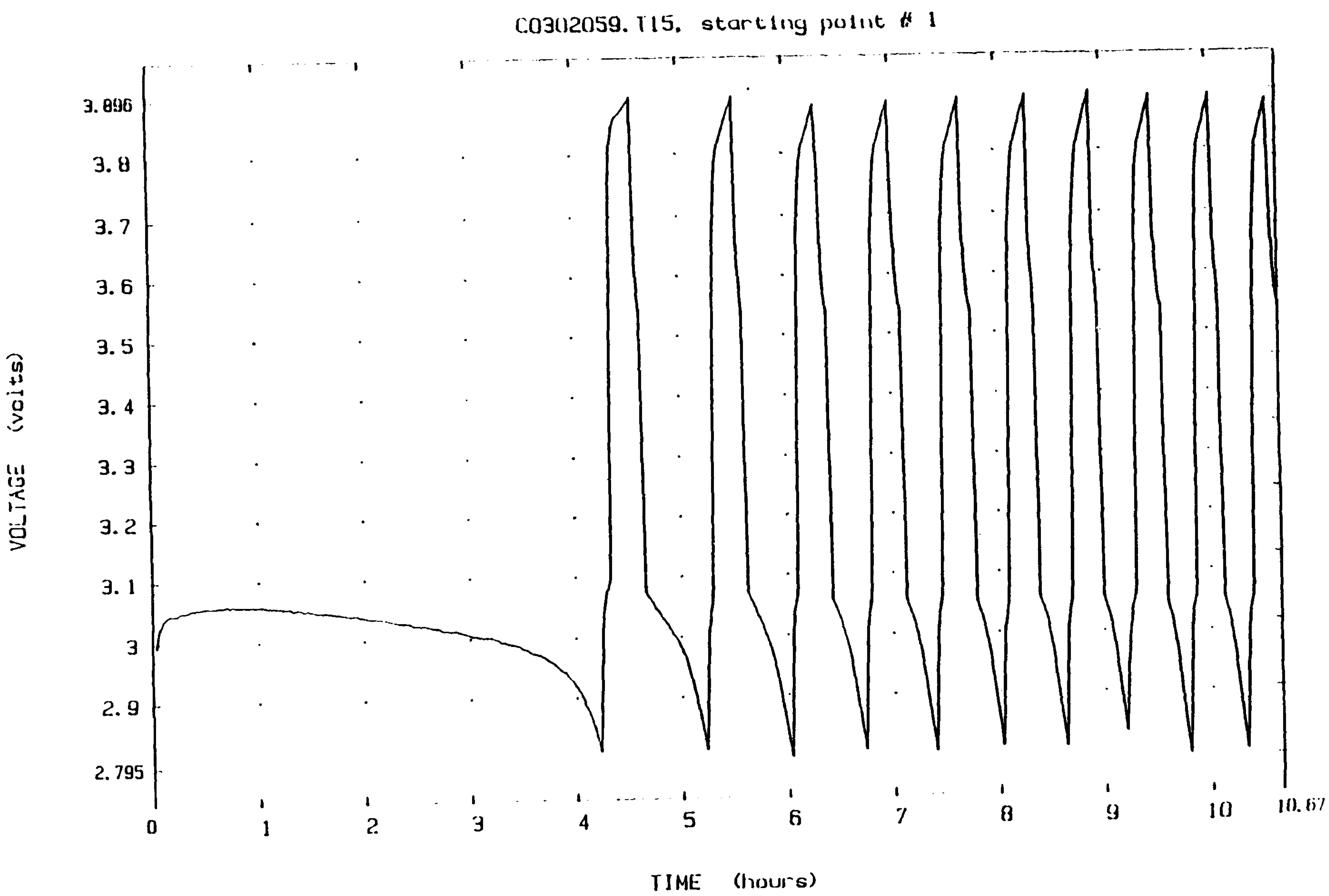

Figure 12: Cycling Voltage Profile of Cell 12

Test Group 6

Test Group 6 was assembled with KB cathodes and activated with $LiAlCl_4 \cdot 6SO_2$ electrolyte. Cells 18 and 25 were shorted during top welding and Cell 26 was shorted after filling with electrolyte . Cells 17, 19, 24, 27, 29 and 30 achieved good capacity. An increase in the charge limit for cell voltage resulted in significant improvement in cycle life. Results are summarized in Table 3.

The voltage profiles of Cells 17, 19 and 24 are shown in Figures 13-24 for selected cycles. An examination of discharge characteristic shows a relatively flat voltage profile down to 3.0 volts. Discharge ends with a sharp decrease in voltage from 3.0 to 2.8 volts which is probably due to increased resistance caused by the formation of a nonconductive film of discharged product on the cathode surface or plugging of the separator. During charge, the voltage profile shows an unusual behavior - voltage increases sharply until it reaches a maximum, then decreases, falls to a minimum and finally increases again until it obtains a plateau. Varying the charge and discharge limit, we found that the appearance of this maximum-minimum during charge is related to the lower limit of discharge voltage. If the cells were discharged to a cutoff voltage of 3.0V, no such maximum-minimum was observed. The resistive film formed during discharge at 3.0 to 2.8 volts apparently breaks down at the region of the maximum during charge and hence drops the voltage.

Figures 25 and 26 show the volumetric and gravimetric cathode utilization capacities delivered to a cutoff voltage of 2.8 volts vs the number of cycles achieved. Cell maintained good discharge capacity over 40 cycles. Cells 19 and 24 were made from the same batch of carbon cathodes which achieved gravimetric capacities of 1.37 and 1.47 Ah/g of carbon, respectively, for the second cycle. The

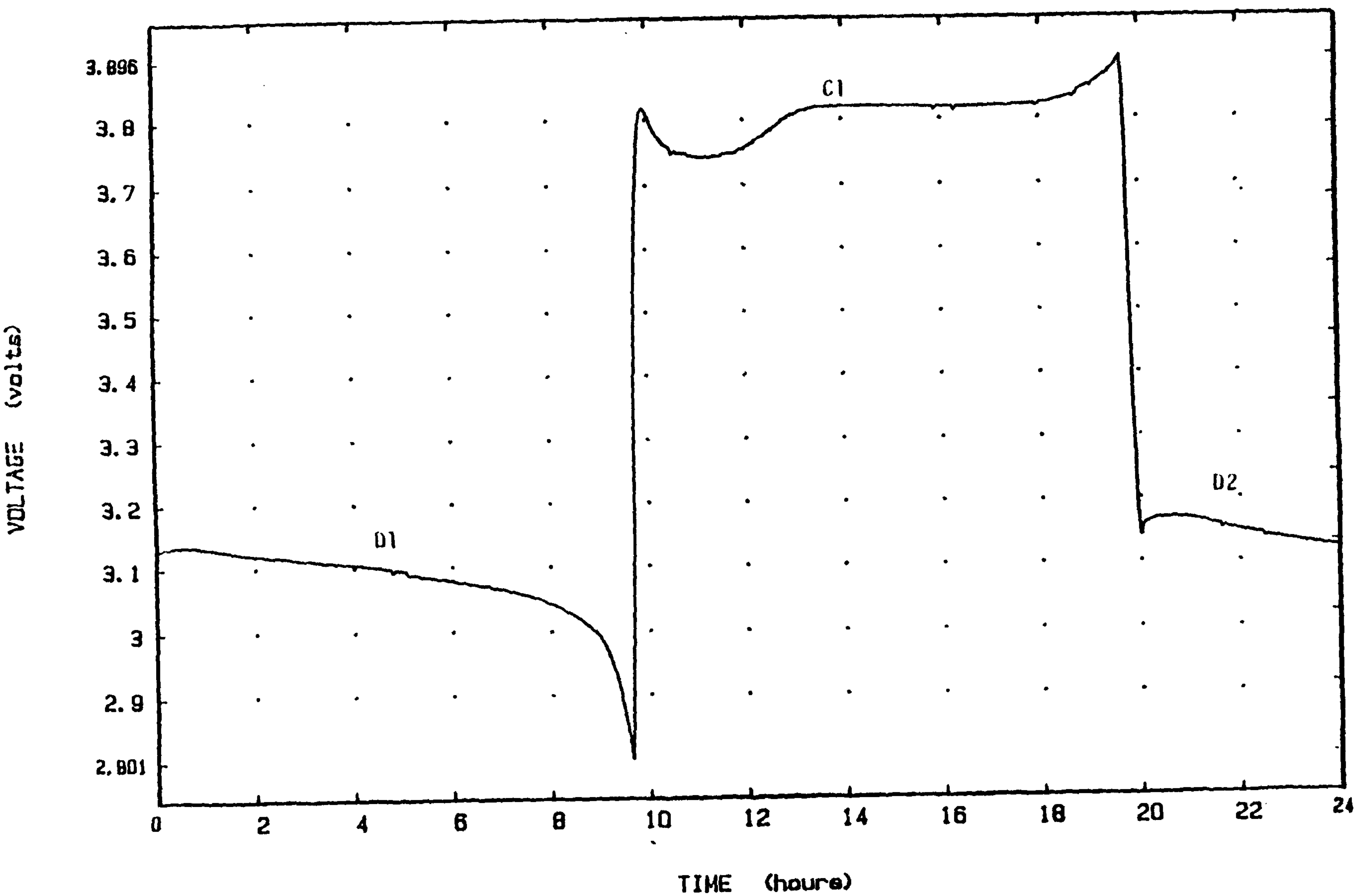

Figure 13: Cycling Behavior of Li/C Cell No. 17 in $LiAlCl_4 \cdot 6SO_2$ Electrolyte with 1.0 mA/cm^2 Discharge and Charge. Cathode and Anode Area: 25 cm^2.

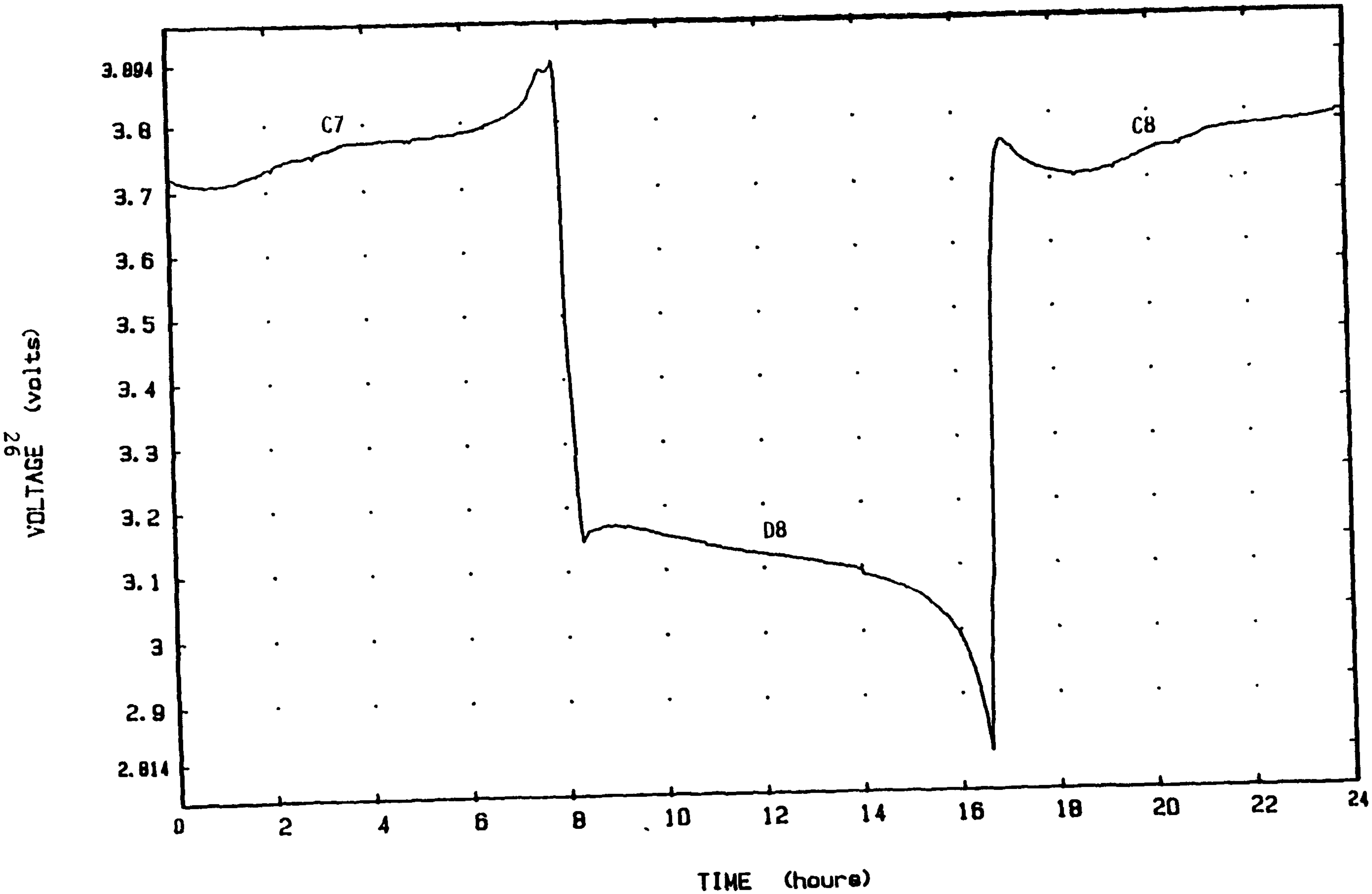

Figure 14: Cycling Behavior of Li/C Cell No. 17 in $LiAlCl_4 \cdot 6SO_2$ Electrolyte with 1.0 mA/cm^2 Discharge and Charge. Cathode and Anode Area: 25 cm^2.

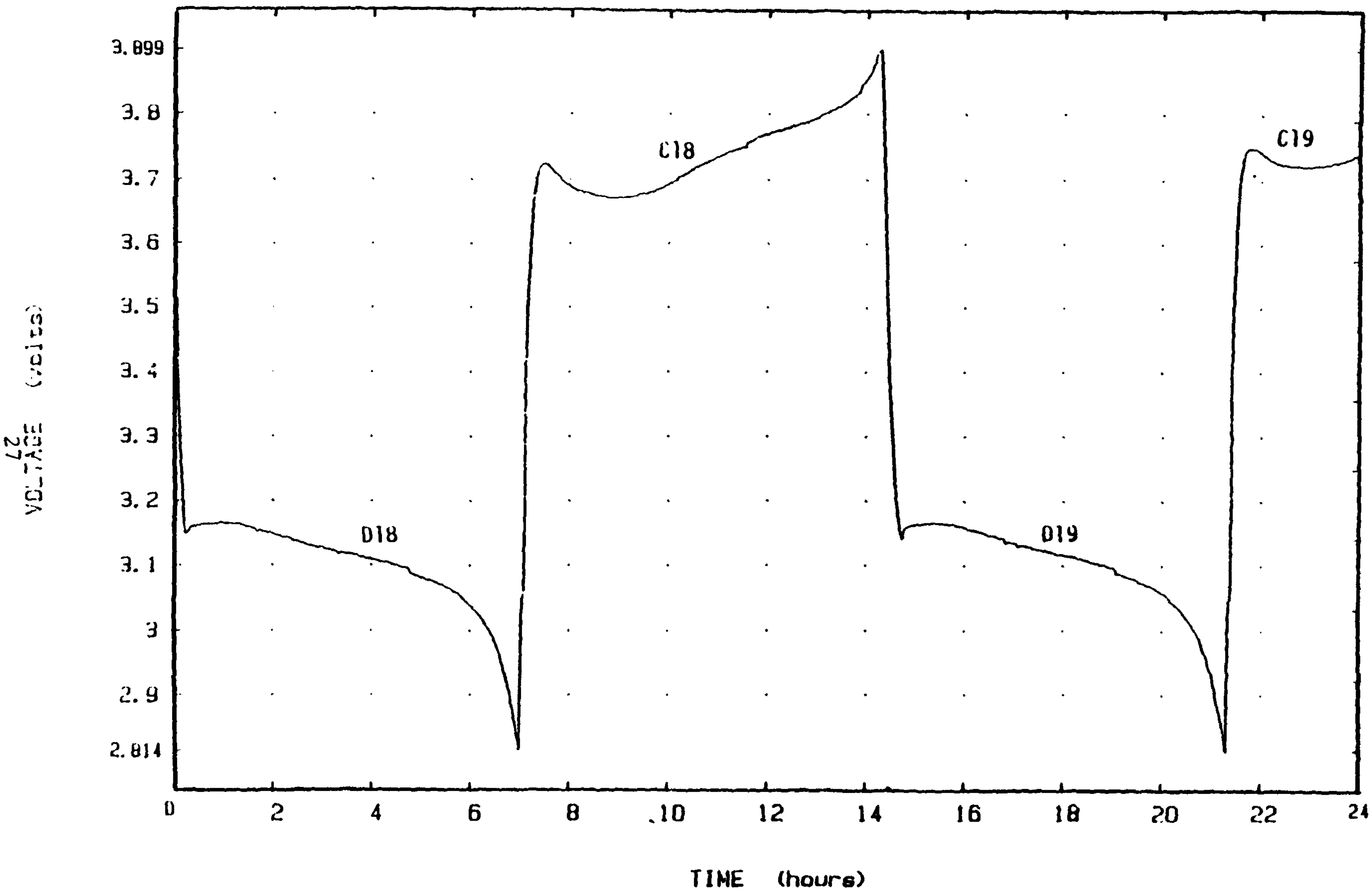

Figure 15: Cycling Behavior of Li/C Cell No. 17 in $LiAlCl_4 \cdot 6SO_2$ Electrolyte with 1.0 mA/cm^2 Discharge and Charge. Cathode and Anode Area: 25 cm^2.

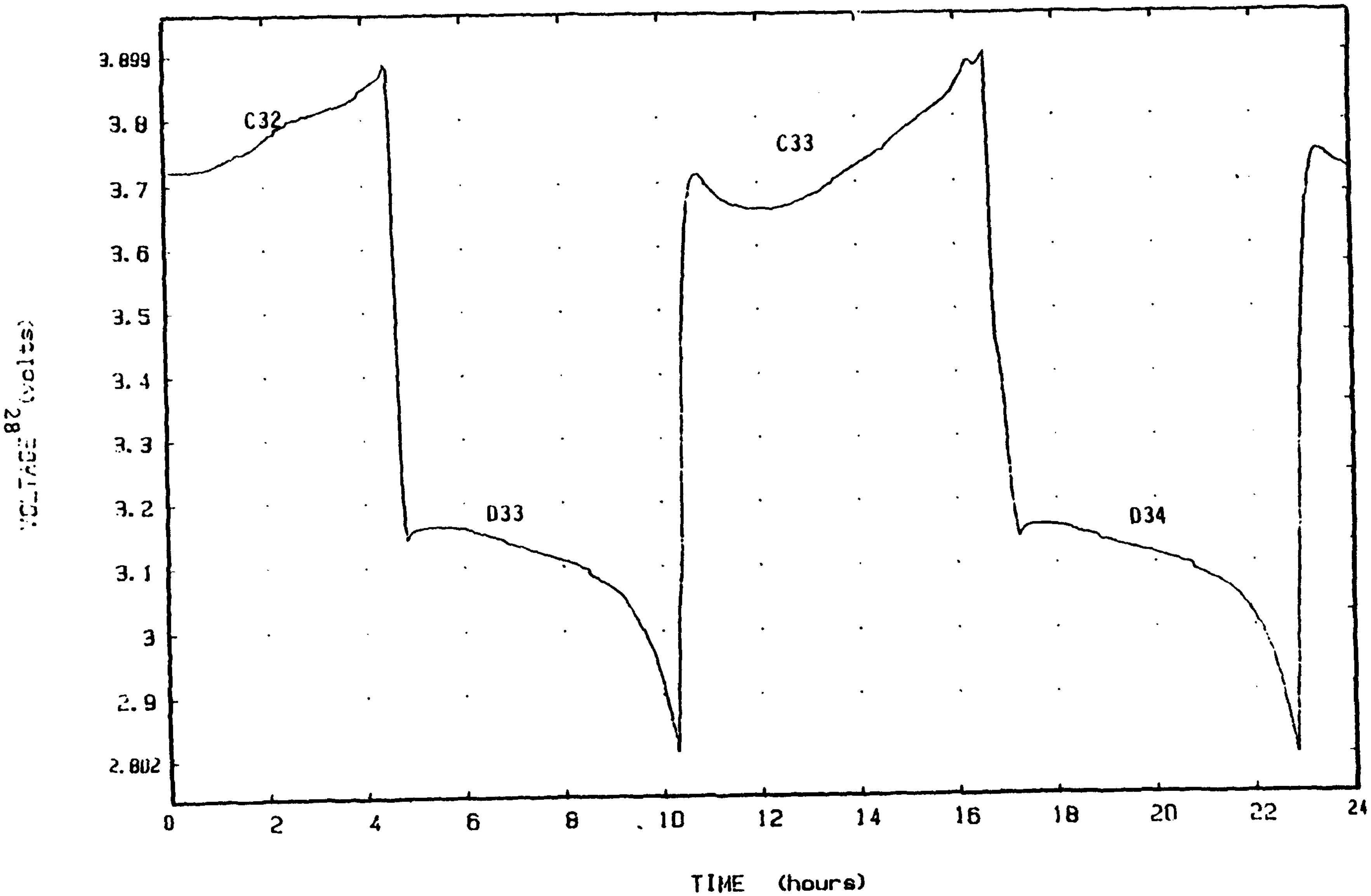

Figure 16: Cycling Behavior of Li/C Cell No. 17 in $LiAlCl_4 \cdot 6SO_2$ Electrolyte with 1.0 mA/cm^2 Discharge and Charge. Cathode and Anode Area: 25 cm^2.

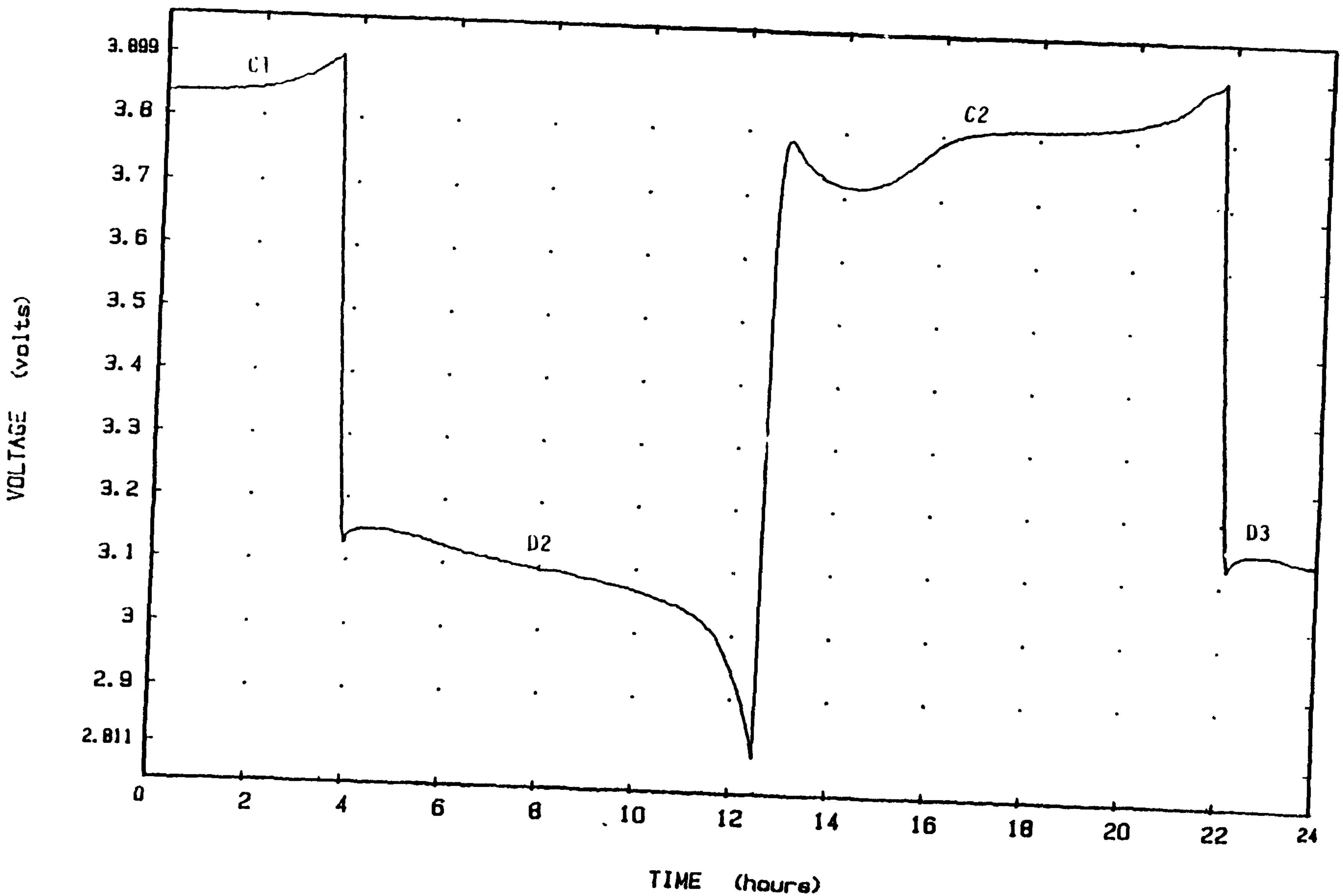

Figure 17: Cycling Behavior of Li/C Cell No. 19 in $LiAlCl_4 \cdot 6SO_2$ Electrolyte with 1.0 mA/cm^2 Discharge and Charge. Cathode and Anode Area: 25 cm^2.

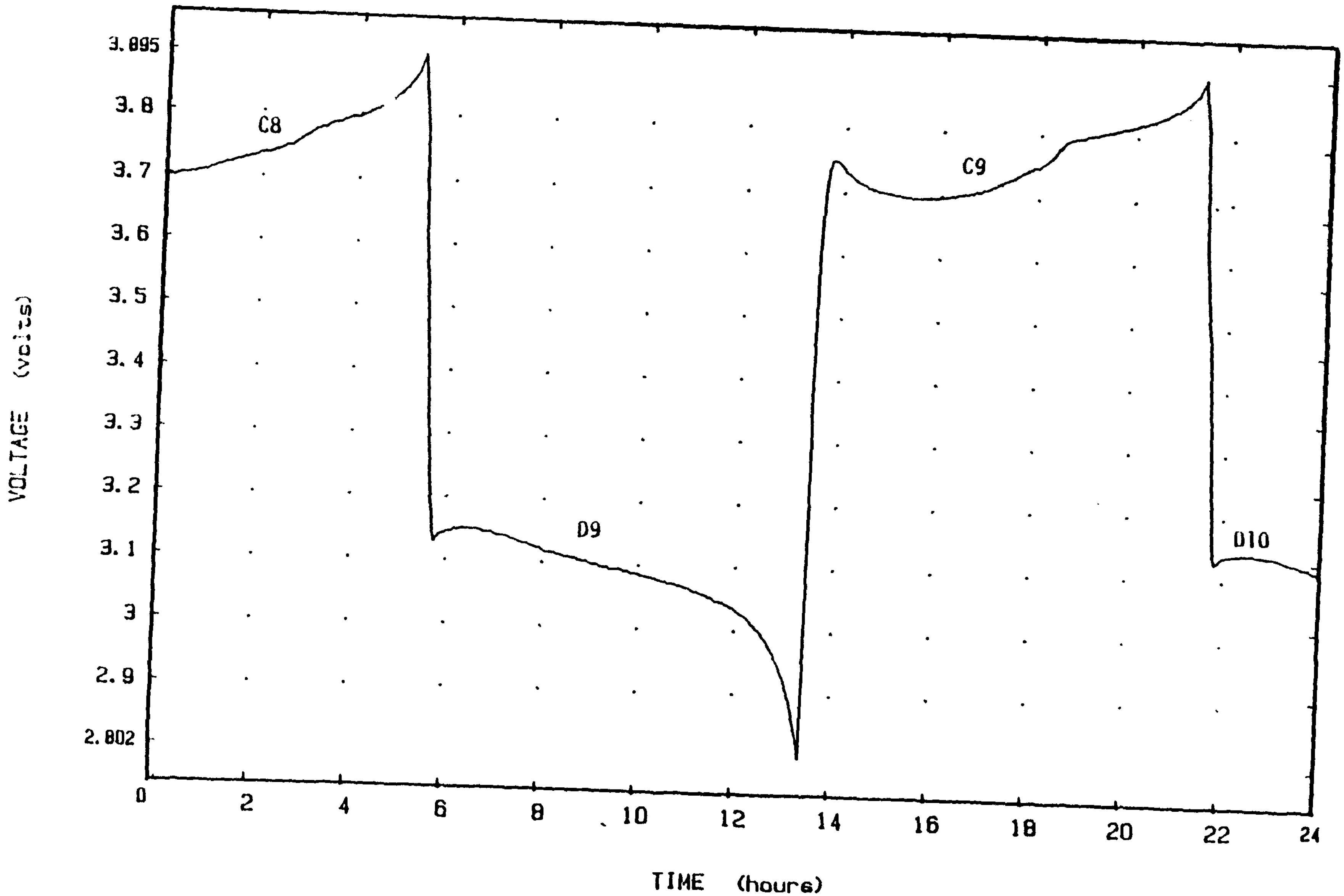

Figure 18: Cycling Behavior of Li/C Cell No. 19 in $LiAlCl_4 \cdot 6SO_2$ Electrolyte with 1.0 mA/cm^2 Discharge and Charge. Cathode and Anode Area: 25 cm^2.

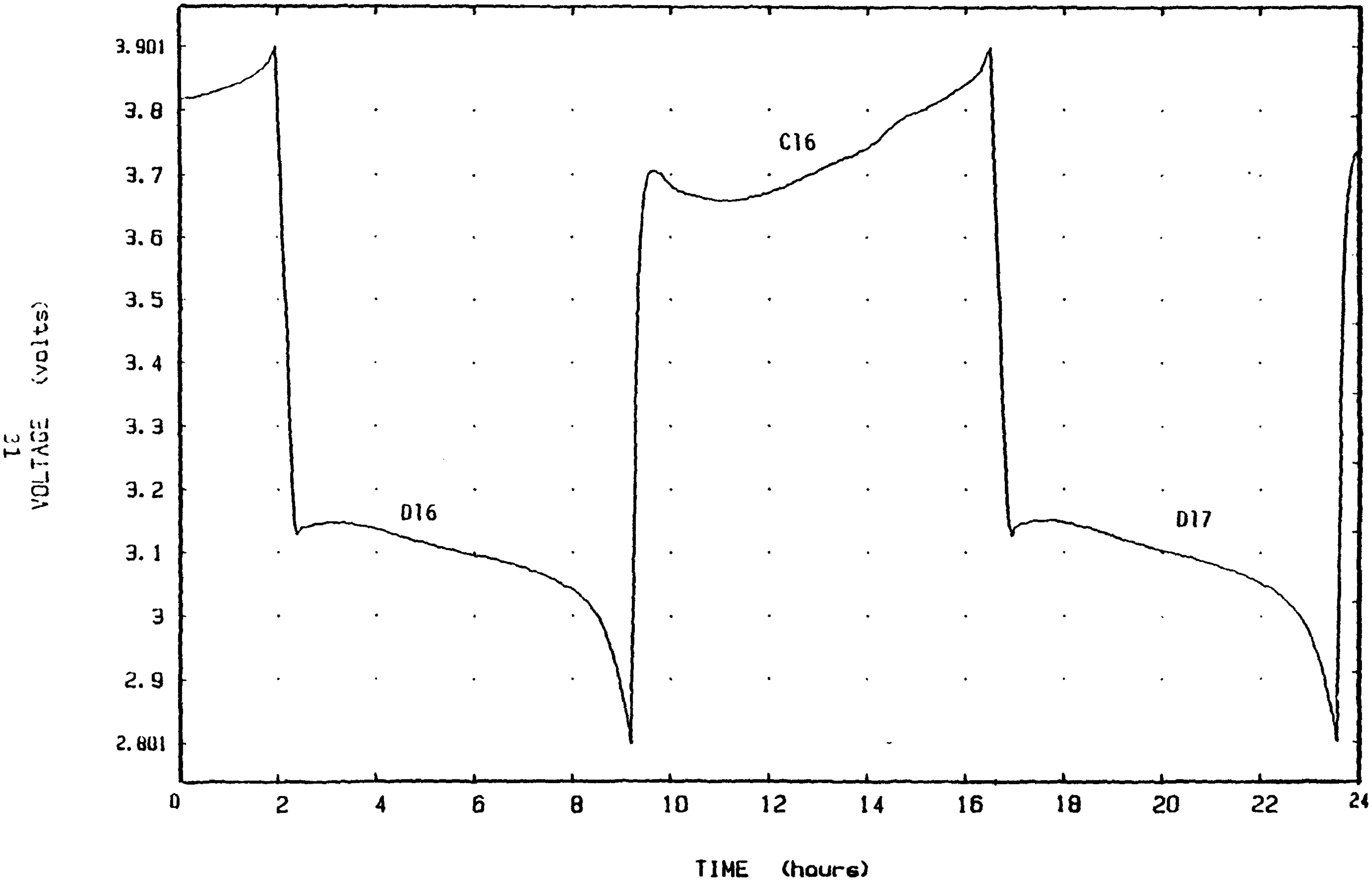

Figure 19: Cycling Behavior of Li/C Cell No. 19 in $LiAlCl_4 \cdot 6SO_2$ Electrolyte with 1.0 mA/cm^2 Discharge and Charge. Cathode and Anode Area: 25 cm^2.

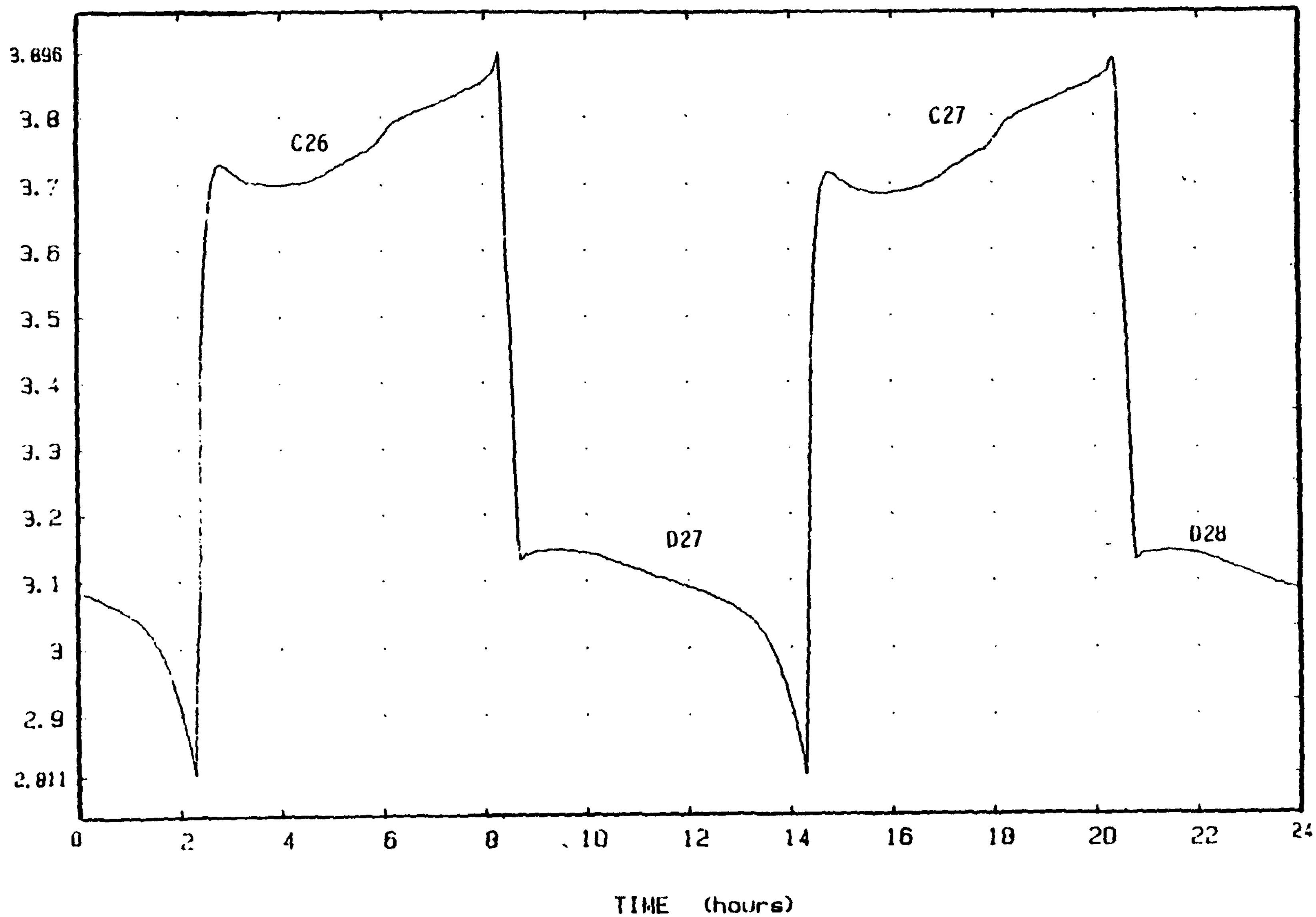

Figure 20: Cycling Behavior of Li/C Cell No. 19 in $LiAlCl_4 \cdot 6SO_2$ Electrolyte with 1.0 mA/cm^2 Discharge and Charge. Cathode and Anode Area: 25 cm^2.

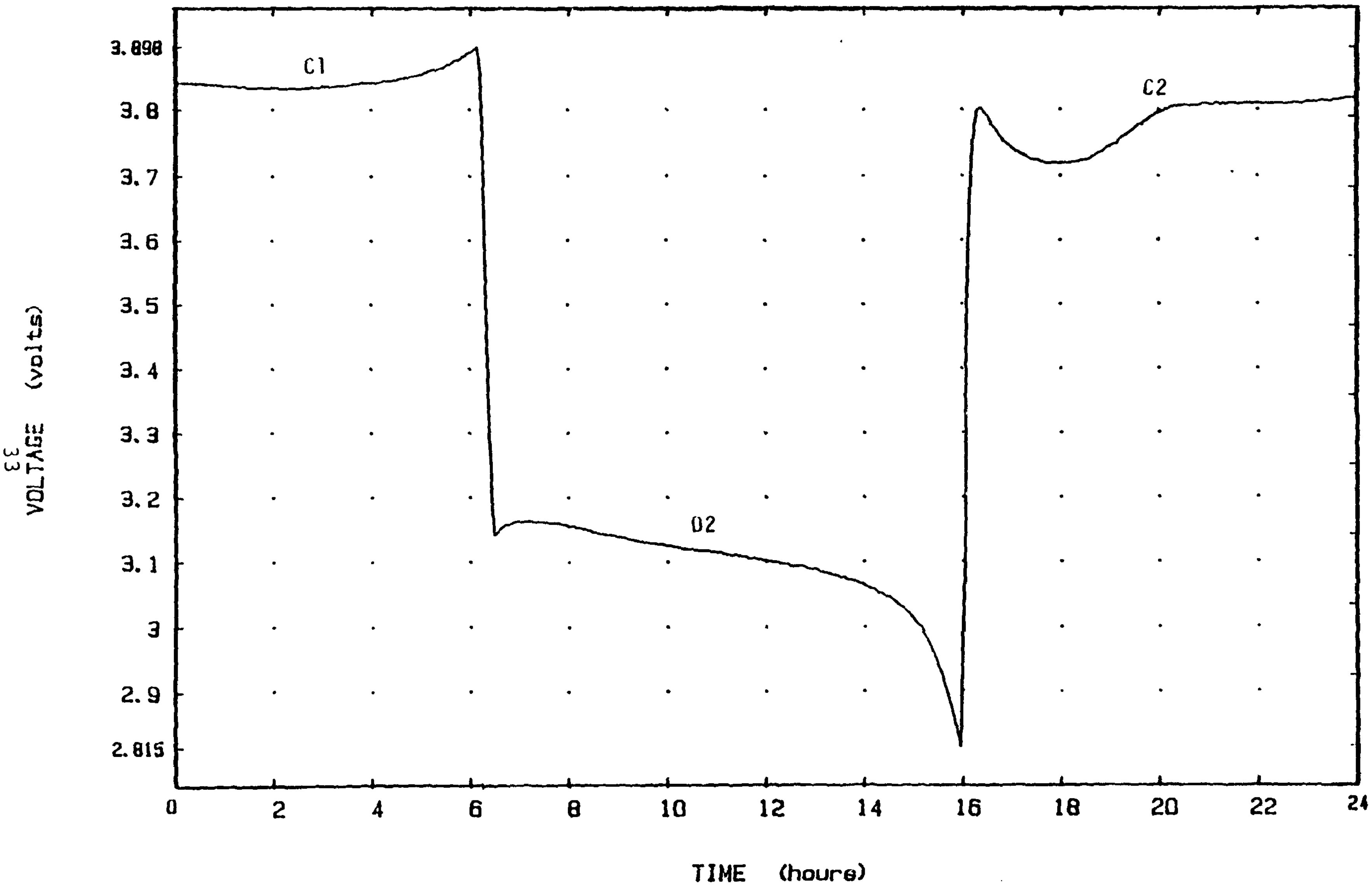

Figure 21: Cycling Behavior of Li/C Cell No. 24 in $LiAlCl_4 \cdot 6SO_2$ Electrolyte with 1.0 mA/cm^2 Discharge and Charge. Cathode and Anode Area: 25 cm^2.

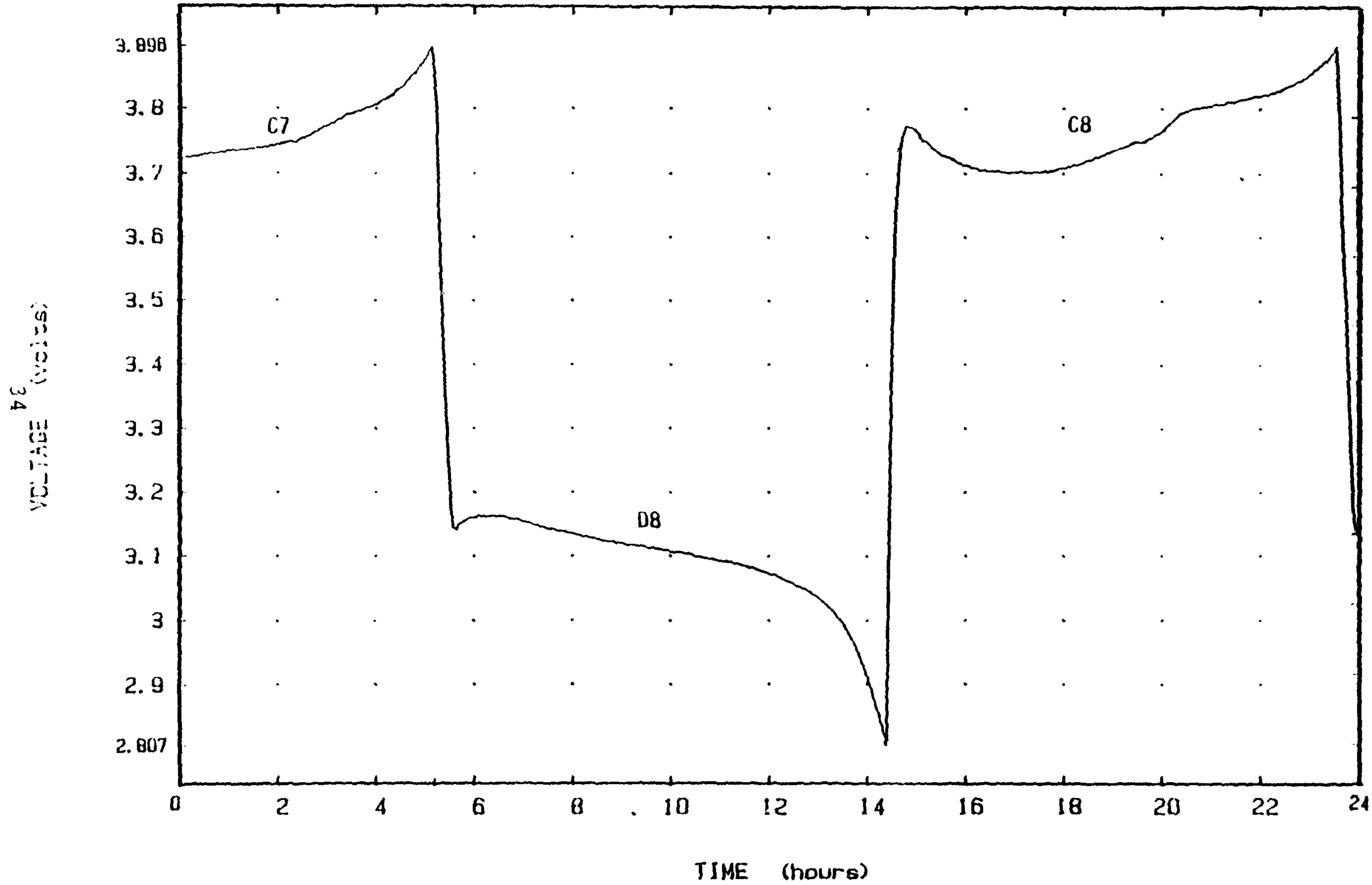

Figure 22: Cycling Behavior of Li/C Cell No. 24 in $LiAlCl_4 \cdot 6SO_2$ Electrolyte with 1.0 mA/cm^2 Discharge and Charge. Cathode and Anode Area: 25 cm^2.

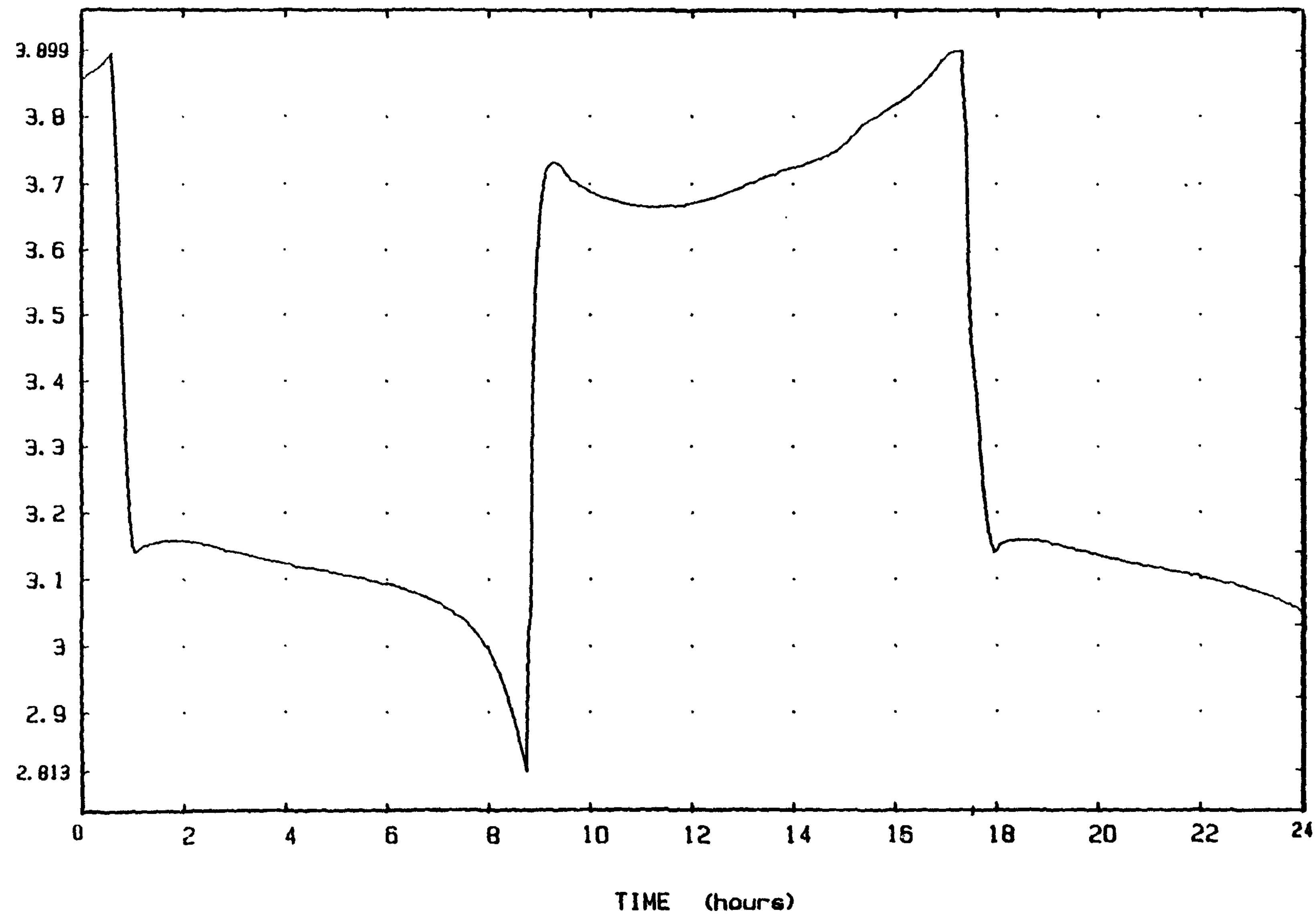

Figure 23: Cycling Behavior of Li/C Cell No. 24 in $LiAlCl_4 \cdot 6SO_2$ Electrolyte with 1.0 mA/cm^2 Discharge and Charge. Cathode and Anode Area: 25 cm^2.

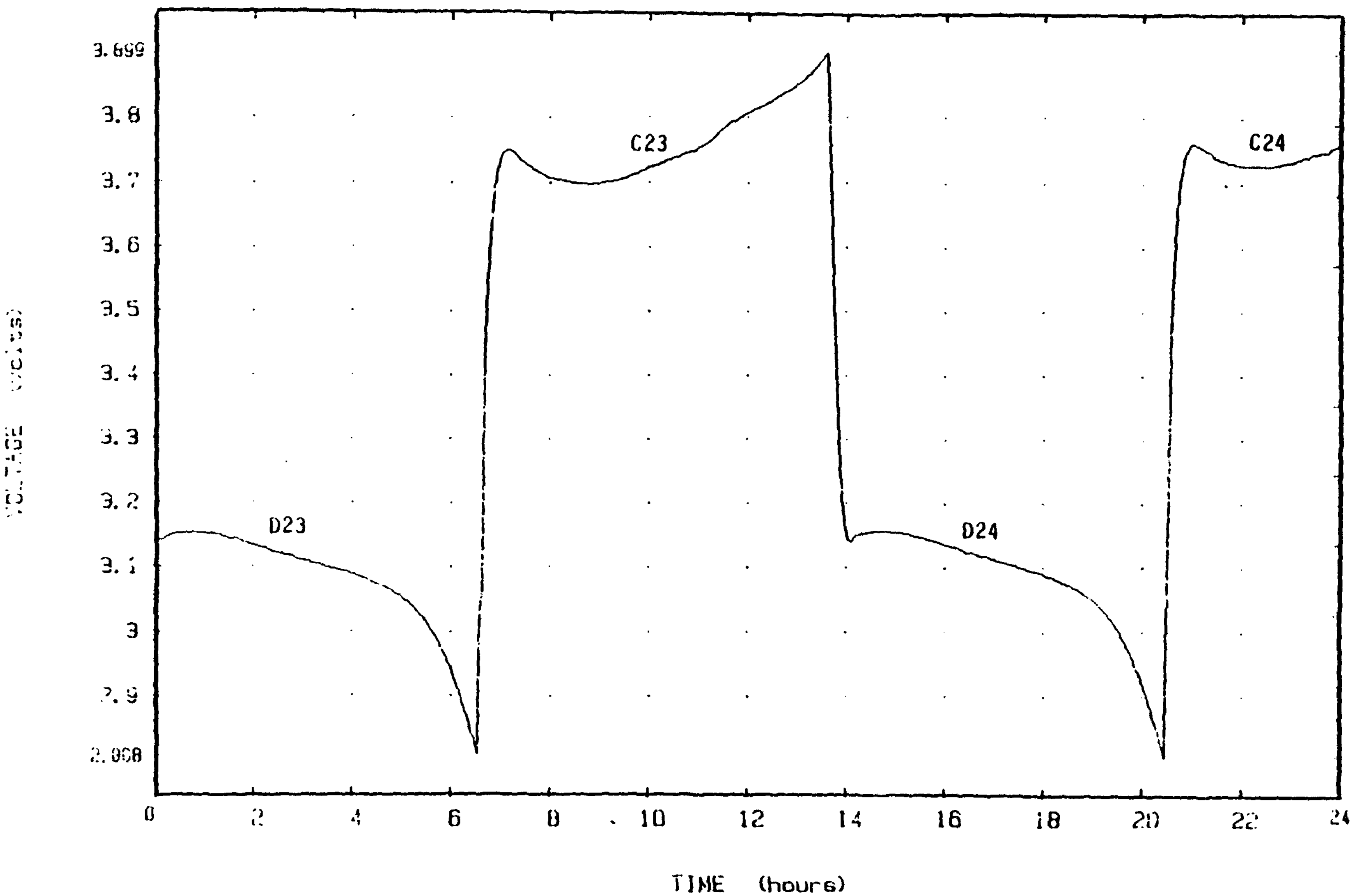

Figure 24: Cycling Behavior of Li/C Cell No. 24 in $LiAlCl_4 \cdot 6SO_2$ Electrolyte with 1.0 mA/cm^2 Discharge and Charge. Cathode and Anode Area: 25 cm^2.

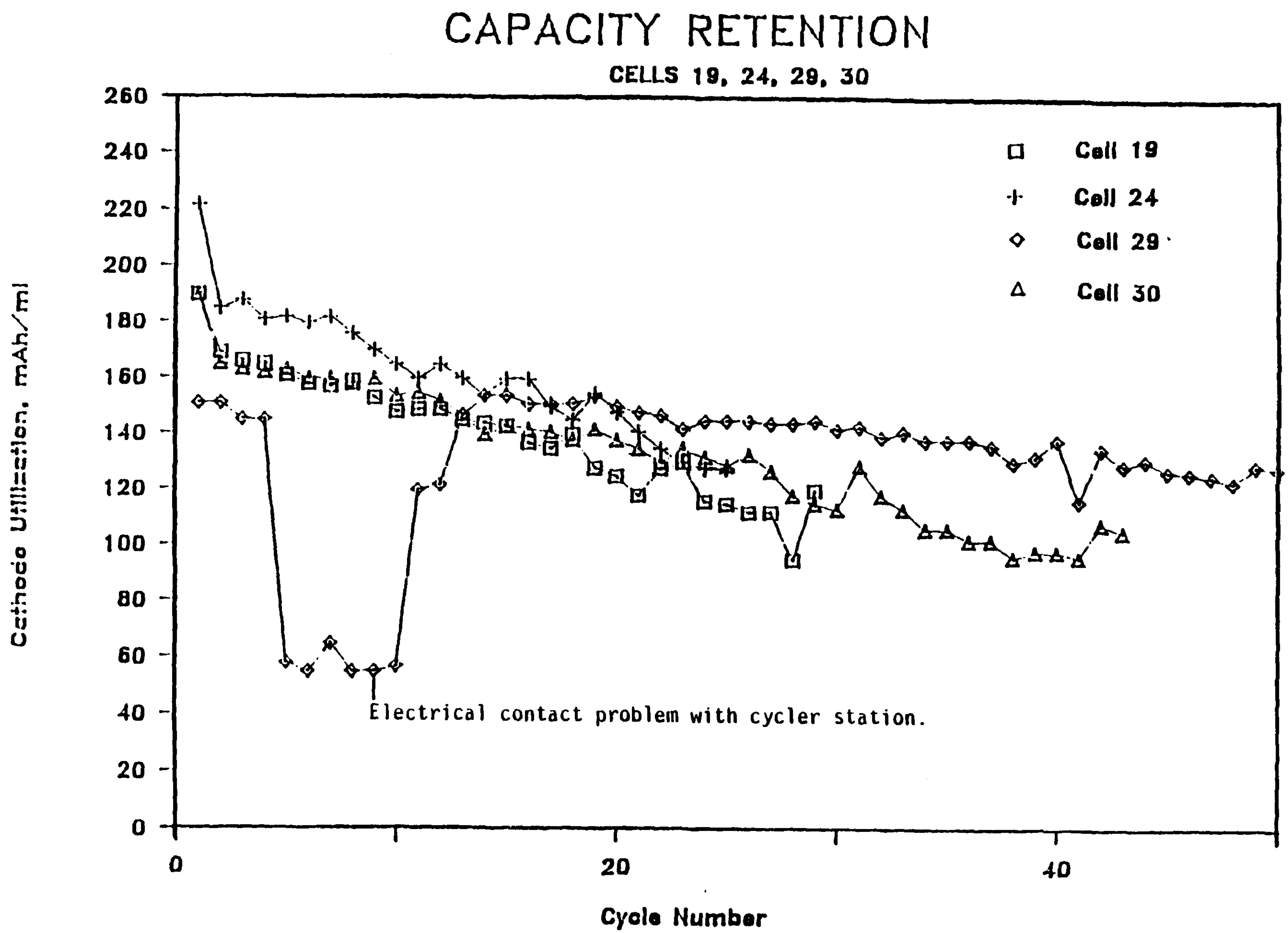

Figure 25: Volumetric Capacity Utilization of Cathode With Number of Cycles for $Li/LiAlCl_4 \cdot 6SO_2/C$ Cells at 1.0 mA/cm^2 Discharge Rate. Cathode Thickness: 0.021" (19 and 24) and 0.015" (29 and 30); Area: 25 cm^2.

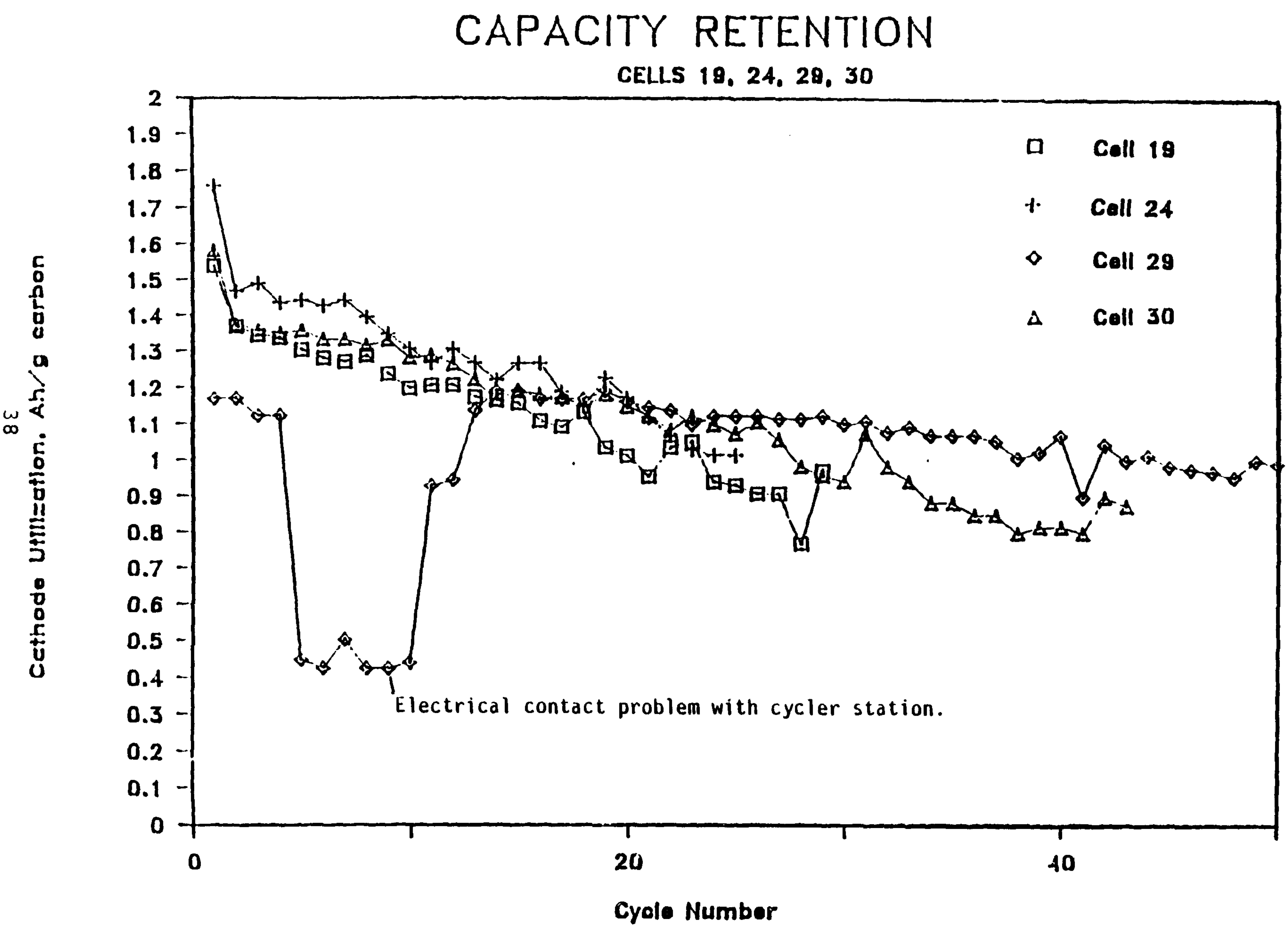

Figure 26: Gravimetric Capacity Utilization of Cathode With Number of Cycles for $Li/LiAlCl_4 \cdot 6SO_2/C$ Cells at 1.0 mA/cm^2 Discharge Rate. Weight of Cathode: ∿0.18 gm (19 and 24) and ∿0.13 gm (29 and 30); Area: 25 cm^2.

capacities dropped to 0.97 and 1.02 Ah/g of carbon for the 29 and 25 cycles, respectively. This capacity loss might be related to the improper voltage limit which might have caused some irreversible reaction to occur.

Cell 24 was constructed with a lithium reference electrode. The voltage profile of reference vs cathode shows only a small anode polarization (≈20-25 mV).

Cell 29 was operating within the voltage limits of 2.8V to 4.0V vs Li. This cell achieved a capacity of 1.17 Ah/g of carbon for the second cycle and 0.99 Ah/g of carbon for the 50th cycle. The capacity loss is about 15 percent. The voltage limits of cell 30 were 2.8 to 3.9 volts. Though this cell showed a good capacity value of 1.38 Ah/g of carbon for the second cycle, the capacity dropped fairly rapidly to a value of 0.88 Ah/g of carbon after completion of only 43 cycles. The loss was about 36 percent. The cell ultimately achieved 106 cycles but vented during charge apparently from excessive heat and vapor pressure.

The cycling performance of several Li/SO_2 cells containing KB cathodes and $LiAlCl_4$ electrolytes has been partly discussed under Test Group 2 and 3 as summarized in Table 3.

Voltage profiles on Li vs Cathode refernece potentials of Cell 24 are shown in Figures 27 and 28. The change in voltage with time for the cell and cathode vs. reference is small indicating little anode polarization at 1 mA/cm^2 charge and discharge rates. This is consistent with observations for Cell 24. The sharp decrease in voltage from 3.0 - 3.8V and corresponding appearance of maximum-minimum near 3.7V has been explained as due to the formation of resistive film during discharge at the region of increased polarization The discharge capacity of cycle Nos. 3 and 25 are 1.47 and 1.0-2 Ah/g of carbon, respectively, which are

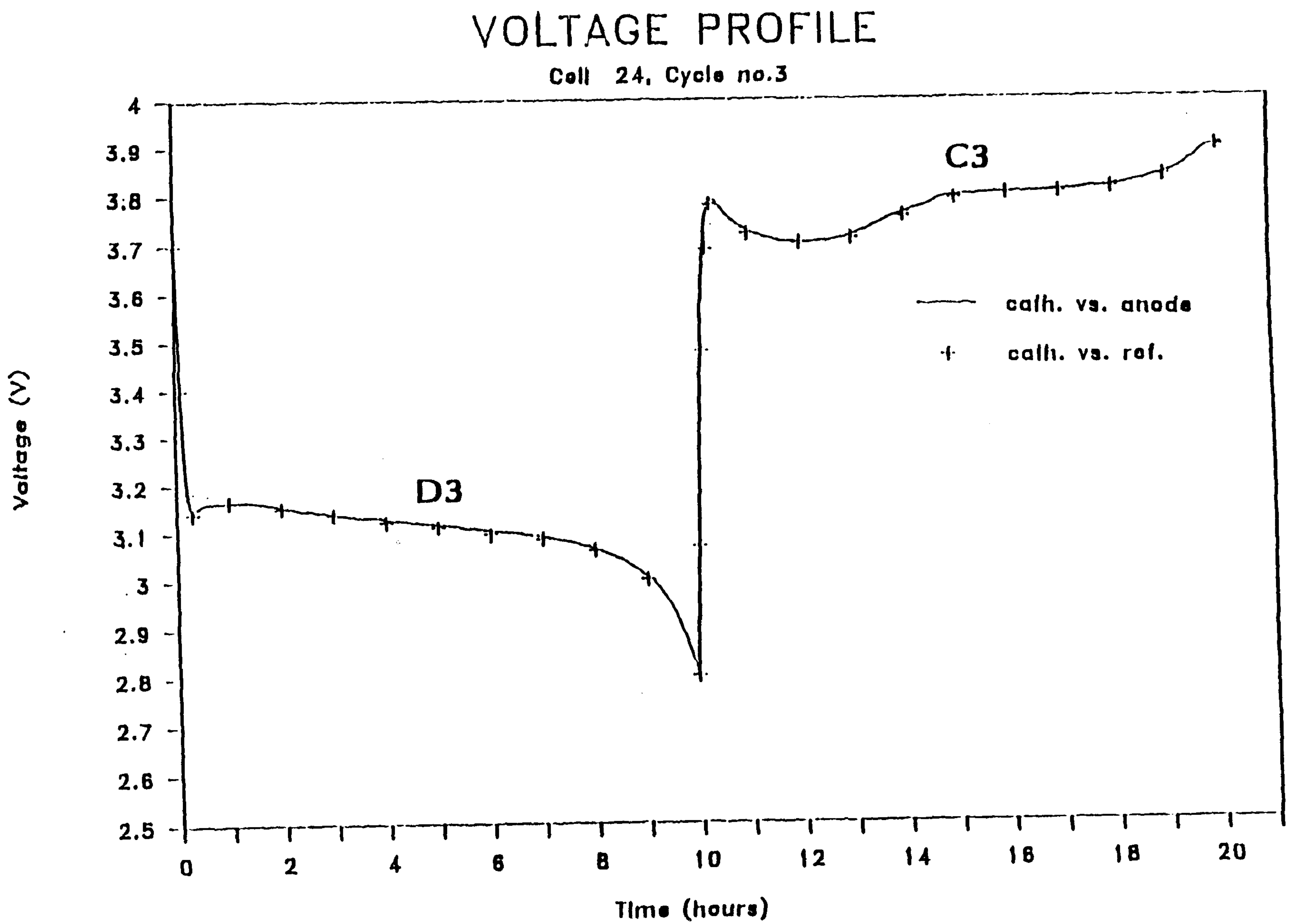

Polarization Behavior of $Li/LiAlCl_4 \cdot 6\, SO_2/C$ Cell No. 24 with $1.0\ mA/cm^2$ Discharge and Charge Rate. Cathode and Anode Area: $25\ cm^2$

Figure 27

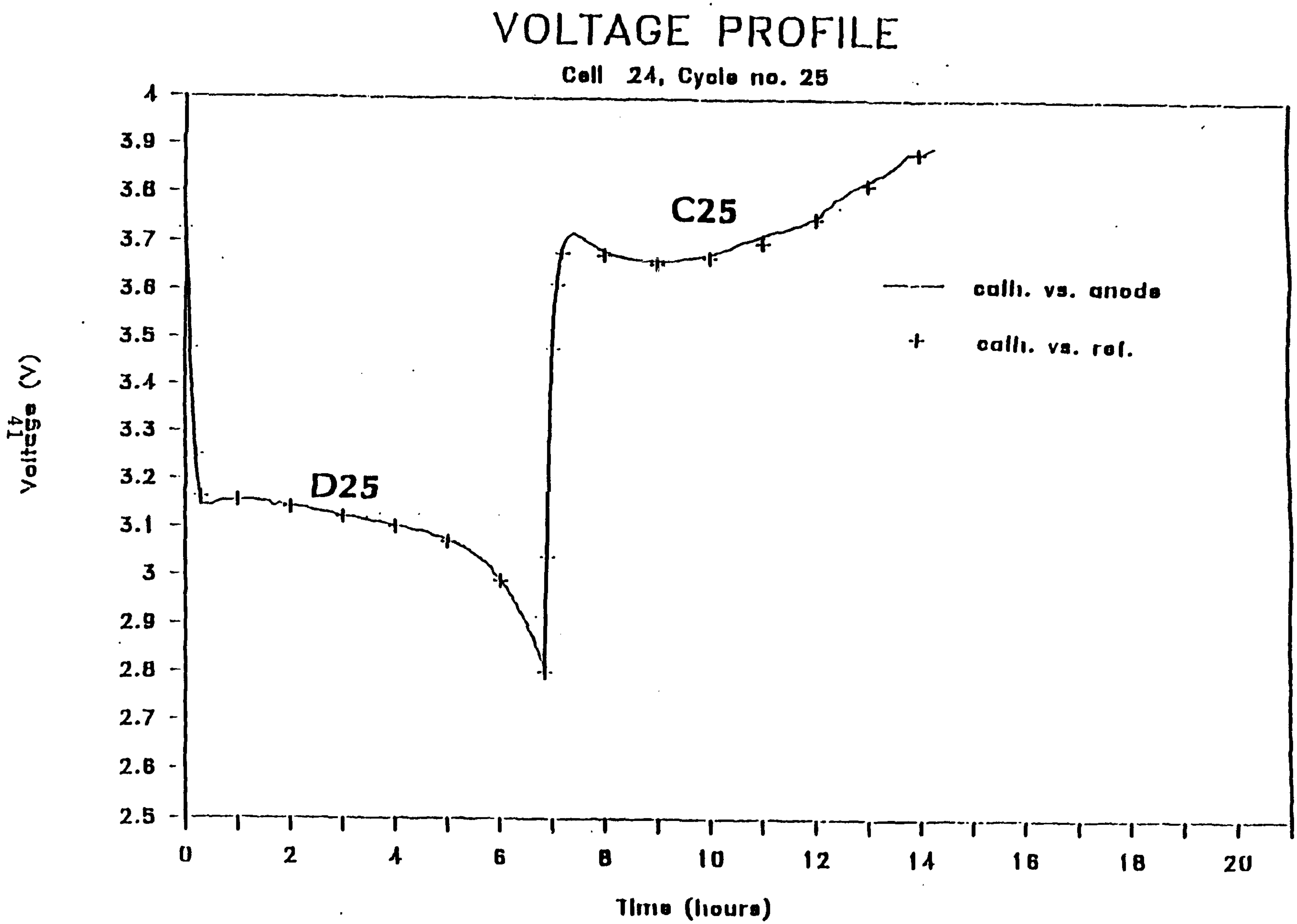

Polarization Behavior of $Li/LiAlCl_4 \cdot 6\ SO_2/C$ Cell No. 24 with $1.0\ mA/cm^2$ Discharge and Charge Rate. Cathode and Anode Area: $25\ cm^2$

Figure 28

significantly higher than 0.44 Ah/g of carbon reported in the literature[1] for the Ketjen Black carbon in $LiAlCl_4$ electrolyte.

Cell 24 was intentionally terminated after completing the 68th cycle of charge to 3.9V and then taken apart for analysis. Similarly, Cell 19 was also taken apart following discharge to 2.8V after completion of the 79th cycle.

Figures 29-31 compare the cathode utilization capacities of a number of cells at different voltage limits vs. the number of cycles. Cells 17 and 27 were made from the same batch of carbon cathodes which achieved gravimetric capacities of 1.35 and 1.20 Ah/g of carbon, respectively for the second cycle in $LiAlCl_4 \cdot 6SO_2$ electrolyte within the voltage limits of 2.8 - 3.9V. After the 50th cycle, the capacity of Cell 17 dropped to 0.71 Ah/g and that of Cell 27 to 0.66 Ah/g which corresponds to about 45 percent capacity loss. the upper voltage limit of Cell 17 was increased to 4.0V after 53 cycles (0.66 Ah/g) which caused an increase of capacity to 0.88 Ah/g. The cell almost retained this capacity until it failed after 72 cycles.

A similar gain in capacity (from 0.59 Ah/g to 0.92 Ah/g) was observed with Cell 27 when the upper voltage limit was increased to 4.0V after 61 cycles. Further extension of upper limit to 4.1V increased the capacity value from 0.90 to 1.16 Ah/g of carbon. In the case of Cell 28, which contained $LiAlCl_4 \cdot 3SO_2$ electrolyte, the effect of capacity increase with increasing upper voltage limit is, however, less significant (Figure 30).

The increased discharge capacity with the increase of upper voltage limit may be associated with one or more of the following: (i) electrochemical regeneration of discharge product at higher charge voltage, and/or (ii) chemical

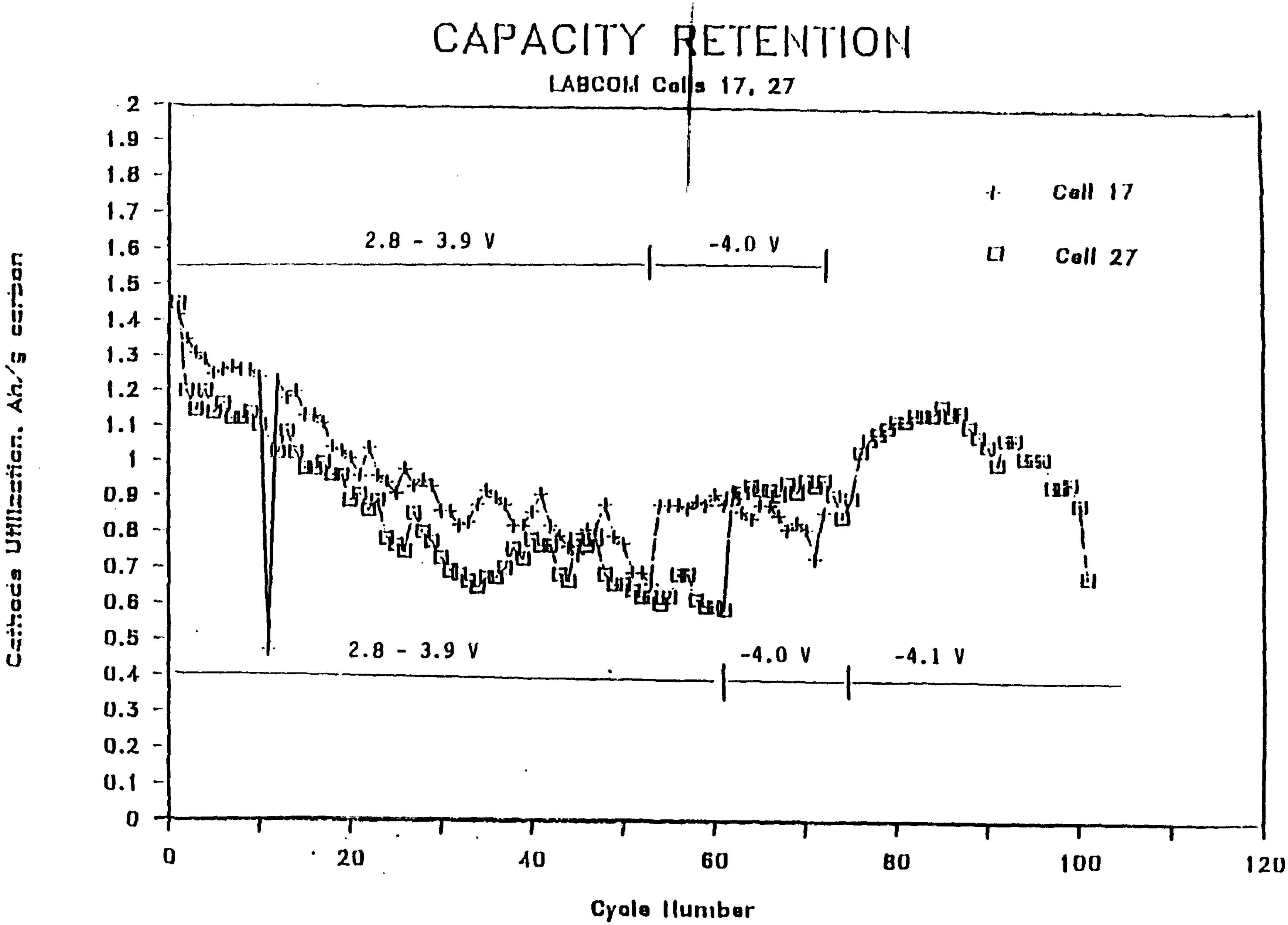

Capacity Utilization of Cathode with Number of Cycles for $Li/LiAlCl_4 \cdot 6SO_2/C$ Cells at 1.0 mA/cm^2 Discharge Rate. Cathode Area: 25 cm^2; Weight: 0.186 gm (#17) and 0.171 gm (#27)

Figure 29

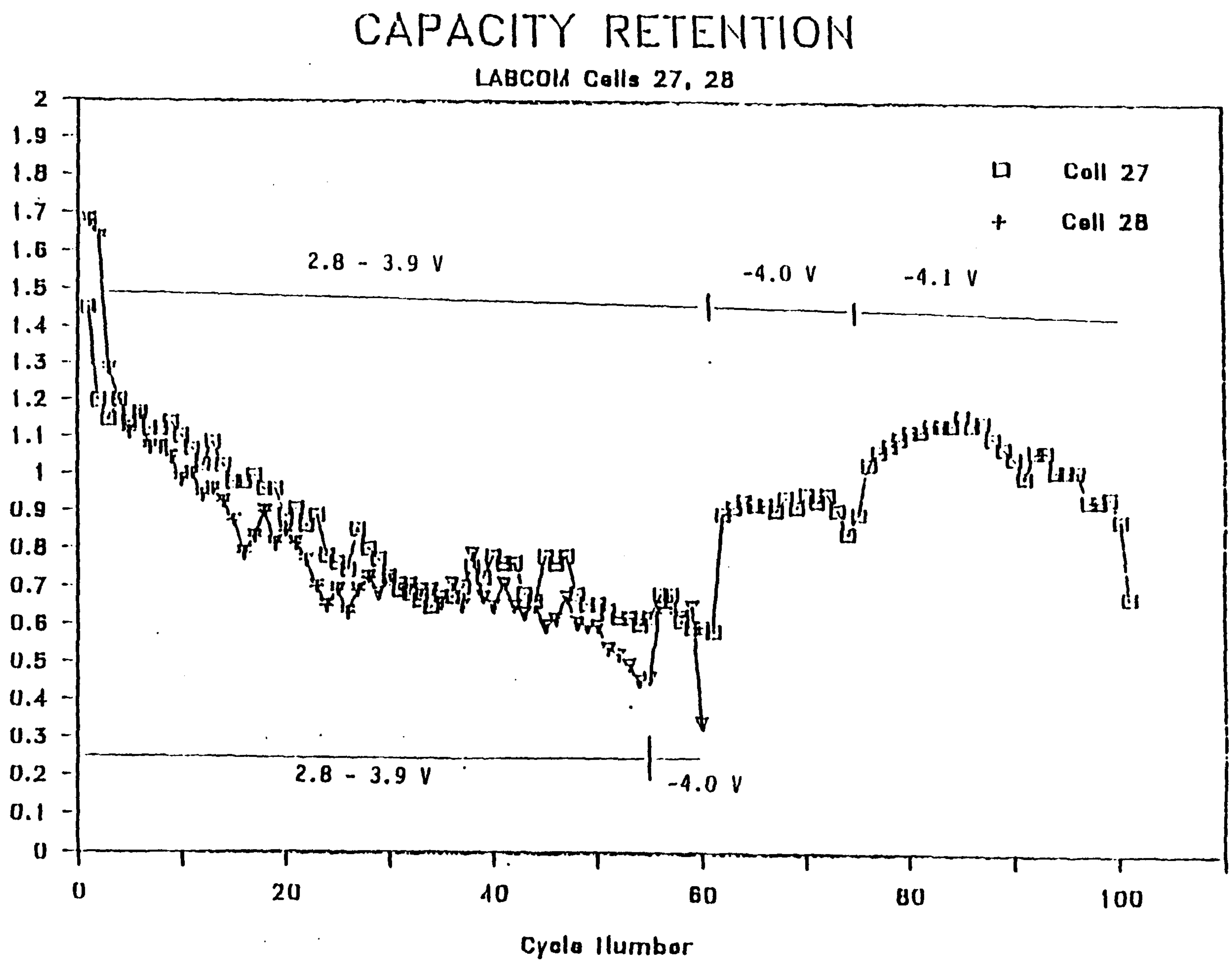

Capacity Utilization of Cathode with Number of Cycles for $Li/LiAlCl_4 \cdot 6\ SO_2/C$ (#27) and $LiAlCl_4 \cdot 3\ SO_2$ (#28) Cells at 1.0 mA/cm^2 Discharge Rate. Cathode Area: 25 cm^2; Weight: 0.17 gm

Figure 30

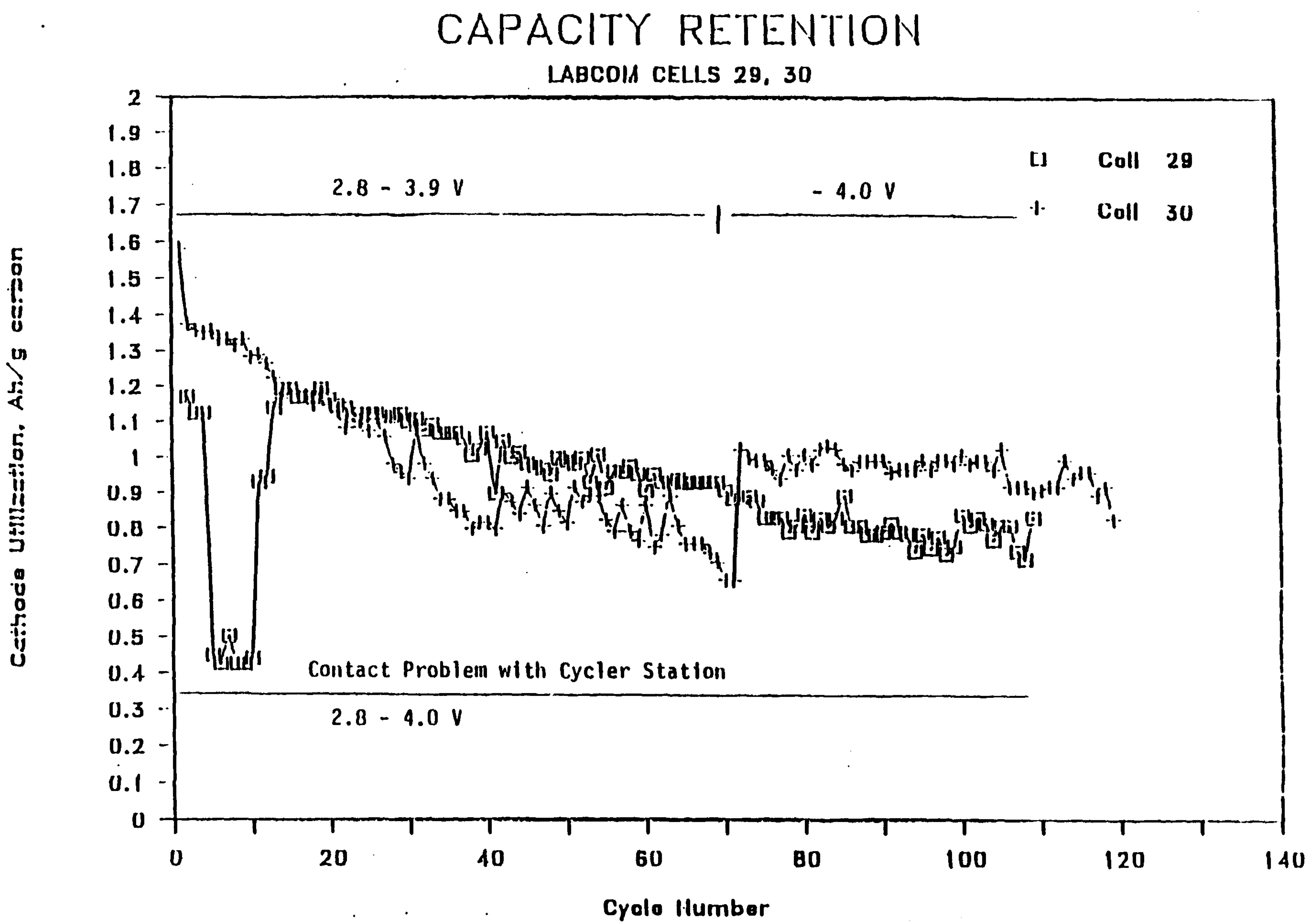

Capacity Utilization of Cathode with Number of Cycles for $Li/LiAlCl_4 \cdot 6\,SO_2/C$ at 1.0 mA/cm^2 Discharge Rate.
Cathode Area: 25 cm^2; Weight: ~ 0.13 gm

Figure 31

regeneration of discharge product with the liberated chlorine at higher voltage, or (iii) the electroreduction of chlorine.

Cell 29 was operating within the voltage limits of 2.8 to 4.0V. The cell achieved a capacity of 1.17 Ah/g of carbon for the second cycle and 0.83 Ah/g for the 109th cycle (see Figure 31). The capacity loss was 29 percent. The initial voltage limits of Cell 30 were 2.8 to 3.9V. Though this cell showed a good capacity value of 1.38 Ah/g for the second cycle, the capacity dropped fairly rapidly to a value of 0.66 Ah/g after completion of only 71 cycles. The capacity loss was about 52 percent. The increase in upper limit to 4.0V caused an increase in capacity to 1.00 Ah/g which corresponds to a capacity loss of about 28 percent compared to second cycle. The cell almost retained this capacity for another 38 cycles.

It is evident from the above experimental results that additional capacity may be achieved by extending the upper voltage limit. But continuous operation of cells at higher voltage limit may degrade solvent or cell components. The selection of electrochemical voltage limits is, therefore, critical in obtaining good capacity and cycle life.

The failure mode analysis of some of the cells were carried out by postmortem observations of cell components, e.g. electrolyte, separator, cathode and anode, and by examination of polarization data. Our observations indicated a common feature of cycled cells was the adhesion and partial incorporation of the separator material (both glass and Tefzel) into the passive film covering the anode.

<u>Test Group 7</u>

The cycling performance of Ketjen Black cathodes in $LiAlCl_4 \cdot 3SO_2$ electrolyte has been examined with a discharge

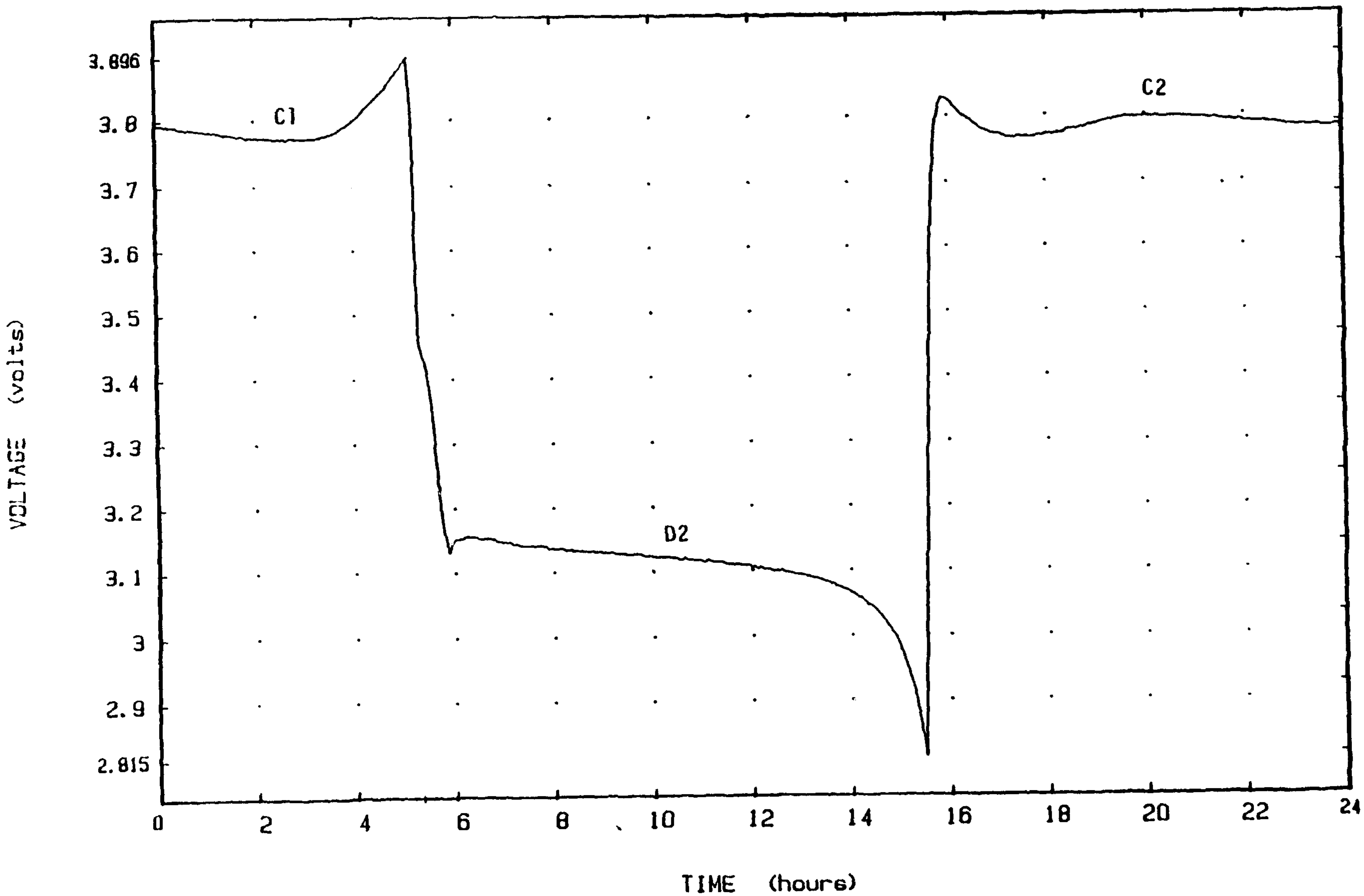

Figure 32: Cycling Behavior of Li/C Cell No. 28 in $LiAlCl_4 \cdot 3SO_2$ Electrolyte with 1.0 mA/cm^2 Discharge and Charge. Cathode and Anode Area: 25 cm^2.

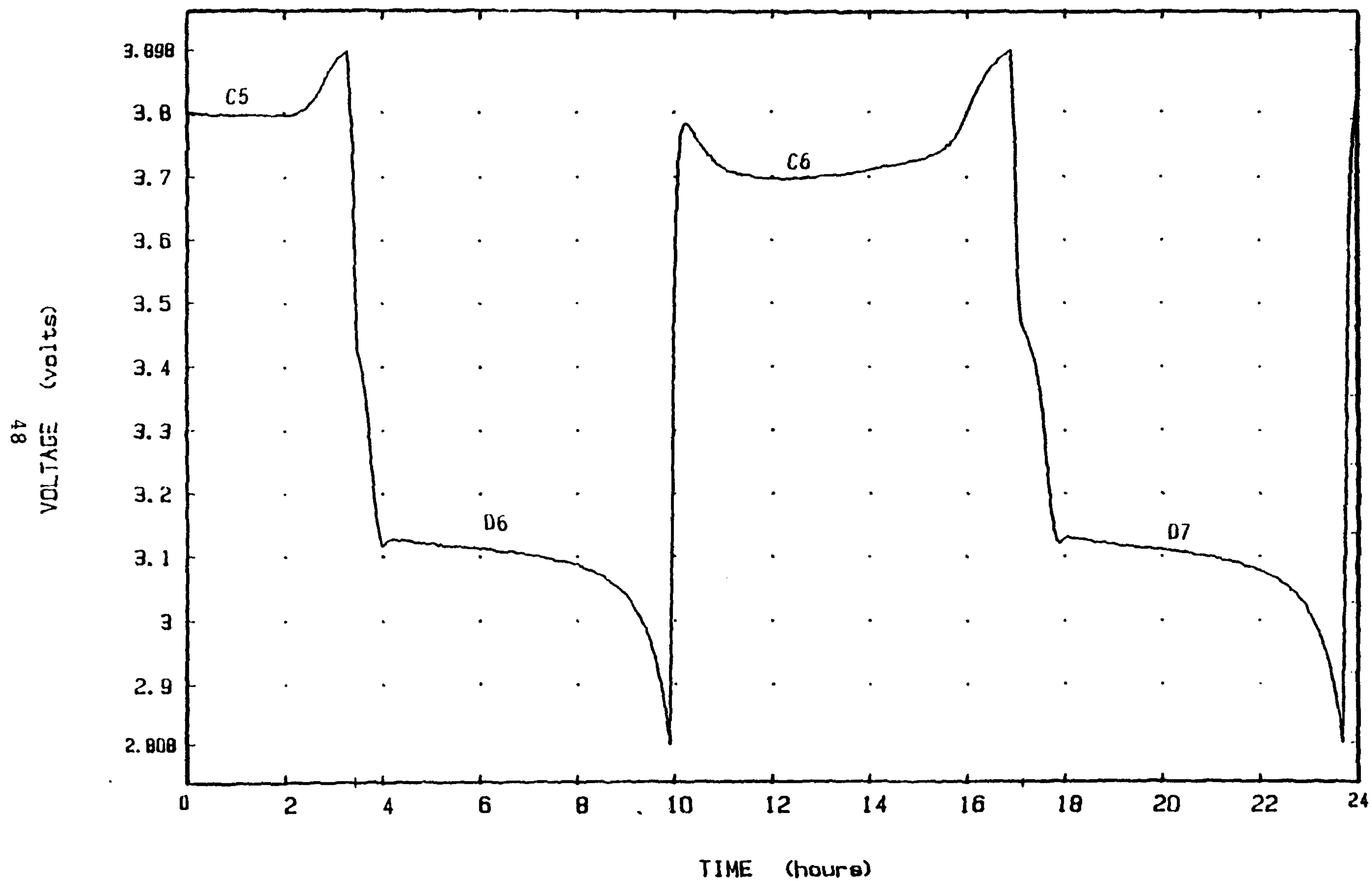

Figure 33: Cycling Behavior of Li/C Cell No. 28 in $LiAlCl_4 \cdot 3SO_2$ Electrolyte with 1.0 mA/cm^2 Discharge and Charge. Cathode and Anode Area: 25 cm^2.

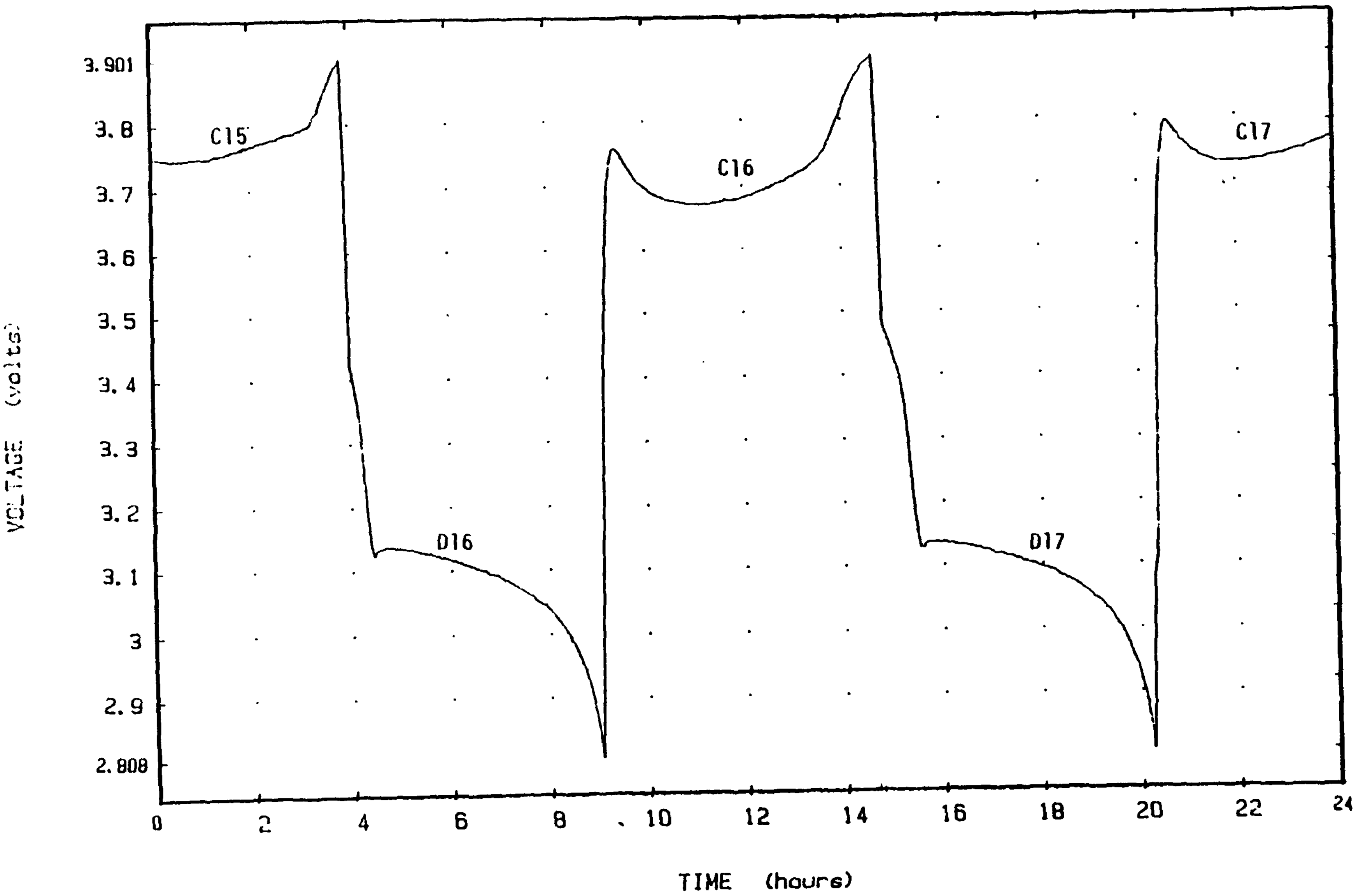

Figure 34: Cycling Behavior of Li/C Cell No. 28 in $LiAlCl_4 \cdot SO_2$ Electrolyte with 1.0 mA/cm^2 Discharge and Charge. Cathode and Anode Area: 25 cm^2.

limit equivalent to 100 mAh/ml of carbon. Before internal shorting, one of the cells achieved 98 cycles without significant capacity loss. The investigation of KB cathode in $LiAlCl_4 \cdot 3SO_2$ electrolyte has been extended to a full depth of discharge. Discharge was limited to a cutoff of 2.8V. Cells 21 and 22 completed two and three cycles before showing inability to accept charge with the second cycle capacity of 1.15 and 1.17 Ah/g of carbon. The voltage profiles of Cell 28 are shown in Figures 31-37 for some typical cycles. The charge/discharge characteristics are similar to those observed with other cells in $LiAlCl_4 \cdot 6SO_2$ electrolyte. Cell 28 was constructed with dendrite getters incorporated within the interelectrode separator. It has been found, from a different project, that the use of dendrite getter helps to prevent dendrite shorting. The cycling performance of Cells 28 and 27 (which also contained dendrite getter) in $LiAlCl_4 \cdot 3SO_2$ and $LiAlCl_4 \cdot 6SO_2$ electrolytes are shown in Figures 29 and 30. These cells showed a capacity value of 1.64 and 1.20 Ah/g of carbon for the second cycles which rapidly dropped to 0.73 and 0.80 Ah/g of carbon for the 28th cycle only. This provided no favorable effect on capacity retention.

It is evident from our results as well as others[2,3] that Ketjen Black carbon shows much better performance in $LiAlCl_4/SO_2$ electrolyte than the lower surface area Shawinigan Black carbon. From a study of different carbon and graphite materials, the Duracell group[1] concluded that the improved performance demonstrated by KB in $LiAlCl_4/SO_2$ was related to its high surface area and pore volume. They also suggested the formation of a complex between the aromatic structure of carbon and electrolyte and involvement of this complex as a redox-couple in the charge/discharge mechanism. Our results of KB cathode in $LiAlCl_4 \cdot 6SO_2$ and $LiAlCl_4 \cdot 3SO_2$ electrolytes support their proposed mechanism. Higher OCV (≈3.33V vs Li), discharge (≈3.1V), and charge potentials (≈3.7V) indicate that redox couple is involved which is different from $SO_2/S_2O_4^=$ (the reduction potential of SO_2 on carbon is about 2.9V vs Li in primary cells).

Table 5 shows the surface area, pore volume and sulfur content of Ketjen Black and Shawinigan Black carbons. KB and SAB not only differ significantly with respect to their surface area and pore volume but also to their sulfur content. One of our task objectives was to examine the effect of sulfur-content in carbon on cathode performance. Cathodes made with the carbon blacks were treated with $SOCl_2$ at 240°C. It was believed that this $SOCl_2$ treatment might increase the sulfur content of the cathode. Cells 16 and 31 were made with the $SOCl_2$ treated SAB and KB as described under Test Group 5, respectively. After first cycle, both of these cells were unable to continue cycling. Their first cycle capacities were also significantly lower than the capacity obtained for untreated cathodes. Thus the $SOCl_2$ treatment actually appears to have destroyed rather than enhanced active sites on the surface of the carbon.

Table 5: Comparison of Surface Area, Pore Volume and Sulfur Content of Shawinigan and Ketjen Black Carbons

Carbon	Surface Area[(a)] m^2/g	Pore Volume[(b)] cc/100 gm	Wt % of S[a]
Shawinigan Black	55	250	0.001
Ketjen Black	1000	360	4.310

(a) Yardney unpublished data
(b) Duracell Data[1]

Cells 20-23, 28 and 31 were activated with the $LiAlCl_4 \cdot 3SO_2$ electrolyte and used KB cathodes. Cells 20 and 23 suffered from shorts and had to be discarded. Cells 21 and 22 would not accept a charge, although they achieved good first cycling capacity. Cell 28 achieved 60 cycles although we believe that the electrolyte fill was probably low. Cell 31 which contained a KB cathode heat-treatment with $SOCl_2$ achieved below average first cycle capacity and could not be charged. Thus the heat treatment destroyed the cathode's ability to cycle between the limits of 2.8 - 3.9 volts.

Test Group 8

Test Groups 1-7 contained laboratory cells with one microporous Tefzel separator. We observed evidence that the material was adhering to the anode face after extensive cycling and the direct contact with metallic lithium may have contributed to this chemical degradation of the Tefzel. With Test group 8, we began using one sheet of Crane .005" non-woven glass paper between the anode and the Tefzel membrane. This combined with the KB cathode and $LiAlCl_4 \cdot 6SO_2$ electrolyte gave us substantially improved cycle life.

With the new cell configuration, twelve experimental "D" cells were built with KB and high surface area (2000m^2/g) carbon felt cathodes. Performance of these cells is shown in Table 3.

Cells 32 and 33 were tested to evaluate the cycle life and discharge capacity at 0°C and -2.5°C respectively. The discharge and charge rates were 1 mA/cm^2 and 0.5 mA/cm^2. The voltage profile of Cell 33 for different charge-discharge cycles are shown in Figure 38. The cell lost about 35% of its capacity after 60 cycles and 60% after 124 cycles. The capacity retention for the discharge cycles of Cells 32 and 33 are shown in Figures 39 and 40, respectively. Both the cells, as expected, showed significantly lower capacity than those operating at room temperature. Cells 32 and 33 delivered 146 and 126 cycles,

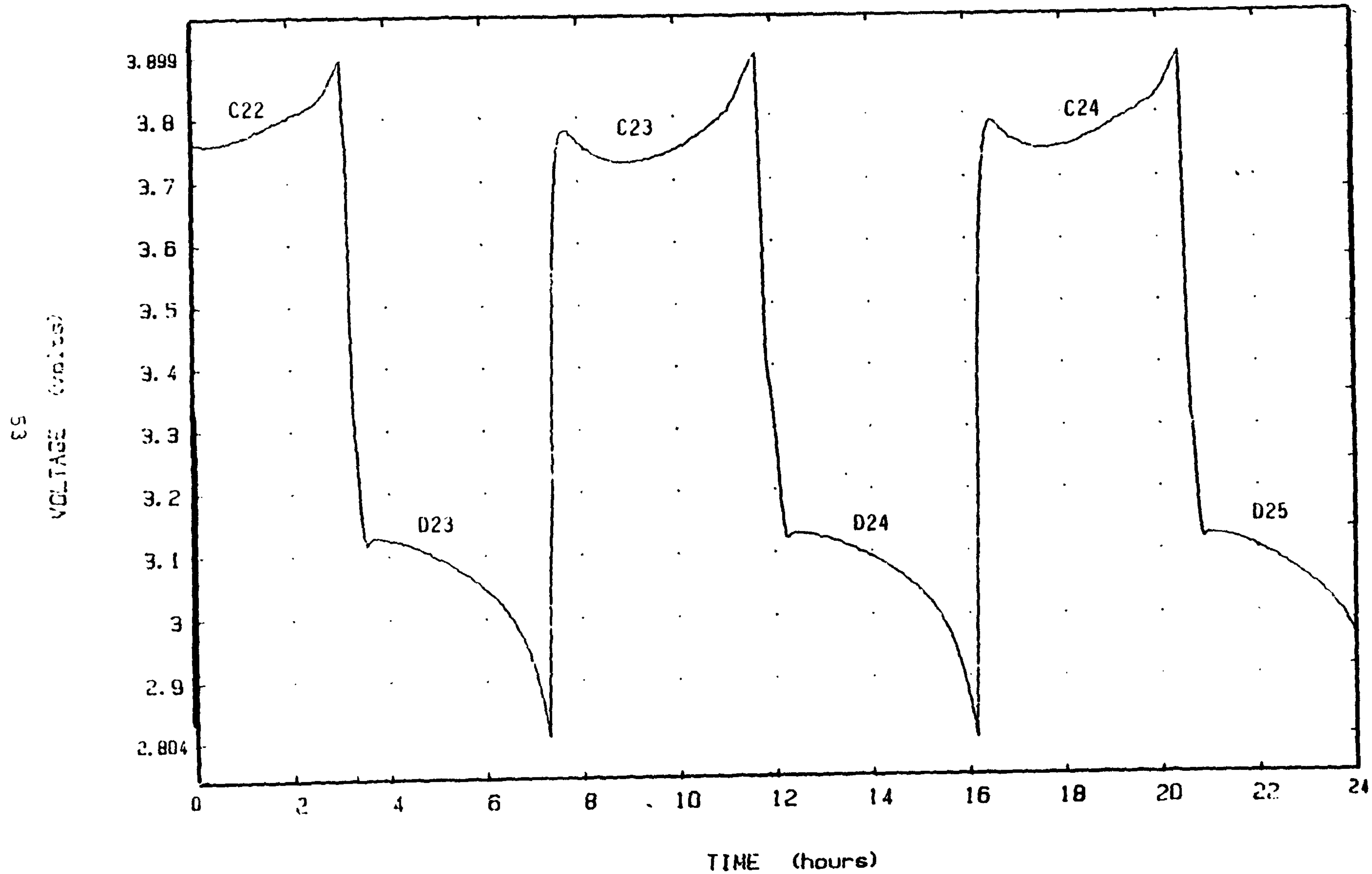

Figure 35: Cycling Behavior of Li/C Cell No. 28 in $LiAlCl_4 \cdot 3SO_2$ Electrolyte with 1.0 mA/cm^2 Discharge and Charge. Cathode and Anode Area: 25 cm^2.

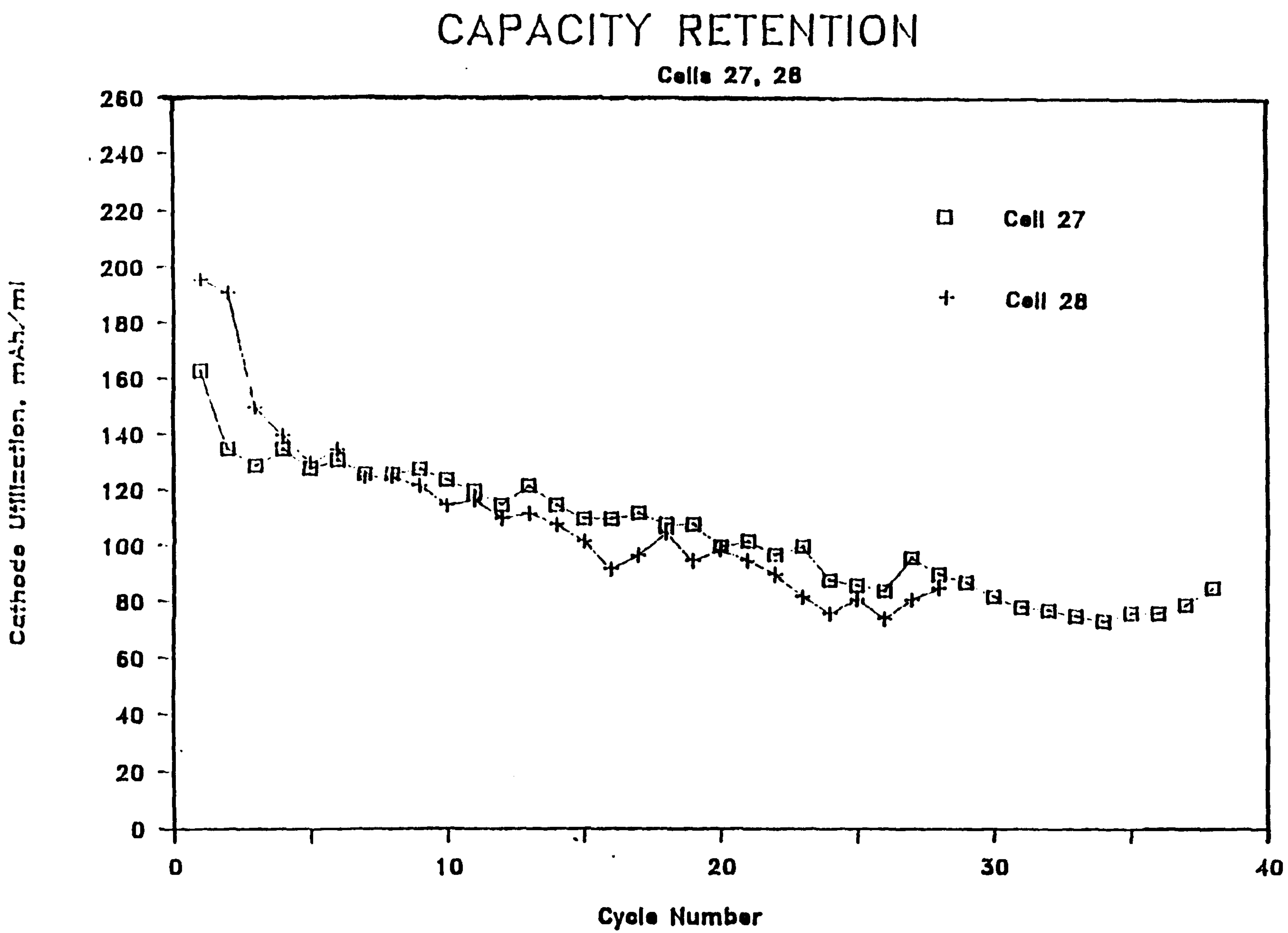

Figure 36: Volumetric Capacity Utilization of Cathode with Number of Cycles for $Li/LiAlCl_4 \cdot 6SO_2/C$ (#27) and $Li/LiAlCl_4 \cdot 3SO_2/C$ (#28) Cells at 1.0 mA/cm² Discharge Rate. Cathode Thickness: ~0.027"; Area: 25 cm².

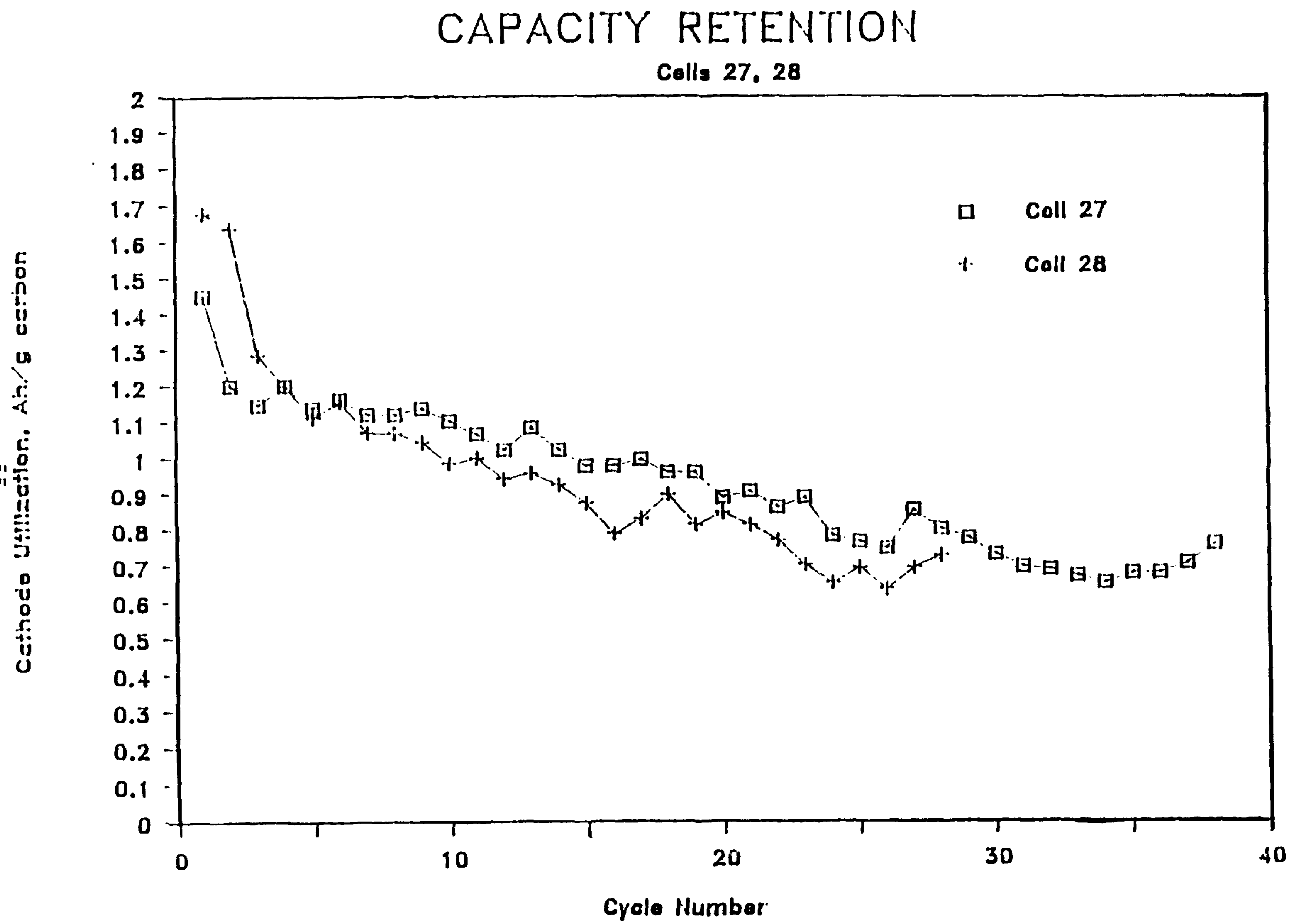

Figure 37: Graviometric Capacity Utilization of Cathode iwth Number of Cycles for $Li/LiAlCl_4 \cdot 6SO_2/C$ (#27) and $Li/LiAlCl_4 \cdot 3SO_2/C$ (#28) Cells at 1.0 mA/cm^2 Discharge Rate. Weight of Cathode: 0.17 gm; Area: 25 cm^2.

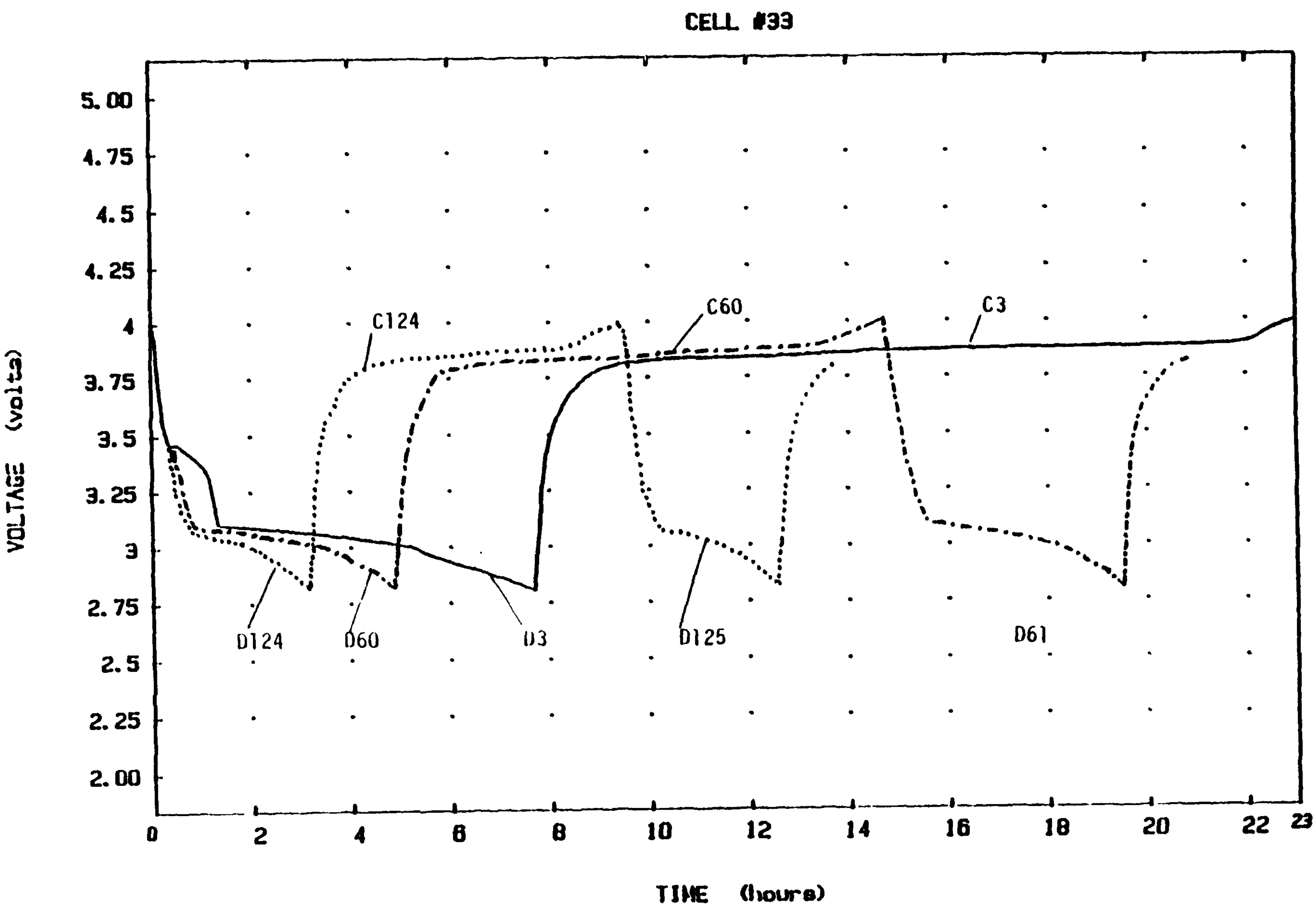

Figure 38: Discharge-Charge Behavior of Li/C Cell (#33) in $LiAlCl_4 \cdot 6SO_2$ Electrolyte with 1.0 mA/cm^2 Discharge and 0.5 mA/cm^2 Charge Rates at -2.5°C. Cathode and Anode Area: 25 cm^2.

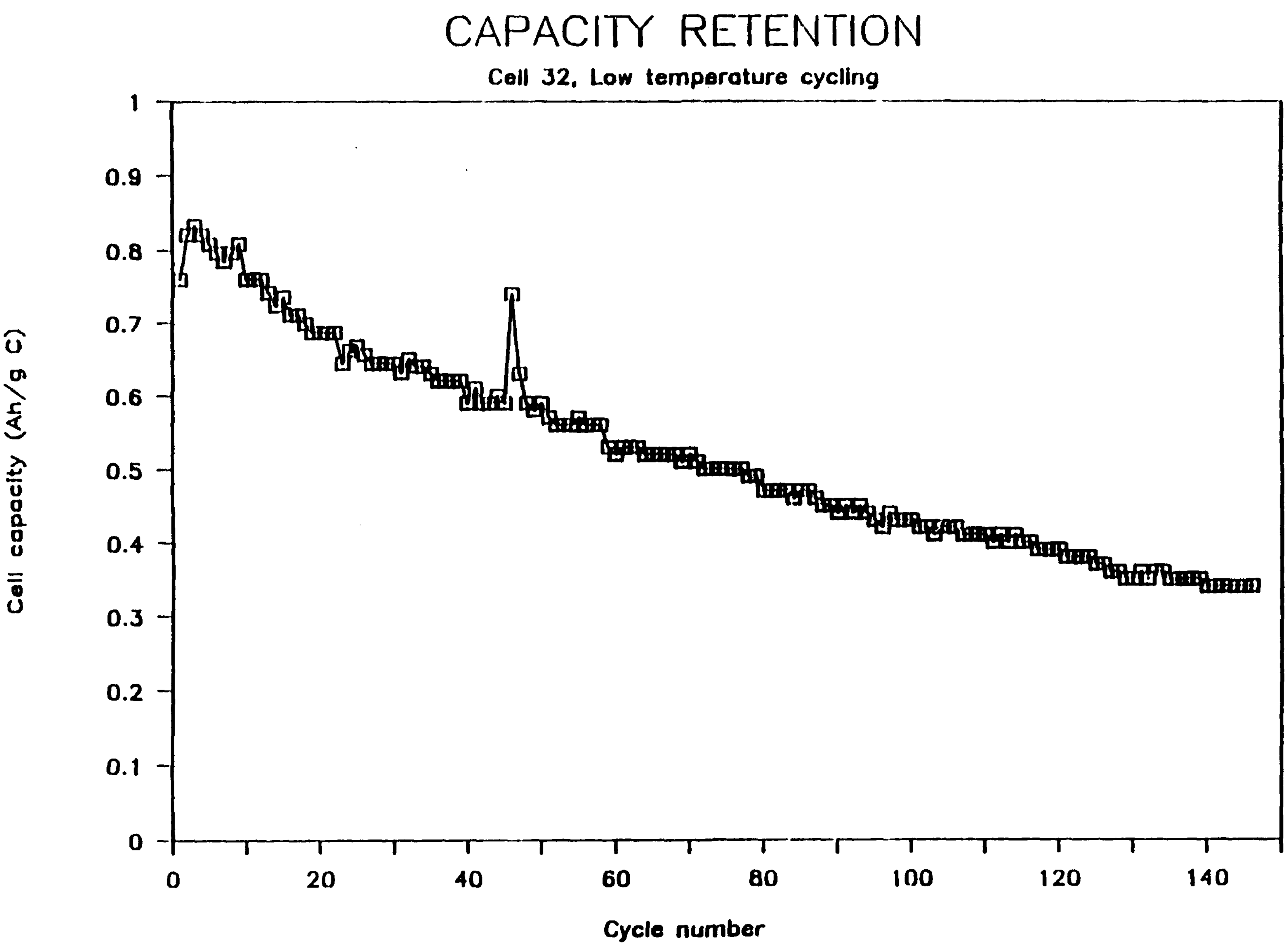

Figure 39: Capacity *vs.* Cycle Number of a $Li/LiAlCl_4.6SO_2/C$ Cell (#32) at 0°C with 1 mA/cm^2 Discharge and 0.5 mA/cm^2 Charge Rates. Voltage Limits: 2.8-4.0 V. Weight of Cathode: 0.225 g; Area: 25 cm^2.

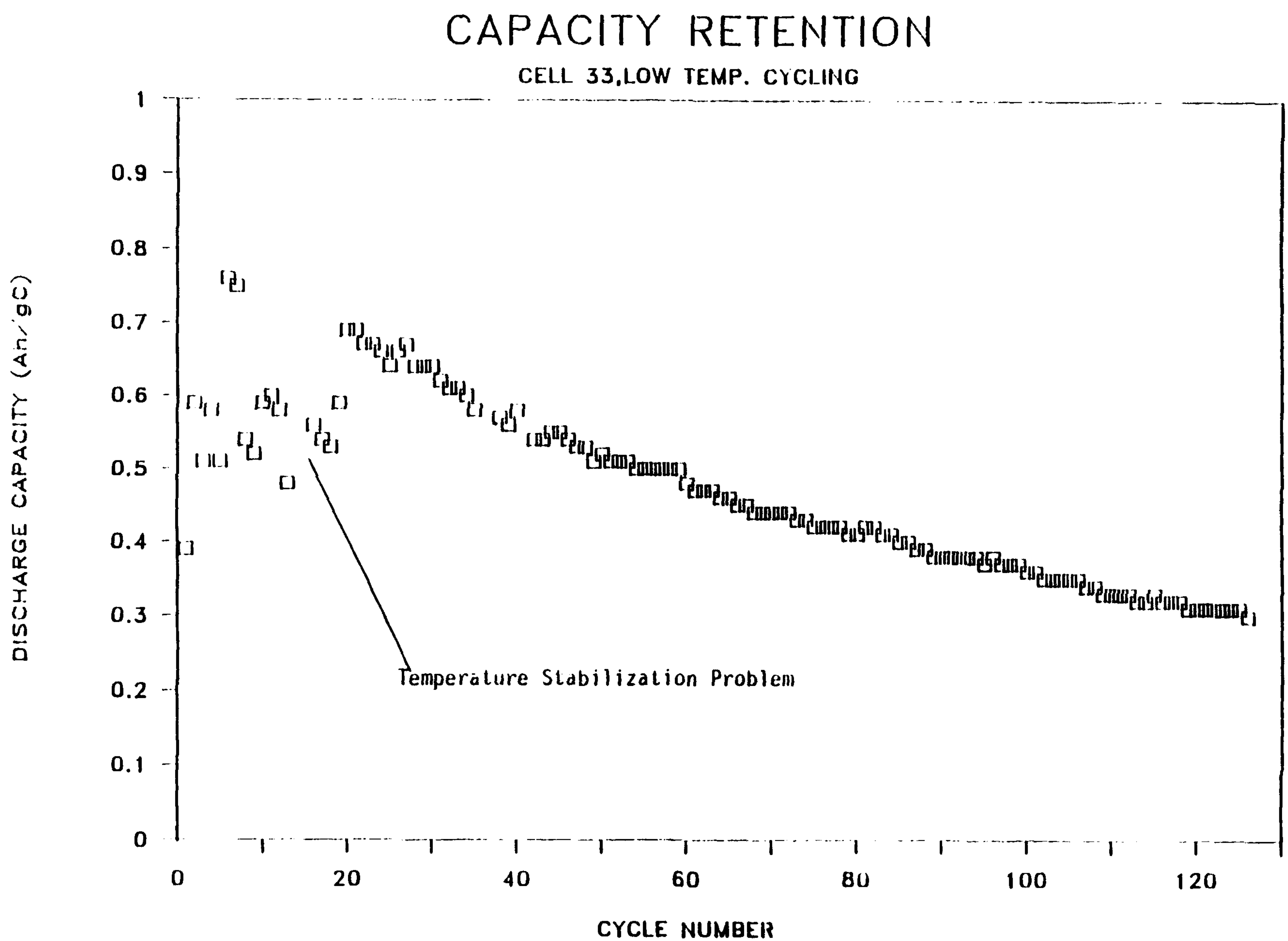

Figure 40: The Cycling Performance of a $Li/LiAlCl_4.6SO_2$/KB Cell (#33) at -2.5°C with 1.0 mA/cm^2 Discharge and 0.5 mA/cm^2 Charge Rates. Voltage Limits: 2.8-4.0 V. Weight of Cathode: 0.271 gm; Area: 25 cm^2.

respectively, and after that were terminated intentionally to examine the cathodes and anodes.

Figure 41 shows the cycling behavior of Cell 34 for the third and 77th cycles. The cell was operating at room temperature with 5 mA/cm^2 discharge and 1 mA/cm^2 charge rates in the voltage limits of 2.8 - 4.0V vs Li. The average operating discharge voltage, at which approximately 90% of the capacity was obtained, was 3.075V for the 3rd cycle and 3.00V for the 77th cycle. The cell after delivering 161 cycles was suspended intentionally to examine the capacity retention and voltage delay after storage for several months.

The capacity retention of discharge cycles is shown in Figure 42. The cell achieved a capacity of 1.22 Ah/g of carbon for the 2nd cycle and 0.84Ah/g for the 50th cycle which corresponds to 31% capacity loss. Though the cell lost about 68% capacity after 160 cycles, the capacity value (0.39 Ah/g) is almost the same as that reported (0.4 Ah/g) in the literature[2] for the first few cycles.

It has been observed that the cycle life and discharge capacity of Li/SO_2 cells depends primarily on the surface area and pore volume of the cathode materials. We, therefore, tested three Li/SO_2 cells, 35, 36 and 37, made with high surface area (2000 m^2/g) carbon felt cathode. These cells showed very poor capacity ($\approx$0.20 Ah/g) and were unable to continue cycling after a couple of cycles. One possible reason of poor cycling performance may have been the formation of resistive networks by electrolyte solution in between the interphase of carbon felt and the substrate (the cathodes were made by placing rather than pressing carbon felt on the Ni-substrate). This material represents the lowest density of carbon cathode evaluated.

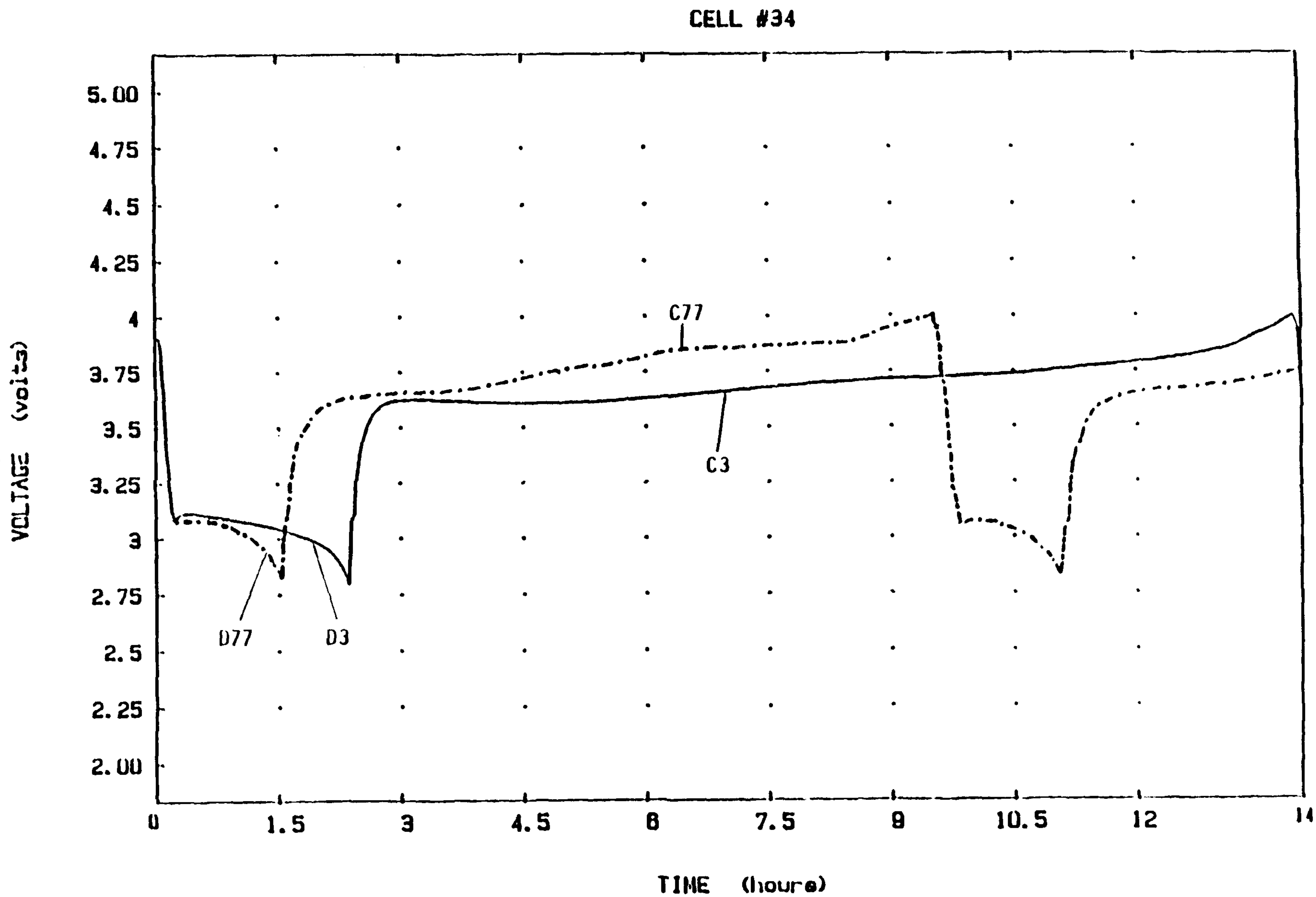

Figure 41: Discharge-Charge Behavior of a $Li/LiAlCl_4.6SO_2/C$ Cell (#34) at 5 mA/cm^2 Discharge and 1 mA/cm^2 Charge Rates. Electrodes Area: 25 cm^2; Voltage Limits: 2.8-4.0 V.

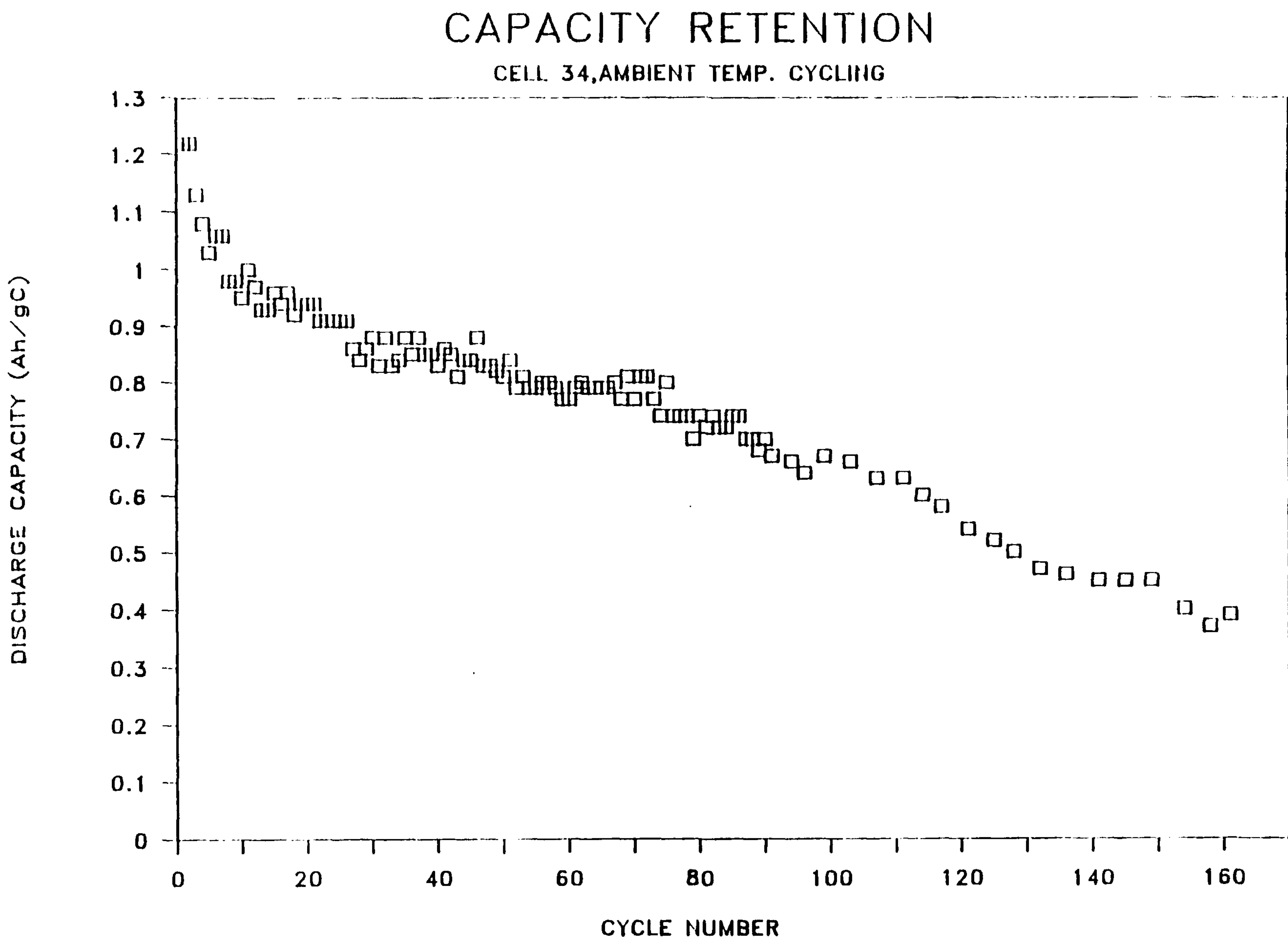

Figure 42: Discharged Capacity *vs.* Cycle Number of a $Li/LiAlCl_4.6SO_2/C$ Cell (#34) at 5 mA/cm^2 and Charged at 1 mA/cm^2. Voltage Limits: 2.8-4.0 V; Electrodes Area: 25 cm^2; Weight: 0.279 g.

Cells 38 and 39 were operating at 1 mA/cm^2 charge and discharge rates. The voltage limits of Cell 38 were 3.0 - 4.0V. A comparison of discharge-charge behavior for cycles Nos. 2, 75 and 166 is shown in Figures 43 and 44. The cell lost almost 50% capacity after 75 cycles and 72% capacity after 166 cycles. The operating voltage of Cell 39 was 2.8 - 4.0V. The cell was cycling within the time limits (12 hours discharge and 12 hours charge) up to 50 cycles with a capacity of 0.94 Ah/g and then within the voltage limits with diminished capacity until vented near the end of 111 charge cycles.

Cells 40 and 41 were cycling at 2 mA/cm^2 discharge and 1 mA/cm^2 charge rates. The voltage limits of Cell 40 were 3.0 - 4.0V. After successful completion of 216 cycles, the cell was suspended from cycling intentionally to examine the cathodes and anodes. Cell 41, which was operating in the voltage limits of 2.8 - 4.0V, vented near the end of the 119th charge cycle. The venting of Cell 43, which was operating a 2 mA/cm^2 discharge and charges rates within the voltage limits of 2.8 - 4.0V, also occurred near the end of charge cycle (101 cycles).

The venting of Cells 39,41 and 43 occurred on charge at the region of can wall where the anode was exposed to the wall through the porous Tefzel separator. Needle-like lithium dendrites formed during charge at the anode probably penetrated the porous separator and thus caused shorting with the case positive can. Resulting heat corroded the metal. We also suspect that the can may have become involved in electrolysis, dissolving when the cathode overpotential became to great for proper charging. These problems of shorting and corrosion can be avoided by placing a nonporous Tefzel sheet around the wall of the can.

Another important observation is that the lower voltage

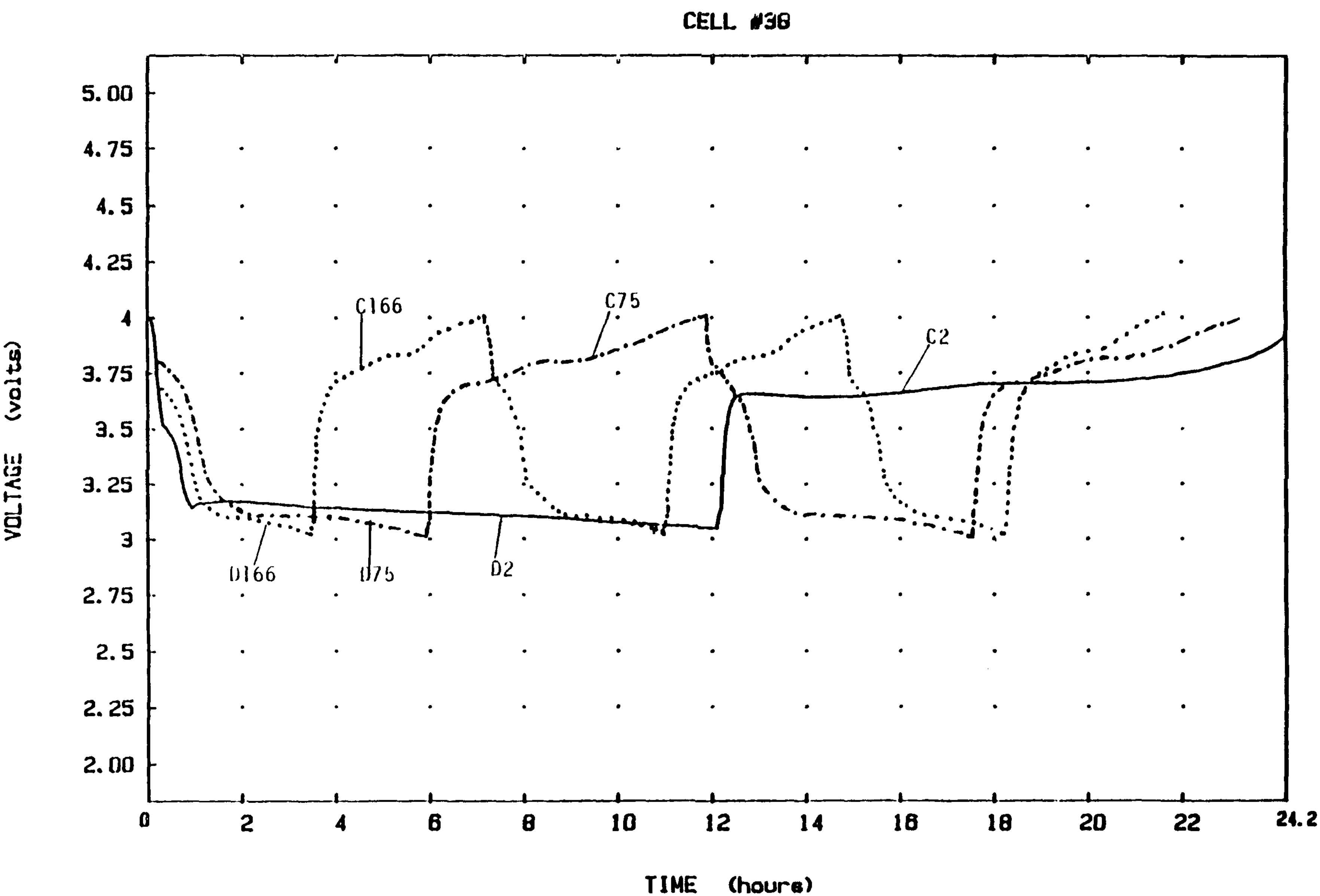

Figure 43: Discharge-Charge Behavior of Li/C Cell (#38) in $LiAlCl_4 \cdot 6SO_2$ Electrolyte at 1.0 mA/cm^2 Discharge and Charge Rates. Cathode and Anode Area: 25 cm^2

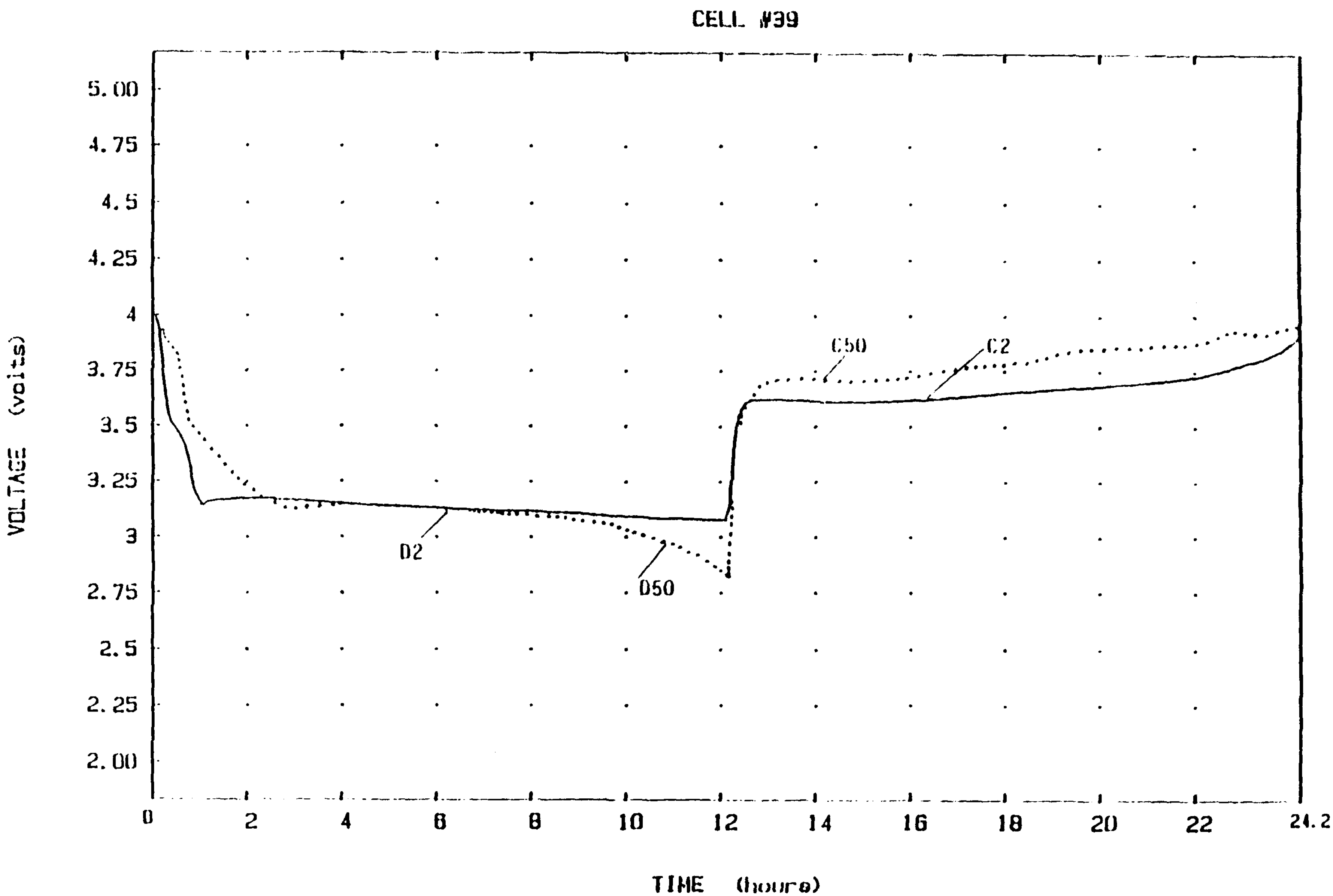

Figure 44: Discharge-Charge Behavior of Li/C Cell (#39) in $LiAlCl_4.6SO_2$ at 1.0 mA/cm^2 Discharge and Charge Rates. Voltage Limits: 2.8-4.0 V. Time Limits: 12 Hours. Cathode and Anode Area: 25 cm2

limits of all the three vented cells was 2.8V. At this voltage region, SO_2 might reduce to form lithium dithionite as the discharge product. Lithium dithionite is known to be hazardous material and believed to be involved actively in the process of cell venting and/or explosion.

Cell 42 was cycling initially at 2 mA/cm^2 discharge and charge rates within the voltage limits of 3.0 - 4.0V. The cell delivered a capacity of 0.92 Ah/g of carbon for the 2nd cycle and 0.31 Ah/g for the 102nd cycle corresponding to a capacity loss of 66%. The charge rate was then decreased to 1 mA/cm^2 which caused an increase in capacity from 0.31 Ah/g to 0.37 Ah/g. The cell delivered another 151 cycles and was terminated for analysis.

<u>Test Group 9</u>

Thirteen additional laboratory cells were prepared as in Test Group 8 for various tests. These are summarized in Table 3. Cells 47 and 51 were additional cells tested at low temperature and are discussed under the appropriate Sections.

CHEMICAL ANALYSIS

In order to distinguish between the desired discharge mechanism described by Duracell:

Anode $\quad Li \dashrightarrow Li^+ + e^-$

Cathode $\quad 3\ C + LiAlCl_4 + SO_2 \dashrightarrow$

$$LiClAl \left\langle \begin{matrix} OSO\text{-}C \\ OSO\text{-}C \\ OSO\text{-}C \end{matrix} \right. + Cl^- - 3e^-$$

and the undesired dithionite formation:

$$\text{Anode} \quad Li \longrightarrow Li^{+} + e^{-}$$

$$\text{Cathode} \quad 2SO_2 + 2e^{-} \longrightarrow S_2O_4^{=}$$

a colorimetric analytical method for dithionite formation was developed.

The use of liquid SO_2 based electrolytes and soluble catholytes has presented an important analytical challenge because of the complex chemistry of sulfur in its many oxidation states. SO_2 contained in salt solutions in lithium metal choride secondary cells can be irreversibly lost by reduction on deep discharge. The reduction and oxidation of SO_2 in Li/SO_2 secondary cells involves very concentrated solutions of SO_2 where molecular adducts (donor-acceptor complexes) such as $LiAlCl_4 \cdot 3SO_2$ play an important role. It has also been suggested that a surface complex involving carbon-oxygen bonds on the cathode are formed.

We have therefore spent some effort under our Independent Research and Development program to develop an analytical technique for the detection and semi-quantitative analysis of lithium dithionite, $Li_2S_2O_4$, the principal but irreversible reduction product in primary Li/SO_2 cells in the presence of other oxysulfur compounds.

The procedure involves the reaction of dithionite (also called hydrosulfite and hyposulfite) with ortho- or paradinitrobenzene in basic alcohol to produce soluble red nitroso-nitrobenzene,

$$S_2O_4{}^{2-} + H_2O \rightarrow NaHSO_2 + NHSO_3$$

$$NaHSO_2 + H_2O \rightarrow NaHSO_4 + 4H^o$$

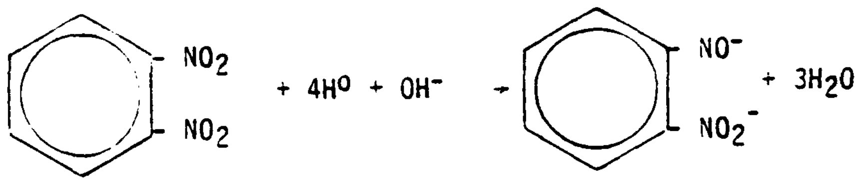

We have produced a rough Beer's law curve (Figure 45) using the absorbence at 400nm. Interference from the strong alcohol absorbence is an important limitation of the techniques's accuracy and we are currently evaluating alternate solvents with lower absorbence cutoffs.

LITHIUM CYCLING EFFICIENCY

A simple electrochemical cell was assembled with a 10 cm^2 lithium electrode, a 10 cm^2 stainless steel foil working electrode and activated with $LiAlCl_4 \cdot 3SO_2$ electrolyte. Lithium was plated onto the steel working electrode and then stripped at the same rate until cell polarization (indicating the complete stripping of the plated lithium). This was repeated at different current densities using a PAR model 173 galvanostat as a current source, a PAR model 179 coulometer to monitor capacities plated and stripped, and a Soltec 2 pen strip chart recorder to monitor cell voltage and capacities. Results are summarized in Table 6.

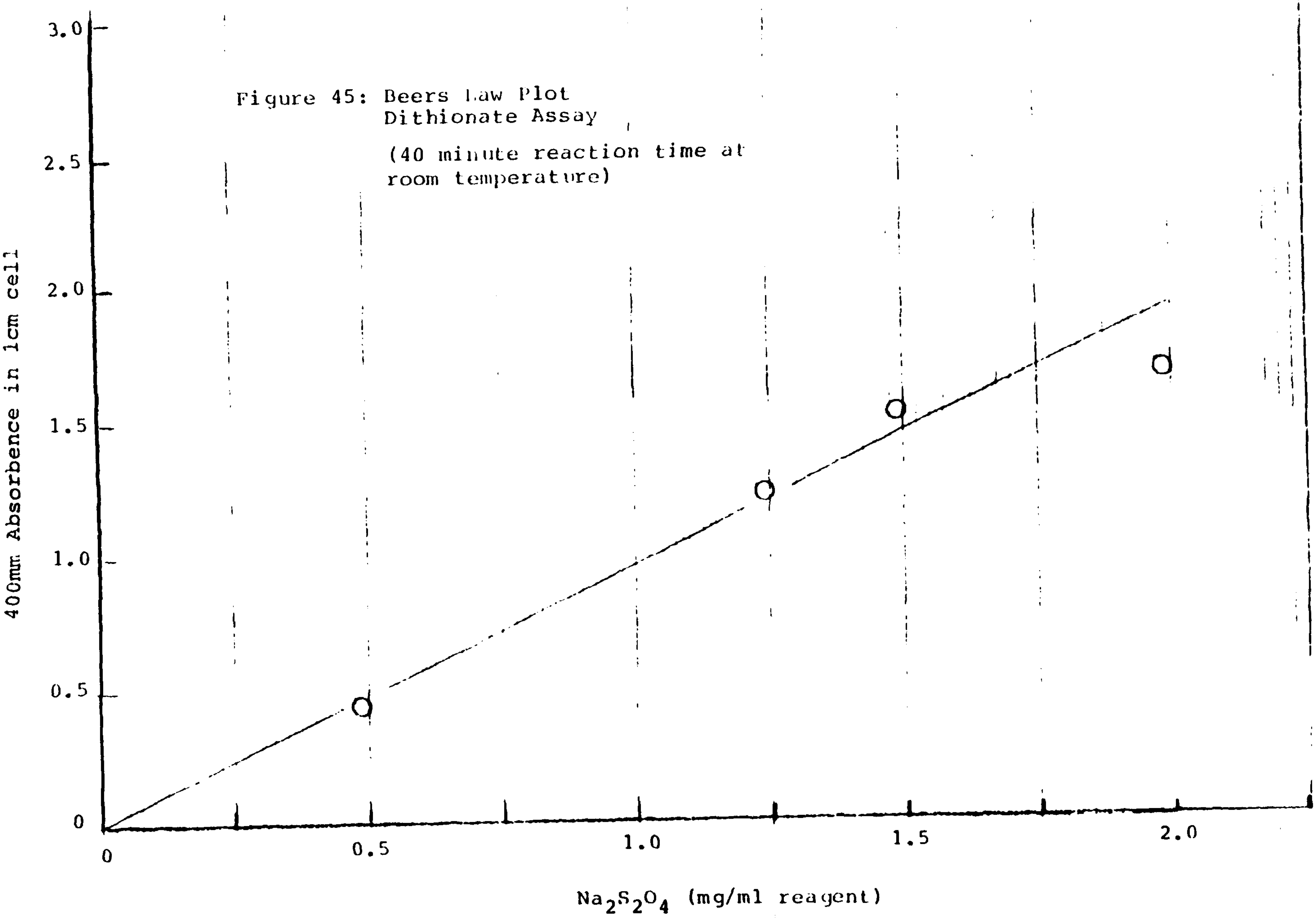

Figure 45: Beers Law Plot
Dithionate Assay
(40 minute reaction time at room temperature)

TABLE 6: Lithium Plating Efficiency

Rate (mA/cm2)		Capacity (C)		Avg. Efficiency $\bar{\xi}$ = 100 Cs/Cp	Cell Polarization
Plate	Strip	Plate	Strip	%	mV
1	1	15.00	8.70	58	30
2	2	15.11	9.76	65	50
5	5	15.01	12.94	86	100
10	10	14.98	13.17	88	150
20	20	17.34	7.54	44	290
5	5	37.51	32.22	86	-
1	1	7.502	5.1	68	-

The lithium plate was gray colored and slightly granular in texture in all cases. No dendrites were evident to the naked eye. Two trends can be seen in the results: efficiency increases with current density up to 10 mA/cm^2 and then decreases at higher rates.

The increases in average efficiency, $\bar{\xi}$, at higher rates can be explained by corrosion effects. At lower plate/strip rates the freshly plated lithium has more time to corrode in the electrolyte solution. The average lithium plating efficiency is defined as Cs/Cp, where Cs and Cp are the capacities of lithium stripped and plated respectively. The inefficiency is the capacity of lithium lost relative to the amount originally plated. That is:

$$\bar{\varphi} = 1 - \bar{\xi} = \frac{Cp-Cs}{Cp} = 1 - {}^{Cs}/Cp.$$

A linear relationship between the lithium cycling inefficiency and the time of the plate/strip experiment would indicate simple zero order kinetics of the corrosion reaction. Figure 46 shows that a more complex relationship exists.

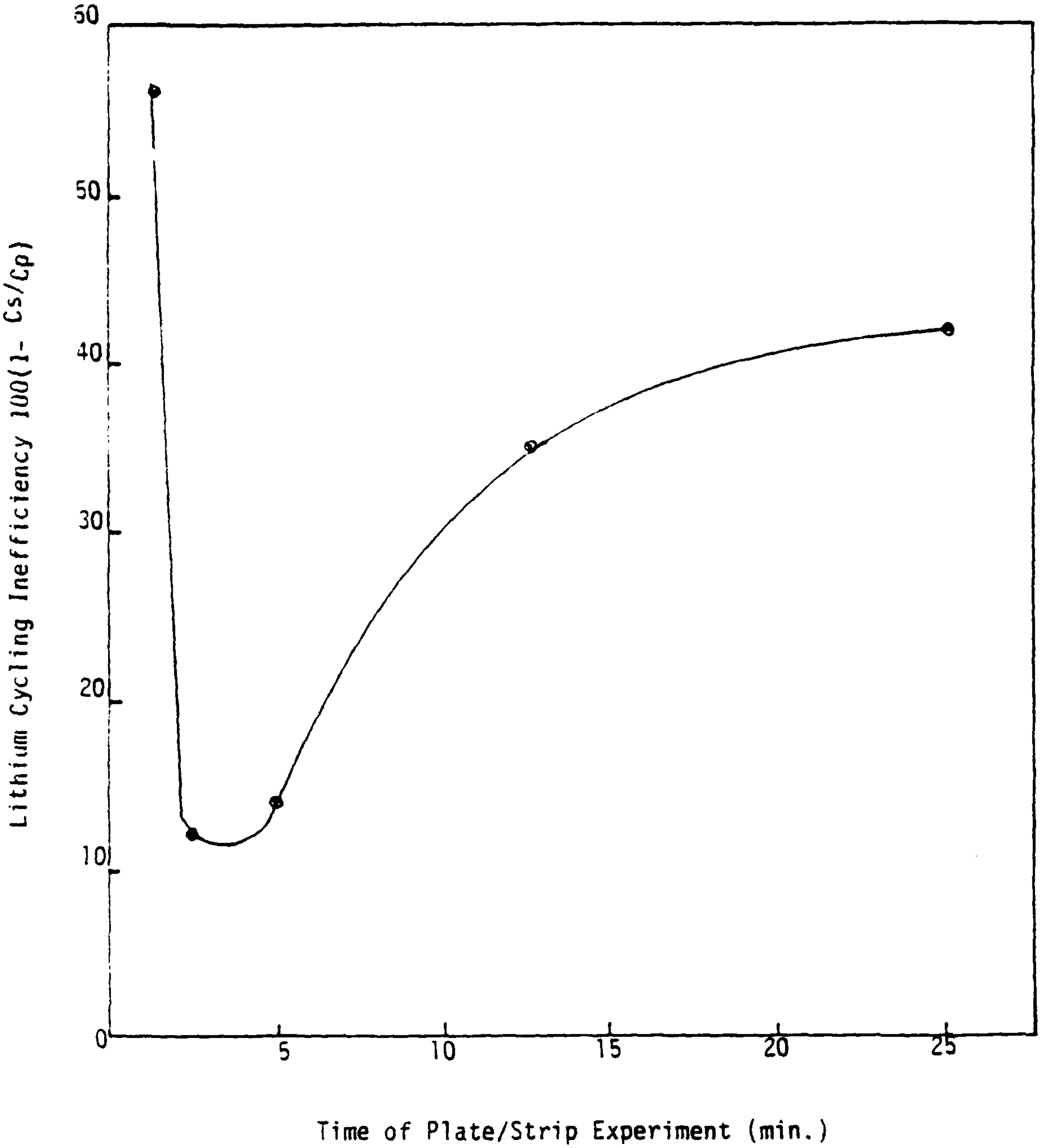

Figure 46: Lithium Cycling Efficiency

STORAGE CAPACITY AND VOLTAGE DELAY

After completion of 161 cycles at 5 mA/cm^2 discharge and 1 mA/cm^2 charge rates, the Li/SO_2 experimental cell no. 34 was stored in the charged state (charged to 4.0V) at room temperature for 120 days. The voltage delay and capacity retention behavior of the cell was examined at 5 mA/cm^2 discharge rate. No voltage delay was observed as shown in Figure 4. The cell was also able to retain the same capacity as observed before storage.

HIGH RATE PULSE DISCHARGE

A fresh experimental Li/SO_2 cell was discharged at 3.2 mA/cm^2 (total 80 mA) to a cut-off voltage of 2.75V. The cell achieved a capacity of 1.41 Ah/g of carbon. The cell was then charged at 1.2 mA/cm^2 to 4.0V, left at OCV for three hours, and then discharged at room temperature by applying a pulse of 0.5 Ampere (20 mA/cm^2) for 20 seconds with 180 seconds rest period. This sequence of pulse was repeated continuously until the cell reached a terminal voltage of 2.5V (the cell achieved 69 pulses). A portion of the pulse discharge behavior is shown in Figure 48. After the high rate discharge cut-off, the cell was drained at 3.2 mA/cm^2 to 2.75V to determine the residual capacity (Figure 49). The cell delivered a total capacity of 1.44 Ah/g of carbon of which 0.80 Ah/g was the pulse capacity and 0.64 Ah/g was residual capacity.

The cell was then charged at 1.2 mA/cm^2 to 4.0V and discharged at 3.2 mA/cm^2 to 2.75V to examine the cycling performance (Figure 50).

LOW TEMPERATURE DISCHARGE

Discharge at -20°C A fresh experimental Li/SO_2 cell (Laboratory cell 51) was discharged at 3.2 mA/cm^2 (total 80 mA) to a cut-off voltage of 2.75V to determine the discharge

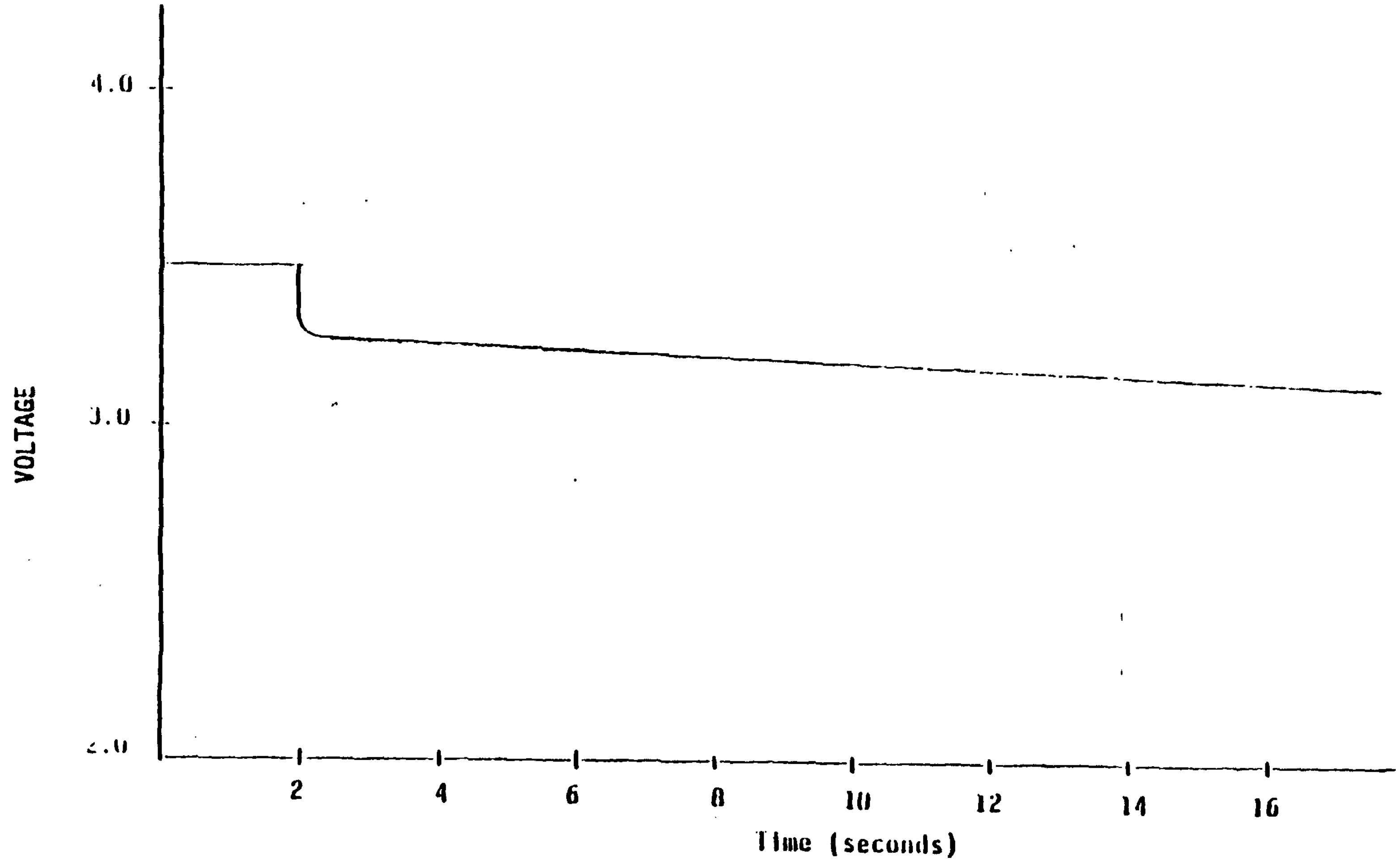

Figure 47: Discharge Behavior of $Li/LiAlCl_4 \cdot 6SO_2$ Cells at 3.2 mA/cm^2 After Delivering 161 Cycles at 5 mA/cm^2 Discharge and 1 mA/cm^2 Charge Rates Within the Voltage Limits of 2.8-4.0 V and Then Storage for Four Months at Room Temperature.

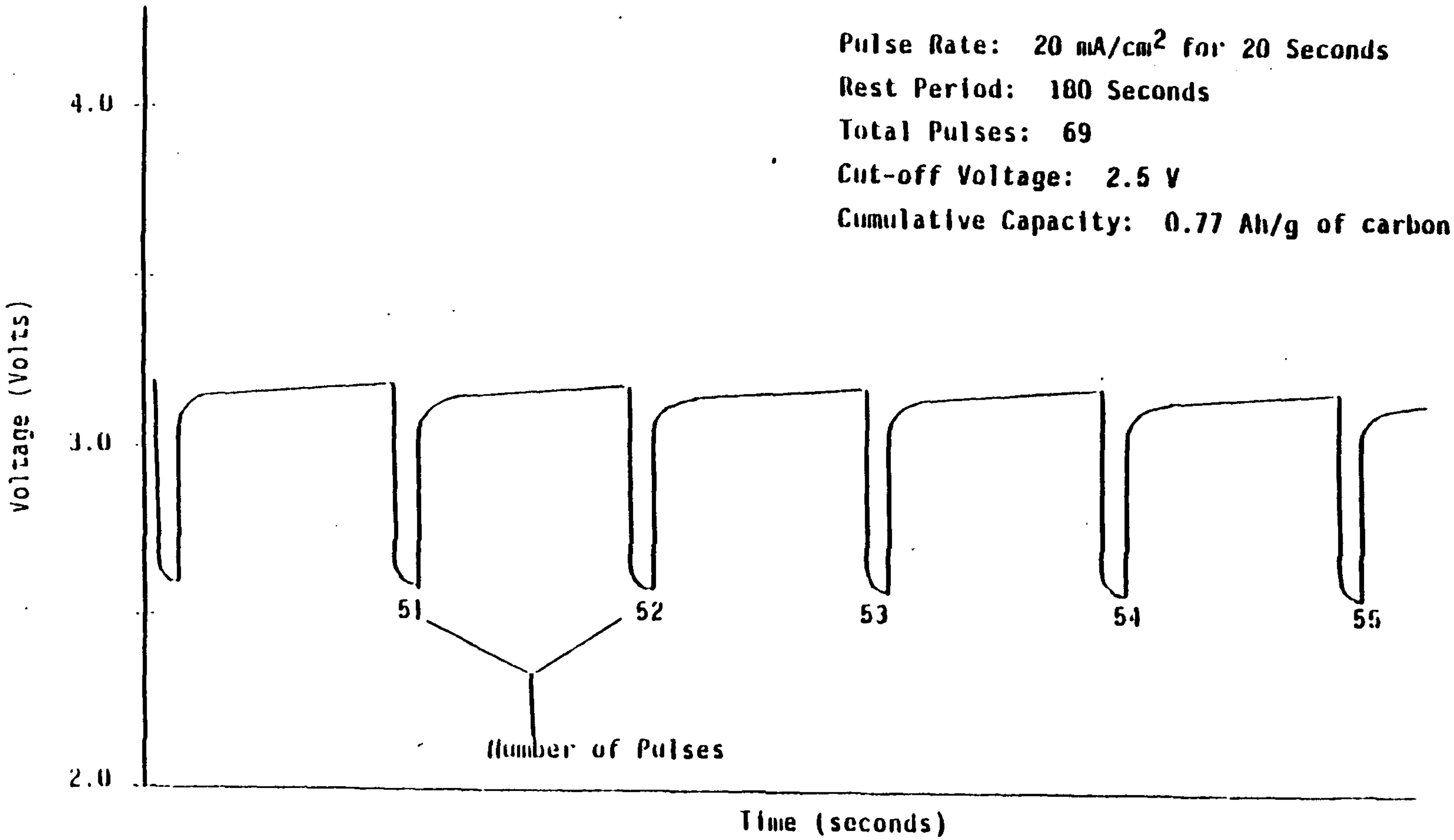

Figure 48: High Rate Discharge of a $Li/LiAlCl_4.6SO_2/C$ Cell by Applying a Pulse of 0.5A (20 mA/cm^2) for 20 Seconds with 180 Seconds Rest Period.

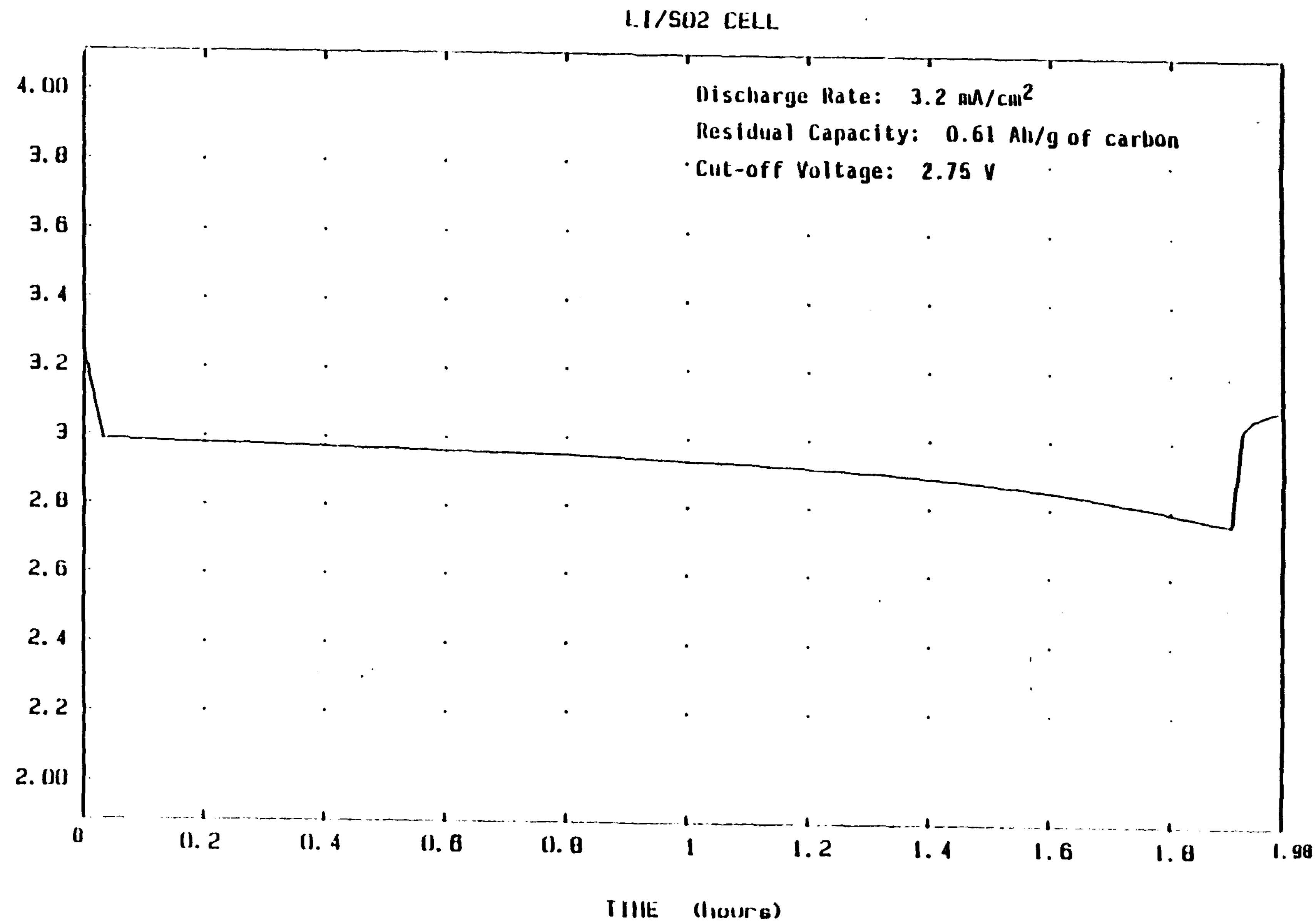

Figure 49: Residual Discharge Behavior of a $Li/LiAlCl_4 \cdot 6SO_2/C$ Cell (After High Rate Pulse Discharge as Mentioned in Figure 3) at 3.2 mA/cm^2. Cutoff Voltage: 2.75 V. Cathode Area: 25 cm^2.

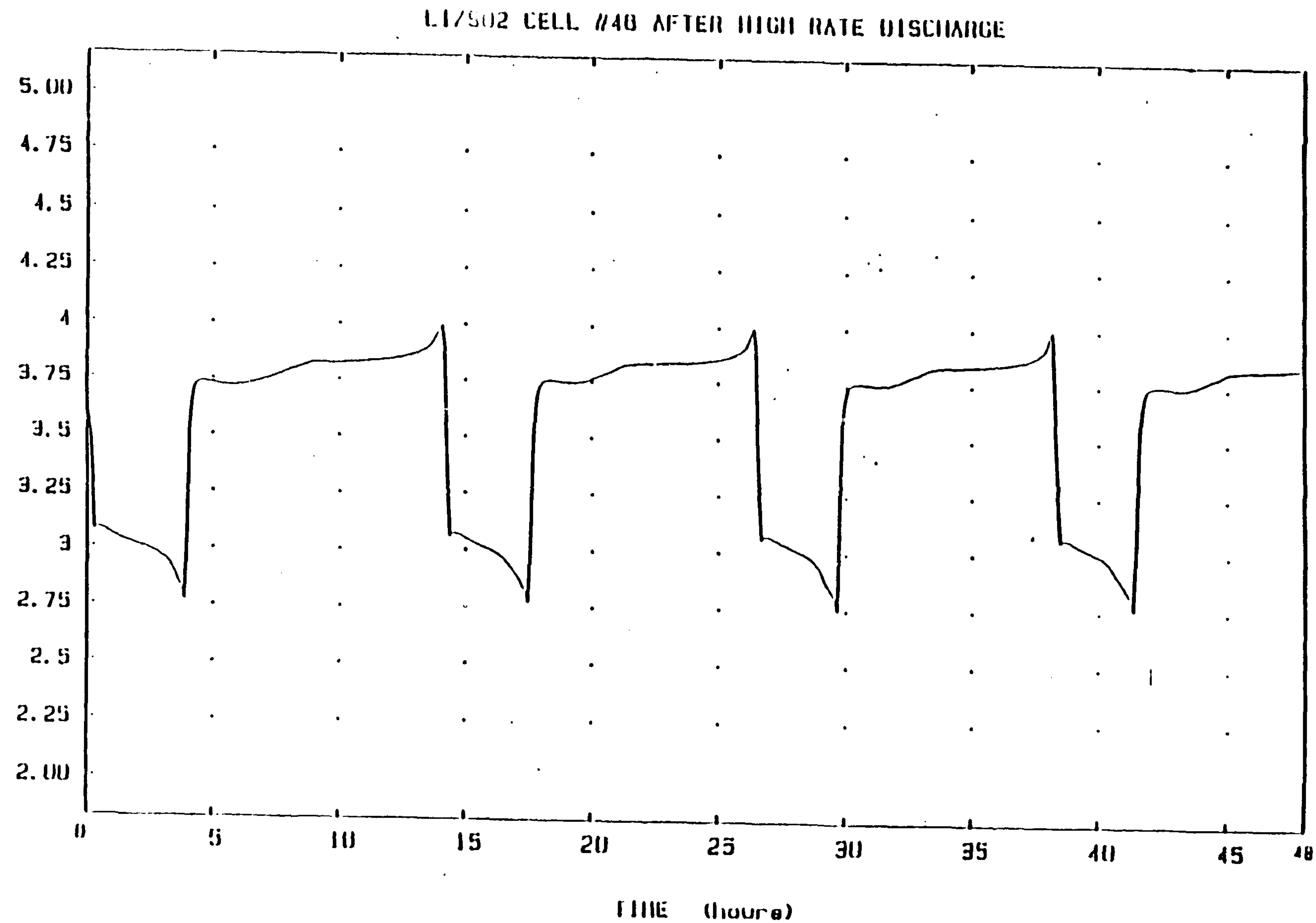

Figure 50: Charge-Discharge Behavior of a $Li/LiAlCl_4 \cdot 6SO_2/C$ Cell (After High Rate Discharge; See Figures 3 and 4) at 1.2 mA/cm^2 Charge and 3.2 mA/cm^2 Discharge Rates. Voltage Limits: 2.75-4.0 V. Cathode Area: 25 cm^2.

capacity at room temperature. The cell was then charged at 1.2 mA/cm^2 to 4.0V, left at OCV for four hours and stored at -20°C in a temperature-controlled bath for 18 hours. The cell was then discharged at -20°C with 3.2 mA/cm^2 to a cut-off voltage of 2.5V (Figure 51). The average operating voltage was 2.77V. No voltage delay was observed. The cell delivered a capacity of 0.28 Ah/g of carbon at -20°C to 2.5V as compared to 1.45 Ah/g at room temperature to a cut-off voltage of 2.75V. The cycling behavior of the same cell after -20°C test was examined at room temperature at 3.2 mA/cm^2 discharge and 1.2 mA/cm^2 charge rates within the voltage limits of 2.75 - 4.0V. The cell delivered more than 100 cycles with 1.39 Ah/g capacity for the first discharge cycle after -20°C test and 0.84 Ah/g for the 100th discharge cycle (Figure52).

The cell was then suspended from cycling after discharge to store at room temperature and examine the capacity retention and voltage delay.

Discharge at -30°C A fresh experimental Li/SO_2 cell (Laboratory cell 47) was discharged at 3.2 mA/cm^2 to 2.75V to determine the discharge capacity at room temperature. The cell was then charged at 1.2 mA/cm^2 to 4.0V, left at OCV for four hours and stored at -30°C in a temperature-controlled bath for 18 hours. The cell was then discharged at 3.2 mA/cm^2 to a cut-off voltage of 2.5V (Figure 53).

The cycling behavior of the same cell after -30°C test was examined at room temperature at 3.2 mA/cm^2 discharge and 1.2 mA/cm^2 charge rates in the voltage limits of 2.75 - 4.0V and is shown in Figure 54.

The cell was then suspended from cycling after charge to store at room temperature and examine the capacity retention and voltage delay.

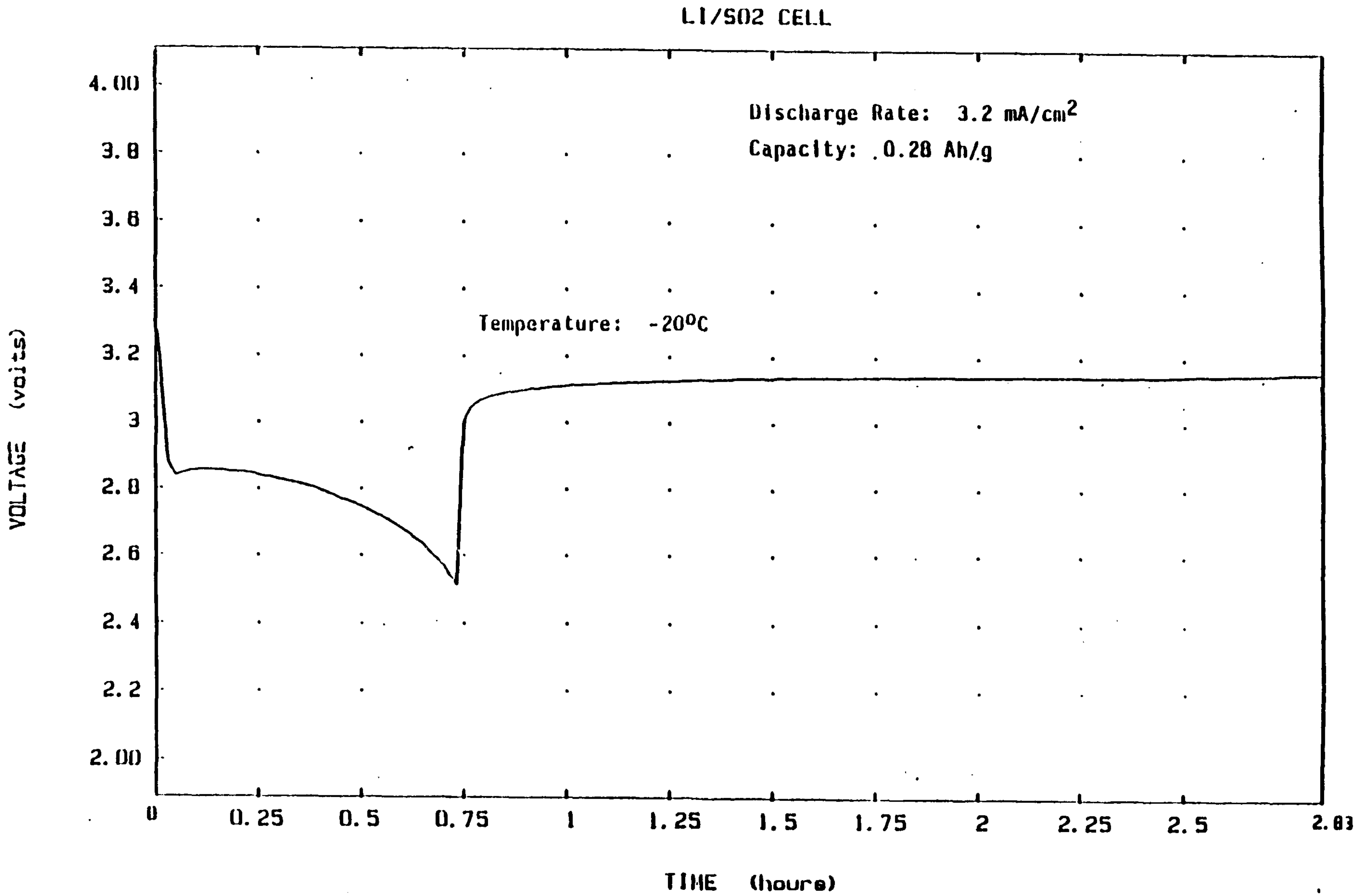

Figure 51: Discharge Characteristics at 3.2 mA/cm^2 and Voltage Recovery (without load) of a $Li/LiAlCl_4.6SO_2/C$ Cell at -20°C. Cathode Area: 25 cm^2.

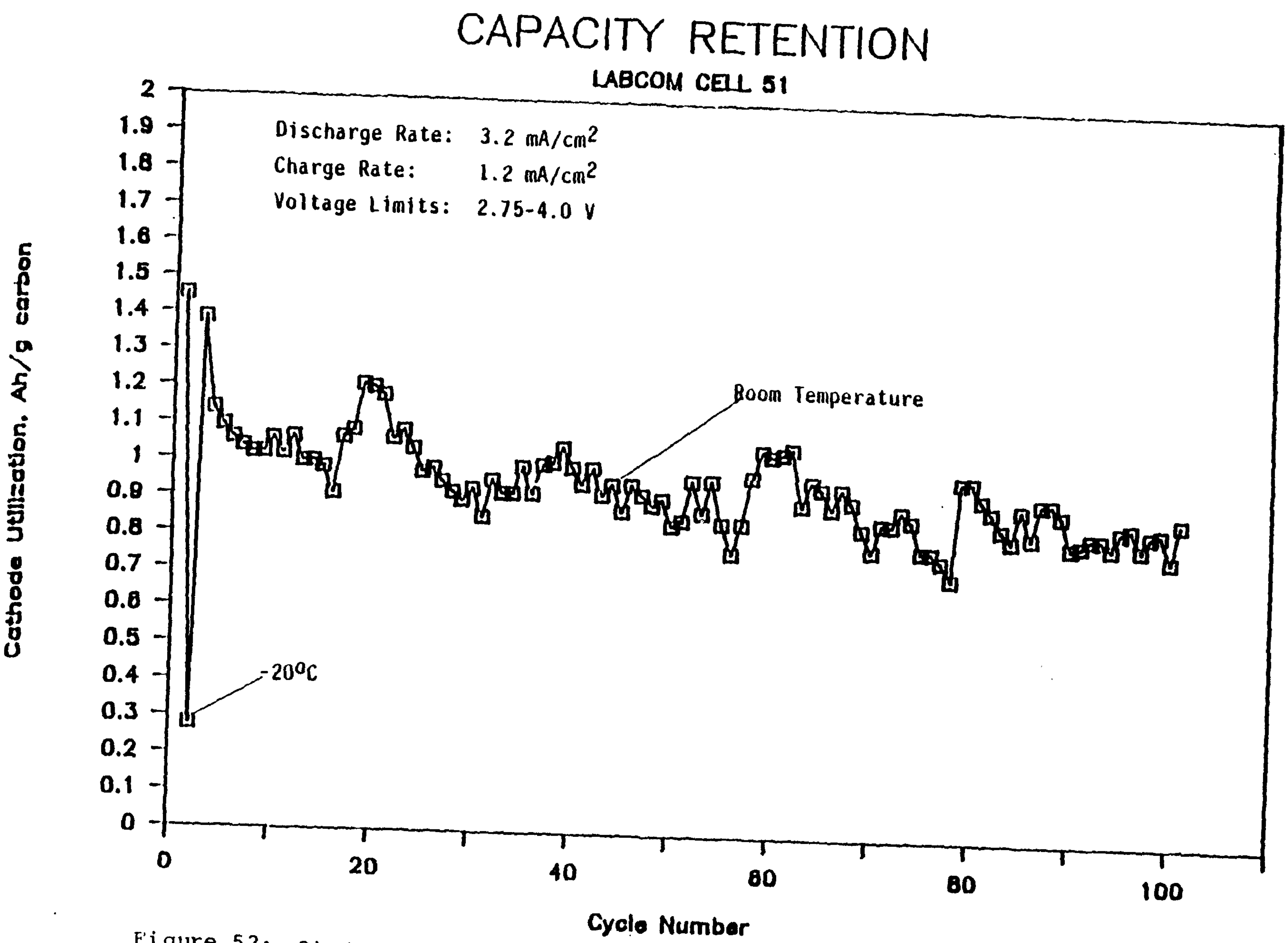

Figure 52: Discharge Capacity vs. Cycle Number of a $Li/LiAlCl_4.6SO_2/C$ Cell at Room Temperature Before and After Discharged at -20°C.

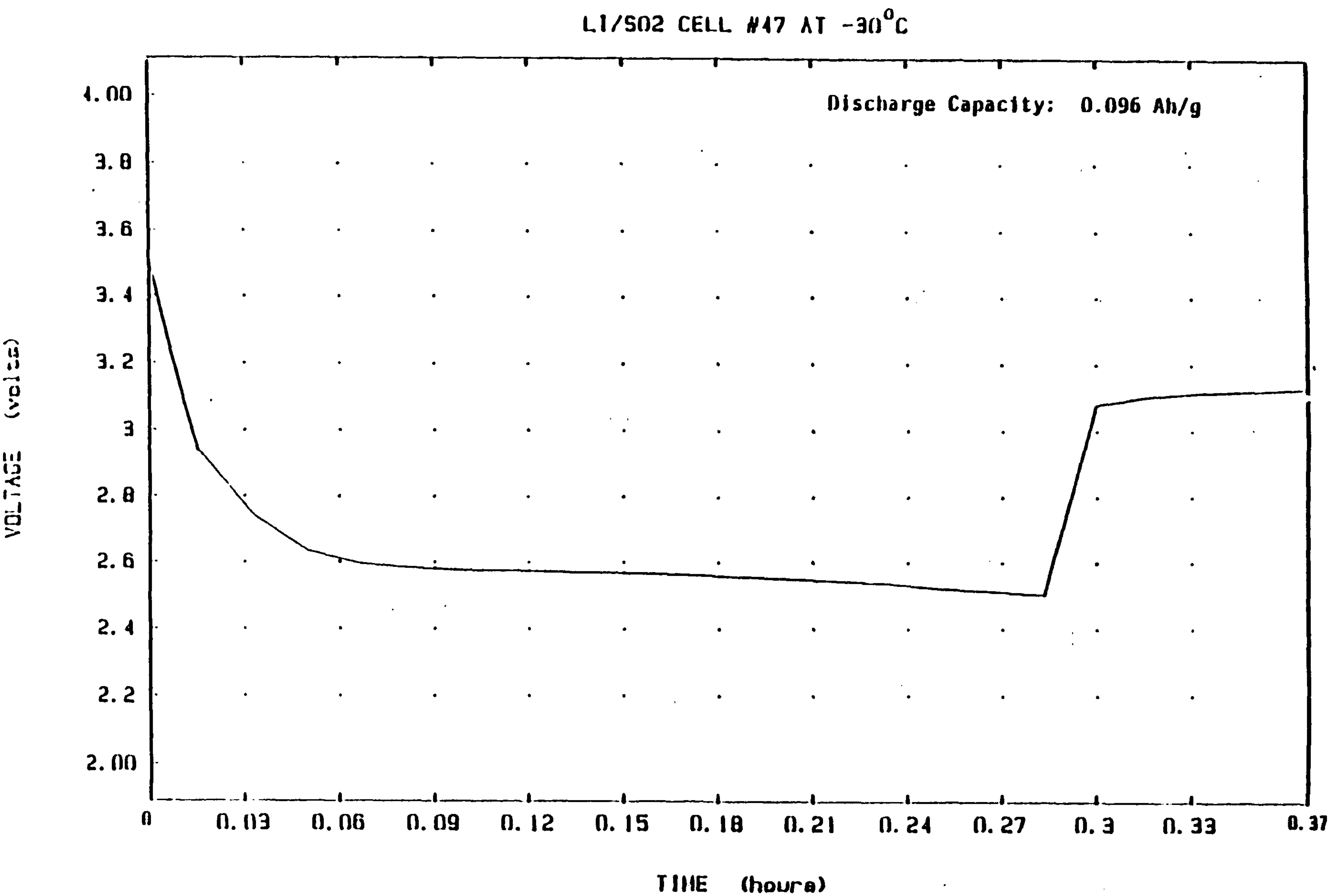

Figure 53: Discharge Characteristics at 3.2 mA/cm^2 and Voltage Recovery (Without Load) of a Li/$LiAlCl_4 \cdot 6SO_2$/C Cell at -30°C. Cathode Area: 25 cm^2.

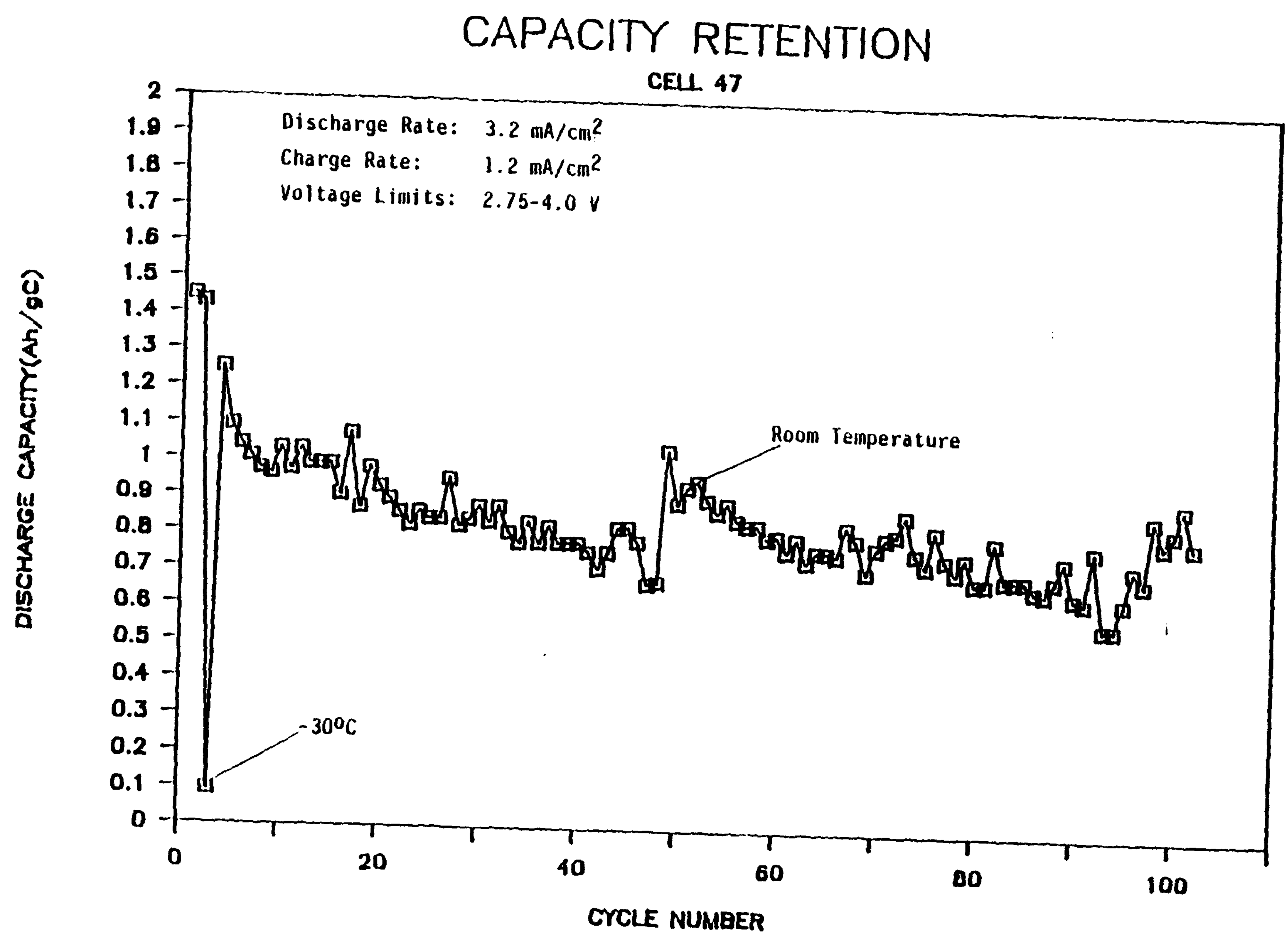

Figure 54: Discharge Capacity *vs*. Number of Cycles of a $Li/LiAlCl_4 \cdot 6SO_2/C$ Cell at Room Temperature Before and After Discharged at -20°C.

PHYSICAL ANALYSIS

The analysis of charged and discharged anodes were carried out using Scanning Electron Microscopy (SEM) and Energy Dispersive X-ray Spectroscopy (EDS) (Figures 55 and 56). SEM and EDS of charged and discharged anodes show the presence of cubic salt crystals containing chlorine but no aluminum or sulfur. These data strongly suggest that LiCl is included on the anode surface as part of the protective film. This film of LiCl might act as a solid electrolyte through which Li^+ can conduct[4]. An amorphous second phase was detected on the surface with a constant Al/S ratio (1:2). This second phase may be formed as a result of absorbed electrolyte complexed with SO_2 on the anode surface.

The charged and discharged cathodes were analyzed by X-ray powder diffraction (XRD). The presence of LiCl on the discharged cathodes (Figure 57) and the absence of detectable amount of LiCl on the charged cathodes (Figure 58) confirms that LiCl is the sole crystalline discharge product.

PHASE TRANSITION IN $LiAlCl_4/SO_2$ ELECTROLYTES

Methods

The technique for determining phase transitions in SO_2 based electrolytes will involve two procedures. First, various electrolyte compositions will be sealed in glass ampules and observed over a wide range of controlled temperatures for signs of phase transitions and salting out. Second, the electrolyte will be cooled and warmed in a double walled glass vessel. Still air will be sealed between the walls to slow the heat flow in and out of the vessel. The ground glass top is fitted with two glass tubes which hold a Teflon coated Type T thermocouple and a nickel stirring rod.

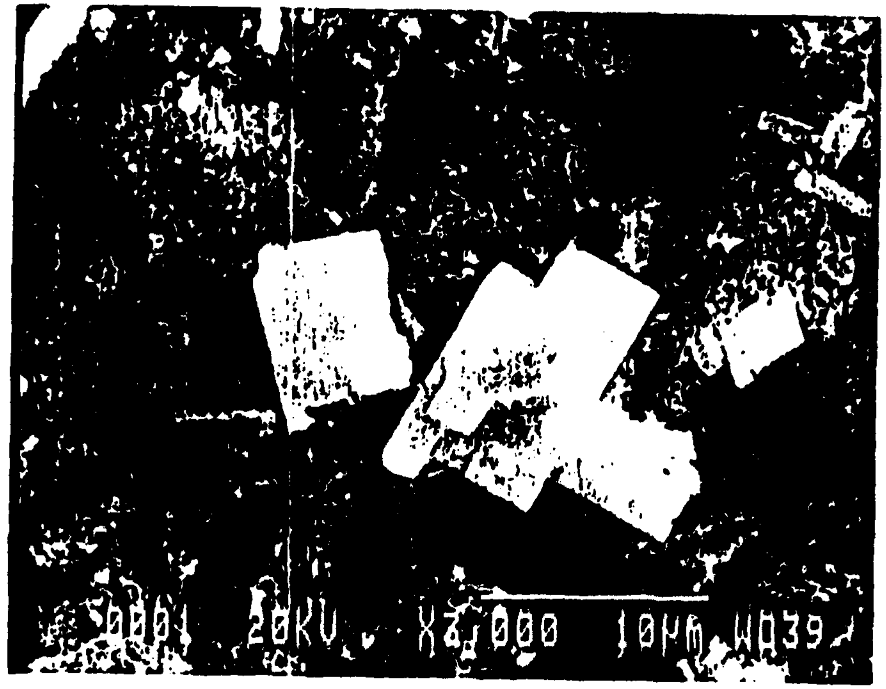

Scanning electron micrograph of Li-Anode after 79 cycles and discharged to 2.8 V at 1.0 mA/cm^2 (Cell #19) in $LiAlCl_4 \cdot 6\,SO_2$ electrolyte.

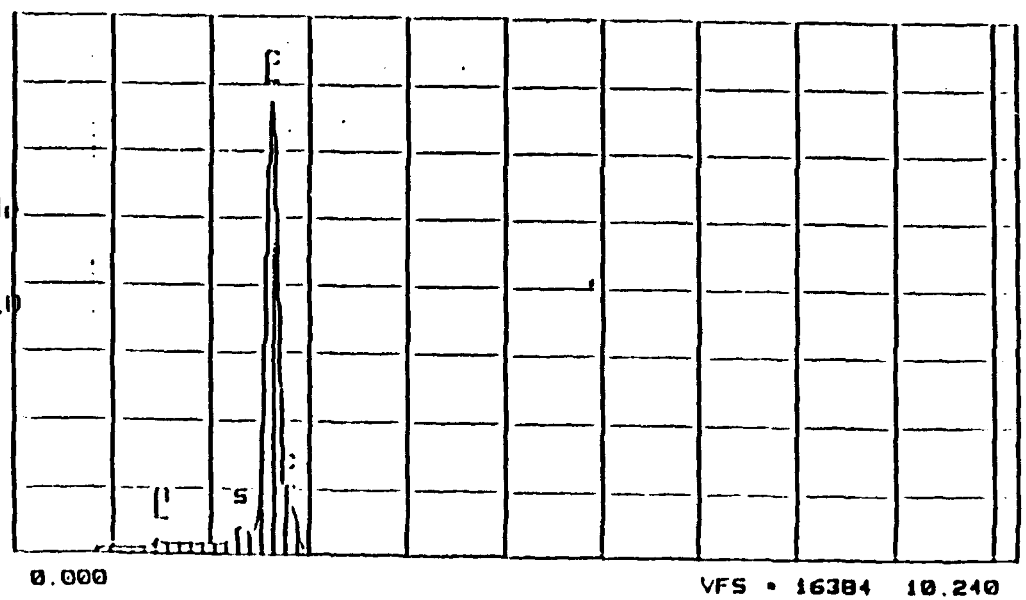

Energy Dispersive Spectroscopy of Li-Anode after 79 cycles and discharged to 2.8 V at 1.0 mA/cm^2 (Cell #19) in $LiAlCl_4 \cdot 6\,SO_2$.

Figure 55

Scanning electron micrograph of Li-Anode after 60 cycles and charged to 3.9 V at 1.0 mA/cm^2 (Cell #24) in $LiAlCl_4 \cdot 6\ SO_2$.

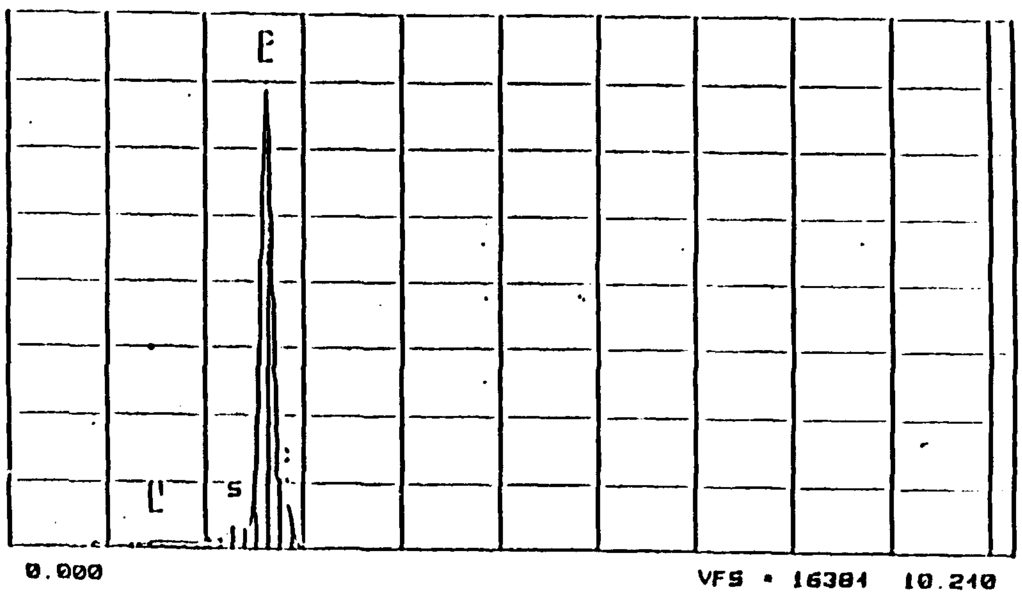

Energy Dispersive Spectroscopy of Li-Anode after 60 cycles and charged to 3.9 V at 1.0 mA/cm^2 (Cell #24) in $LiAlCl_4 \cdot 6\ SO_2$.

Figure 56

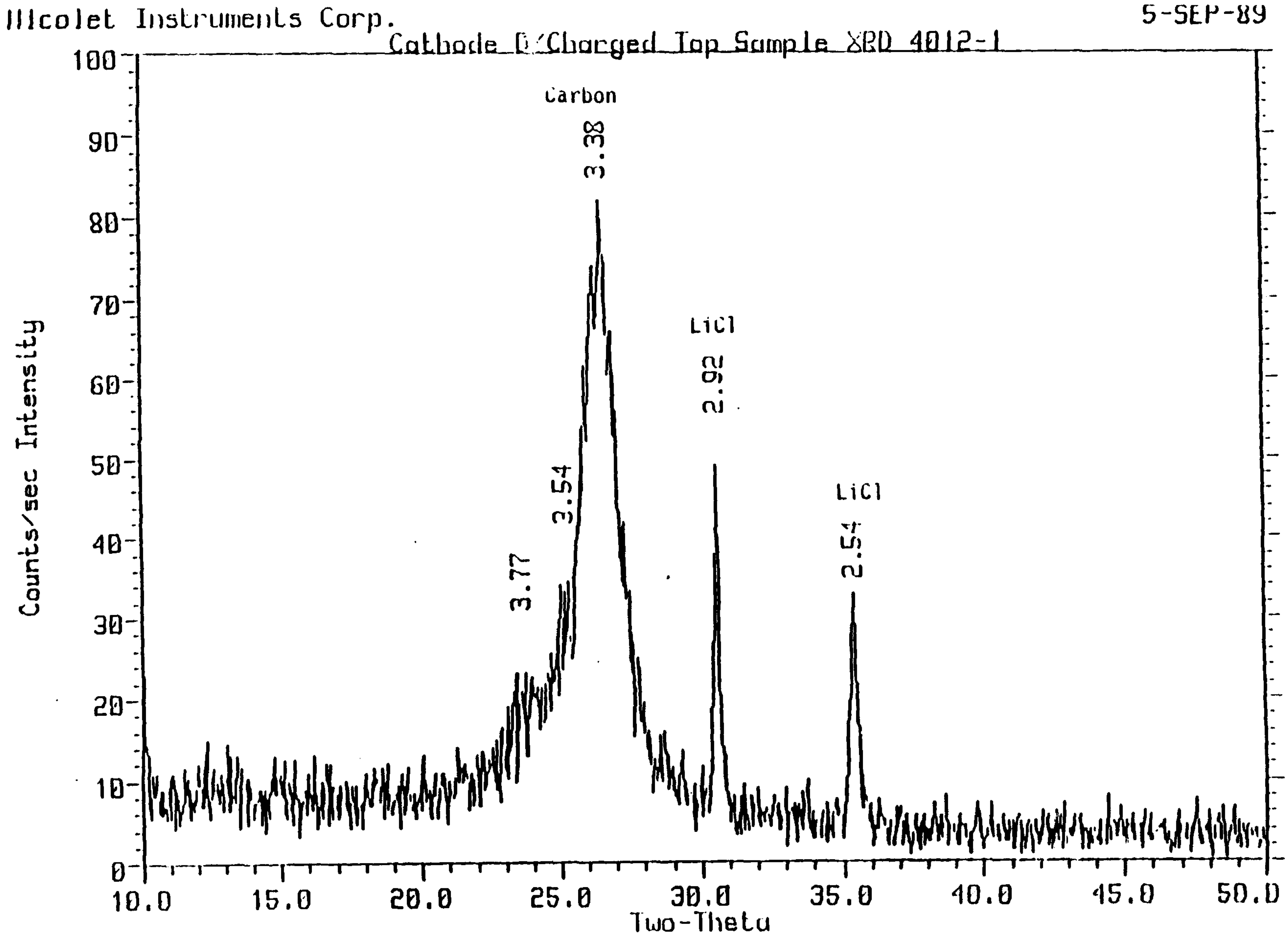

X-ray Diffraction Pattern of Discharged Cathode (rinsed in liquid SO_2) of Cell 19

Figure 57

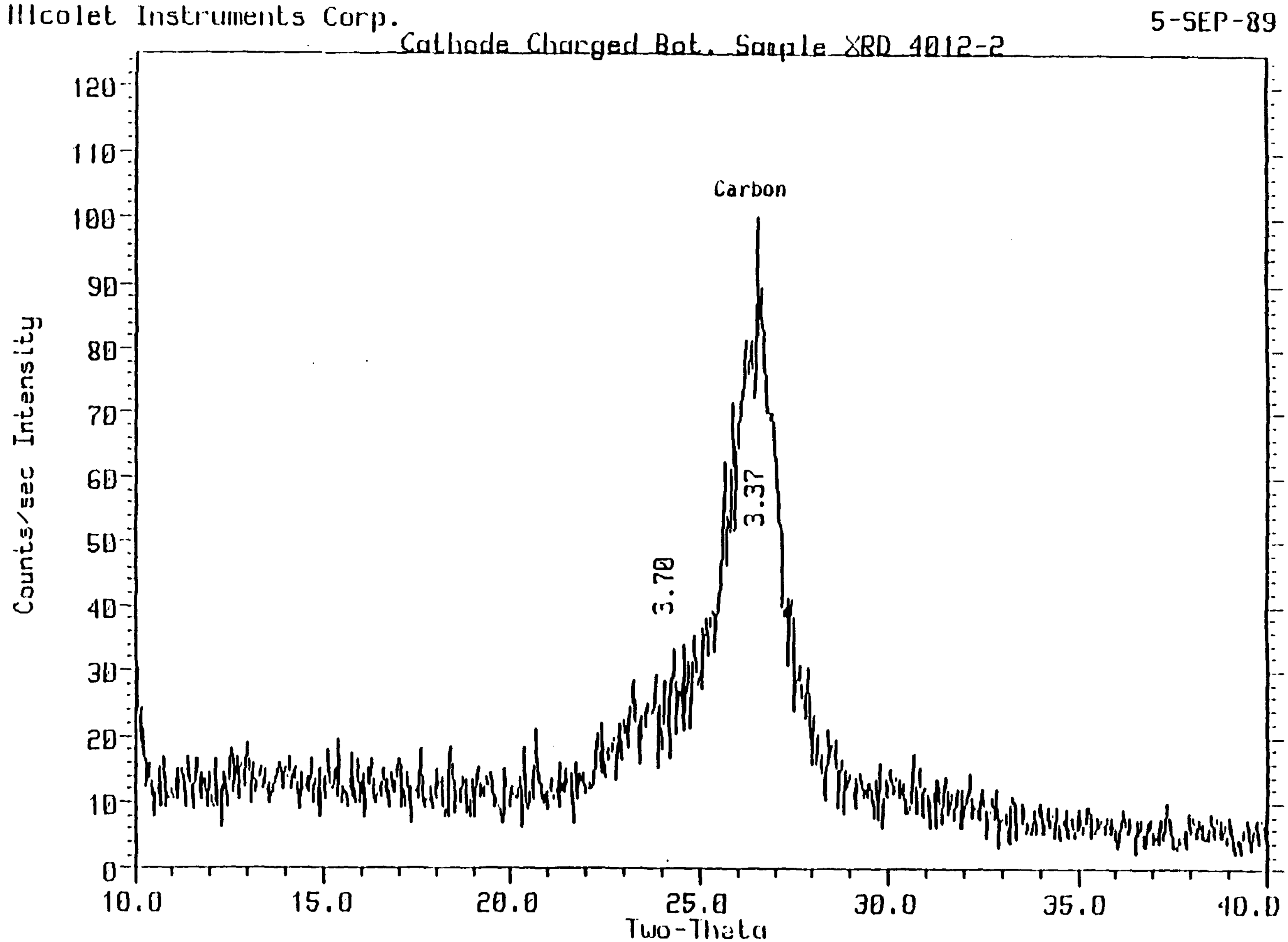

X-ray Diffraction Pattern of Charged Cathode (rinsed in liquid SO_2) of Cell No. 24

Figure 58

In the second technique, the solution is cooled over an appropriate range of temperature while stirring. The thermocouple is connected to a cold junction potential whose output can be recorded continuously on a plotter at 10 mV full scale with offset capability. Transition temperatures can be read directly from the appropriate conversion table.

$\underline{LiAlCl_4 \cdot 3SO_2}$

5.42 grams of $LiAlCl_4 \cdot 3SO_2$ were quickly transferred into the melting point Dewar in dry air. The Teflon coated thermocouple and nickel loop stirrer were inserted and the Dewar capped. The chart recorder was set to 10 mV full scale, 70 percent offset, 5 mm/min. The Dewar was placed in a dry ice-acetone bath without stirring. The solution super cooled to -16°C in about 20 minutes and then warmed to +16°C from the latent heat of freezing or salting out. The mixture was all solid at -16°C.

The same material was allowed to warm to room temperature and was warmed briefly with a hot air gun to 47.9°C. The mixture was then plunged into dry ice-acetone and the temperature monitored on the recorder, this time with continuous stirring.

The temperature decreased uniformly until a plateau occurred at +19.0°C. The temperature continued to fall, while continuously stirring, until a second transition occurred at about -16°C. The mixture had super cooled several degrees just prior to the transition and the solution became rubbery preventing any further stirring. This material continued to cool until -35.3°C where it was allowed to warm in air. Neither transition was apparent in the warming curve.

$\underline{LiAlCl_4 \cdot 6SO_2}$

The phase behavior of $LiAlCl_4 \cdot XSO_2$ (x = 5.714) was observed in the melting point apparatus. The solution was first prepared from ACS grade LiCl, $AlCl_3$ and 99.9 percent pure SO_2 gas condensed at low temperature. The complex was allowed to form at room temperature in a pressure bottle.

Koslowski[5] determined that a solution with 80 mole percent SO_2 undergoes a transition at about +17°C, probably the offset of salting out. We were able to super cool the solution with an ice-KCI mixture to -8°C in order to transfer it into the melting point tube. During transfer, a small amount of SO_2 escaped changing the composition from 85.1 to 81.7 percent SO_2. The loss of SO_2 triggered salting out to produce a slurry. The mixture was at -1.5°C.

The glass Dewar was quickly transferred to dry ice-acetone (-70°C) and cooled with continuous stirring. The output voltage of the cold junction potential was monitored with a recorder set at 10 mV full scale, 80 percent offset running at 60 mm/min.

One plateau was observed for the mixture at -36.7°C. The mixture was allowed to cool further, after the plateau, to -38°C and then warmed in ambient (+23°C) dry air.

The mixture showed no transitions on warming, appearing as a salt-solution mixture. The volume ration of liquid to solid increased continuously. However, before all the salt had a chance to redissolve, bubbling of SO_2 began at +2.7°C in the unpressurized vessel. At +9.5°C, the recorder was turned off.

<u>Summary of Phase Transition Results</u>

The freezing behavior of $LiAlCl_4 \cdot xSO_2$ mixtures with 75 (x=3.0) complex) and 82 (x=4.5 complex) mole percent SO_2 was observed. Both mixtures exhibit two transitions. The 75 percent begins to salt out at +19°C while the 82 percent begins to salt out at a temperature above -1.5°C where the

SO_2 vapor pressure is well above one atmosphere. The 75 percent mix then freezes completely at -16°C while the 82 percent mix undergoes a glass transition to a rubbery consistency at -36.7°C.

With these two preliminary measurements, two conclusions are apparent. First, for $LiAlCl_4 \cdot XSO_2$ mixtures in excess of x = 3, phase behavior is similar to familiar salt solutions where salting out can occur over a wide range of temperatures before the entire mixture is frozen. This is quite different from $LiAlCl_4$ solutions in $SOCl_2$ which freeze entirely at a particular temperature. Reversal of these transitions for the SO_2 complex on warming is sluggish.

Second, the SO_2 vapor pressure is too high for X>3 to accurately measure the salting out temperature in the unpressurized double walled vessel.

SPIRAL WOUND CELLS RESULTS

Construction of high rate spiral wound cells is described in the Experimental Section. Individual cell characteristics and test results are given in Table 7. The first cathodes prepared for wound cell assembly actually contained less carbon than originally planned. With an electrode thickness of 0.03 inch for the whole cathode/substrate component, the carbon thickness was only about 0.025 inch. Once wound to the proper diameter to fit in the cell cases, each stack or winding contained a cathode with about 4.0g active material, corresponding to a capacity of about 5.5 Ah initially. The first two wound cells, DW-1-01 and DW-1-02, were activated with about 51g $LiAlCl_4 \cdot 6SO_2$ electrolyte (about 33ml). Assuming the discharge reaction described by Duracell,

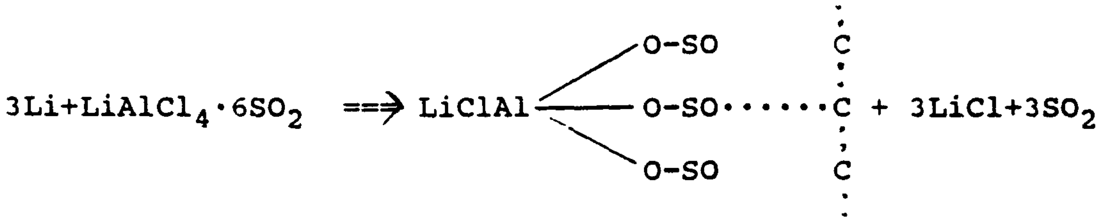

the capacity available from the electrolyte was approximately 6Ah (224 mAh/ml). In practice a lower capacity is expected since the electrolyte solution becomes more dilute (less conductive) during discharge.

Cycling conditions imposed on the wound cells are detailed in Table 8 below.

Table 8
Cycling Conditions for Wound Cells

Cell	I (mA)	i (mA/cm^2)	Discharge Limits		Charge Limits	
			time (h)	Volt (V)	time (h)	Volt (V)
DW-1-01	361	1	7	2.8	7	4.0
DW-1-02	361	1	10	2.8	10	4.0

TABLE 7: SPIRAL WOUND CELL SUMMARY

Cell Number	Case Type	Electrode Surface Area	Electrolyte Weight	Approx. Cathode Density	Cathode Weight	Discharge Limits		Charge Limits		First Cycle Capacity	Cycle Achieved	Comments
		(cm3)	(grams)	(g/cc)	(grams)	Time(hr)	Volts	Time(Hr)	Volts			
DW-1-01	D	361	51	.17	4.10	7	-	7	-	2.5	21	Venting with flame on charge
02	D	361	51	.17	4.0	10	-	10	-	3.6	32	
03	3/2 C	284	-	-	3.5	-	-	-	-	-	-	Failed to Poor
04	3/2 C	284	-	-	3.8	-	-	-	-	-	-	Aluminum/Nickel Welds
05	3/2 C	284	22	.14	2.0	-	2.8	-	4.2	0.9	19	
06	3/2 C	284	19	.15	2.2	-	2.8	-	4.2	1.6	11	High internal resistance
07	3/2 C	284	26	.15	2.2	-	2.8	-	4.2	0.9	3	Limited cycle life
08	3/2 C	284	26	.15	2.2	-	2.8	-	4.2	0.4	8	
09	BA5590	675	37	.089	2.8	-	2.8	-	4.0	1.0	2	Terminated for analysis
10	BA5590	675	37	.089	2.8	-	2.8	-	-	-	-	Leaked during high temperature storage
11	BA5590	675	37	.089	2.8	-	2.8	-	-	-	-	Not tested
12	BA5590	675	37	.089	2.8	-	2.8	-	4.0	0.7	10	Terminated due to short cycles
13	BA5590	675	37	.089	2.8	-	2.8	-	4.0	2.6	38	Terminated for analysis
14	BA5590	675	37	.089	2.8	-	2.8	-	4.0	3.0	45	Terminated for analysis
16	BA5590	675	37	.09	2.8	-	2.8	-	4.0	-	-	Untested
17	BA5590	675	37	.09	2.8	-	2.8	-	4.0	-	-	Untested
18	BA5590	675	37	.09	2.8	-	2.8	-	4.0	-	-	Untested
19	BA5590	675	37	.09	2.8	-	2.8	-	4.0	-	-	Untested
20	BA5590	675	37	.09	2.8	-	2.8	-	4.0	-	-	Untested
21	BA5590	675	37	.09	2.8	-	2.8	-	4.0	-	-	Untested
22	BA5590	675	37	09	2.8	-	2.8	-	4.0	-	-	Untested
23	BA5590	675	37	.09	2.8	-	2.8	-	4.2	1.0	8	Vented on charge
24	BA5590	675	37	.09	2.8	-	2.8	-	4.2	1.0	4	Vented on open circuit just after charge
25	BA5590	675	37	.09	2.8	-	-	-	-	-	-	Leaked during high temperature storage

The voltage profiles of the first and twentieth cycles of cell DW-1-01 are shown in Figures 59 and 60. Throughout the life of the cell both discharge and charge were limited by the time setting on the automated cycling equipment. The cell vented with flame on the twenty-first cycle during charge. The voltage profile of this cycle is shown in Figure 61. There were no indication of voltage fluctuation or dendrite shorting previous to the venting. Capacity of discharge and charge were identical and uniform throughout the cell life.

The second wound cell, DW-1-02, was also cycled at $1mA/cm^2$ galvanostatically. The discharge time was limited to 10 hours (3.6 Ah), otherwise the two cells were cycled identically. The profiles of the first and twentieth cycles are shown in Figures 62 and 63 as a comparison to the first cell. The cell capacity decreased gradually as shown in Figure 64 through 32 cycles and then very rapidly for the next three cycles. Examination of the voltage profile of the 32nd cycle showed evidence of dendrite shorting during that cycle. At this point the cell was disassembled for failure analysis. It was frozen in liquid nitrogen and cut open. The electrode package detonated about ten seconds after being exposed to the atmosphere even though it was frozen. There are two possible causes for this - dendritic lithium may have reacted explosively with moisture condensed on the cold stack or some combination of unstable reaction products was present on the surface of the lithium electrode. It was clear, however, that the reaction involved the lithium electrode.

At this point the wound cell design was reviewed to increase the safety level. The following changes were incorporated into the cell design. Aluminum expanded mesh was considered for the cathode substrates. Under some conditions, nickel substrates have been associated with unstable reaction

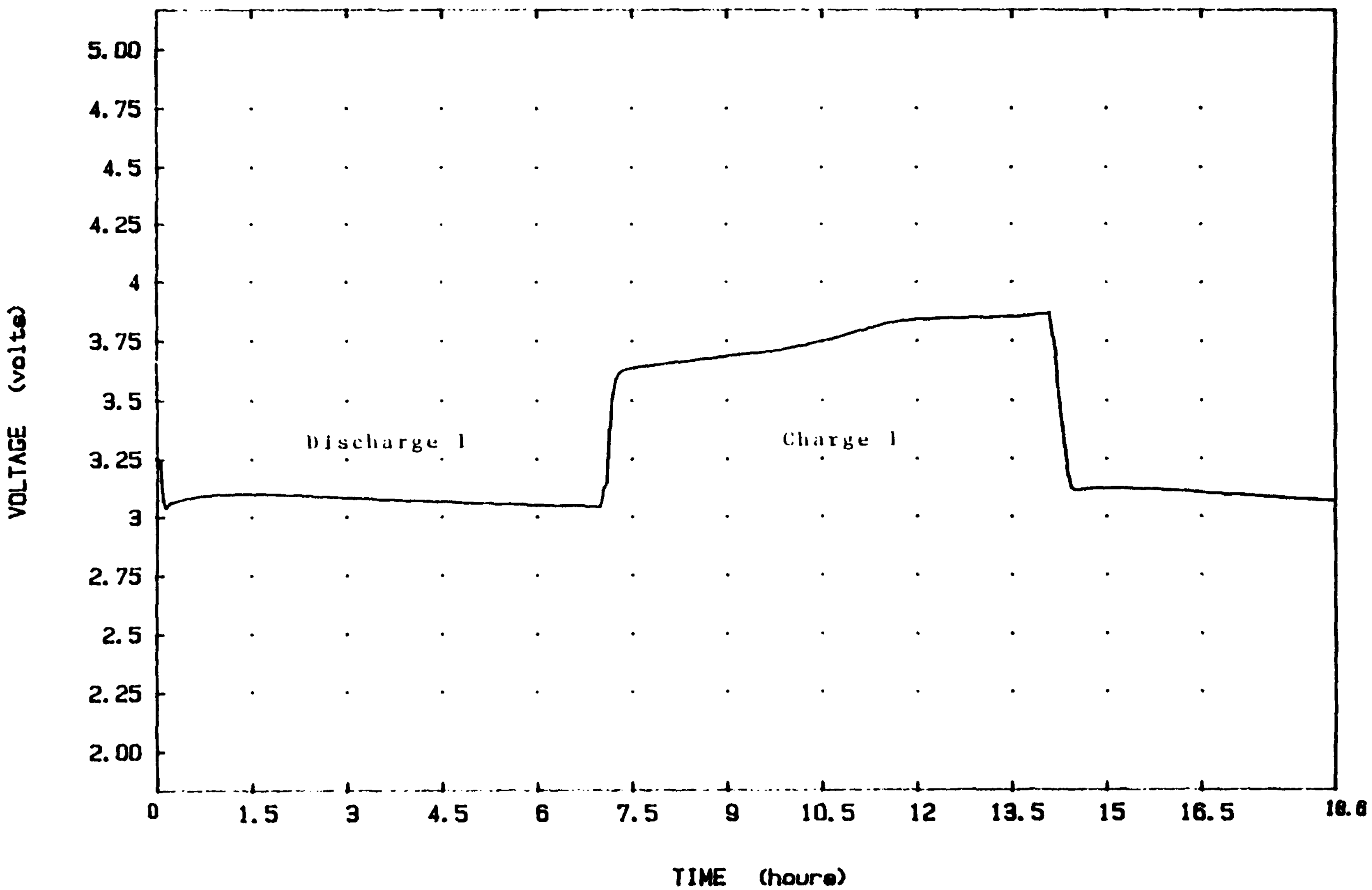

Figure 59: Voltage Profile of Cell DW-1-01, Cycle 1

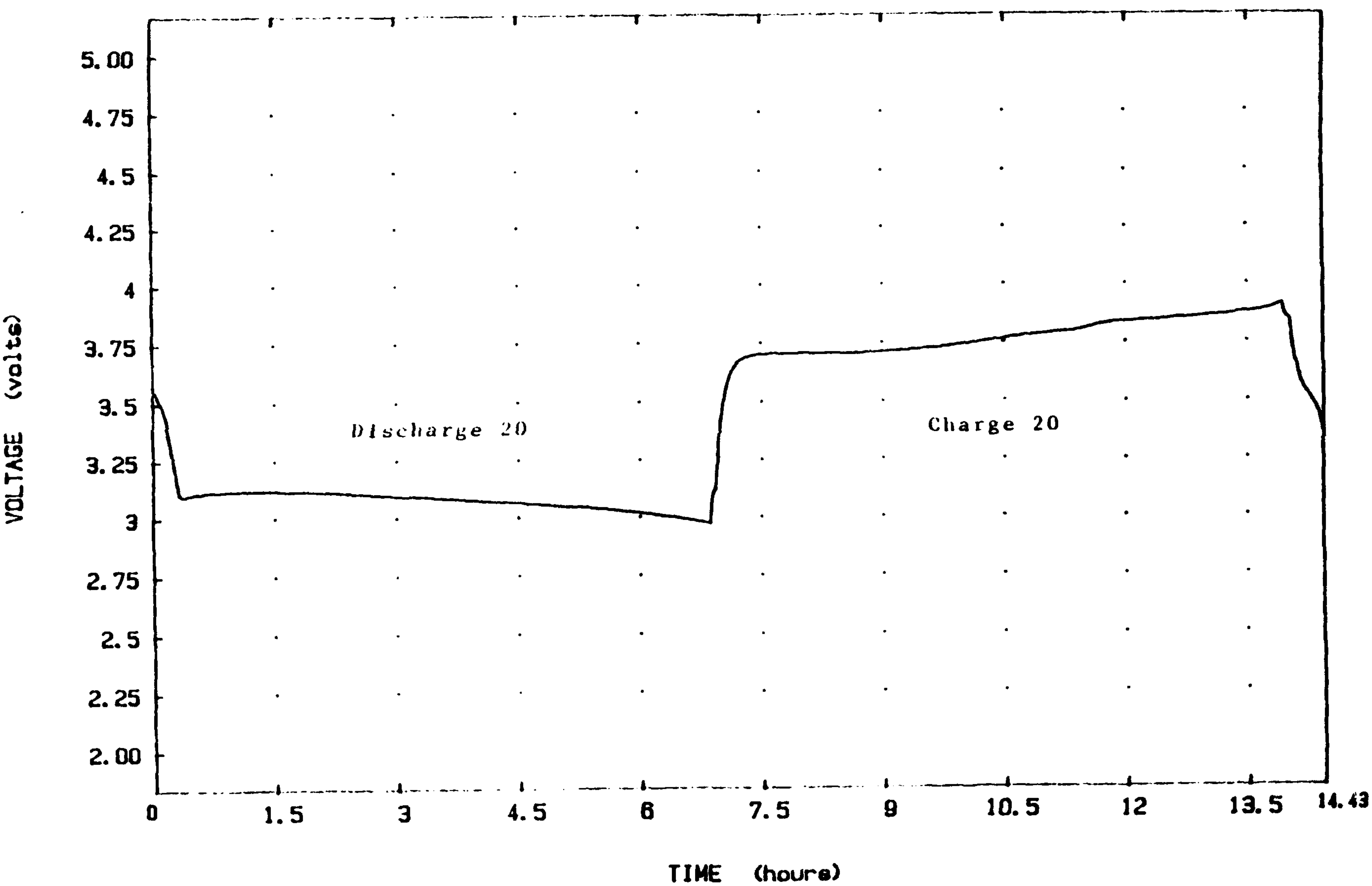

Figure 60: Voltage Profile of Cell DW-1-01, Cycle 20

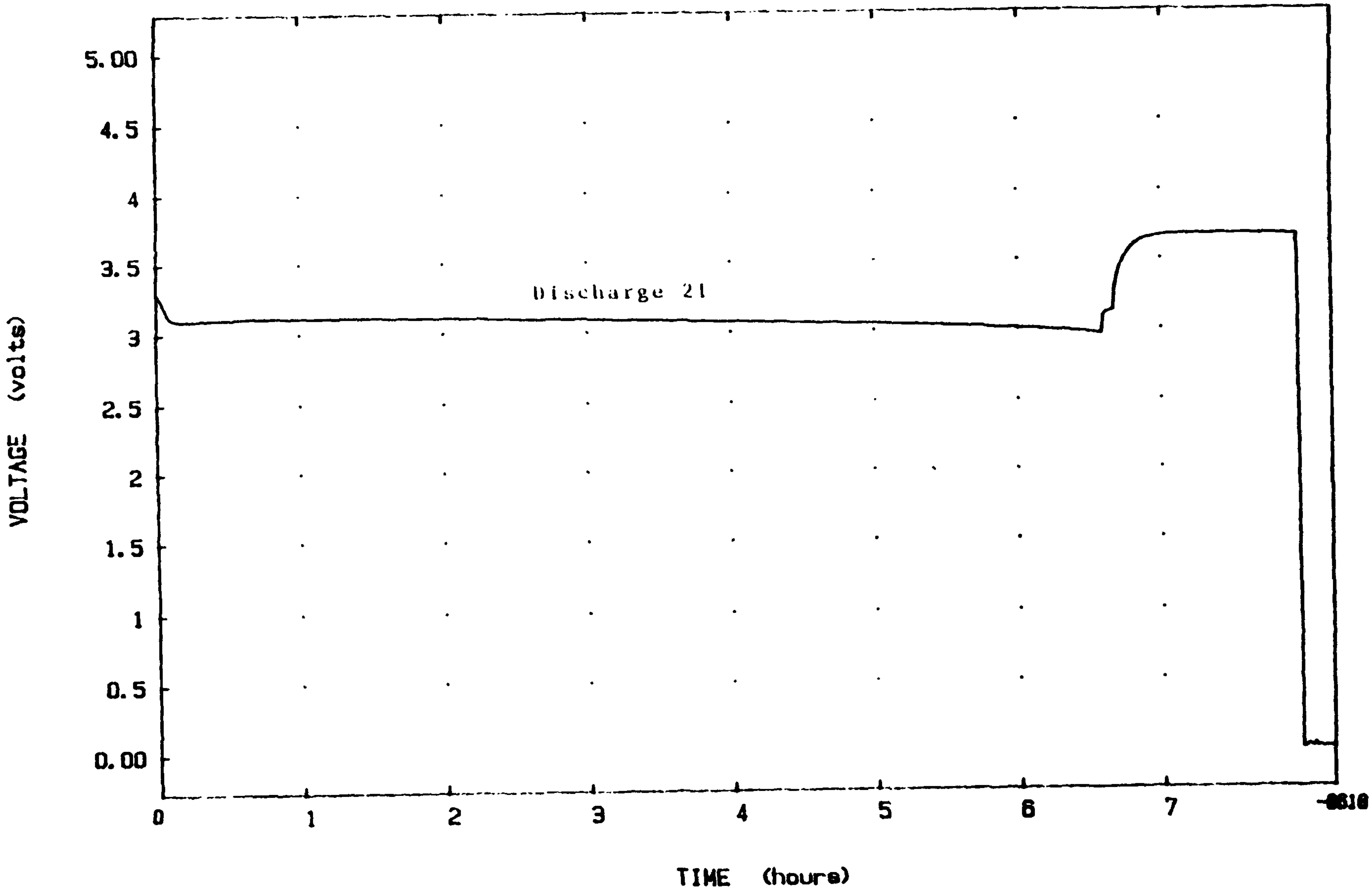

Figure 61: Voltage Profile of Cell DW-1-01, Cycle 21

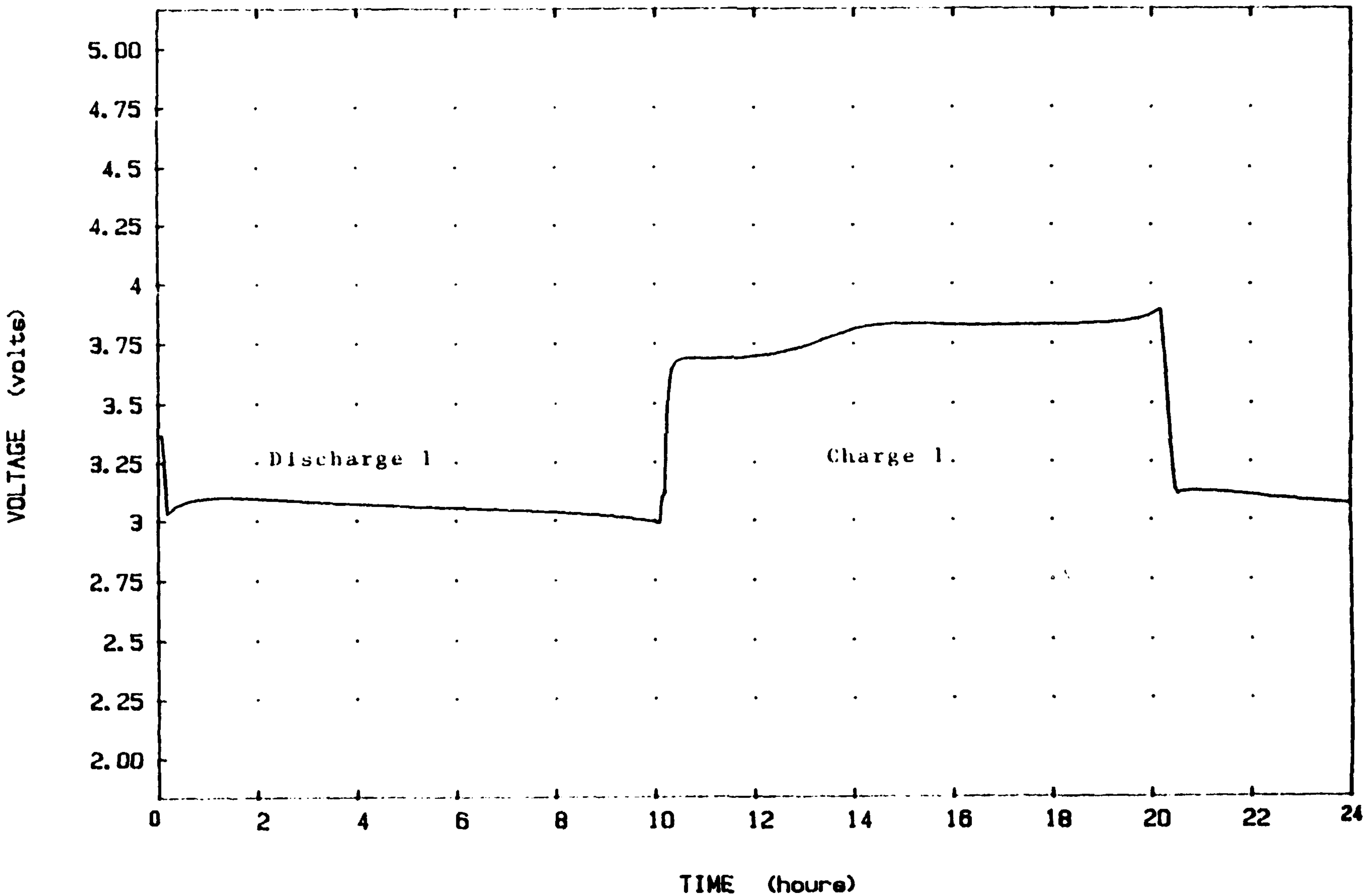

Figure 62: Voltage Profile of Cell DW-1-02, Cycle 1

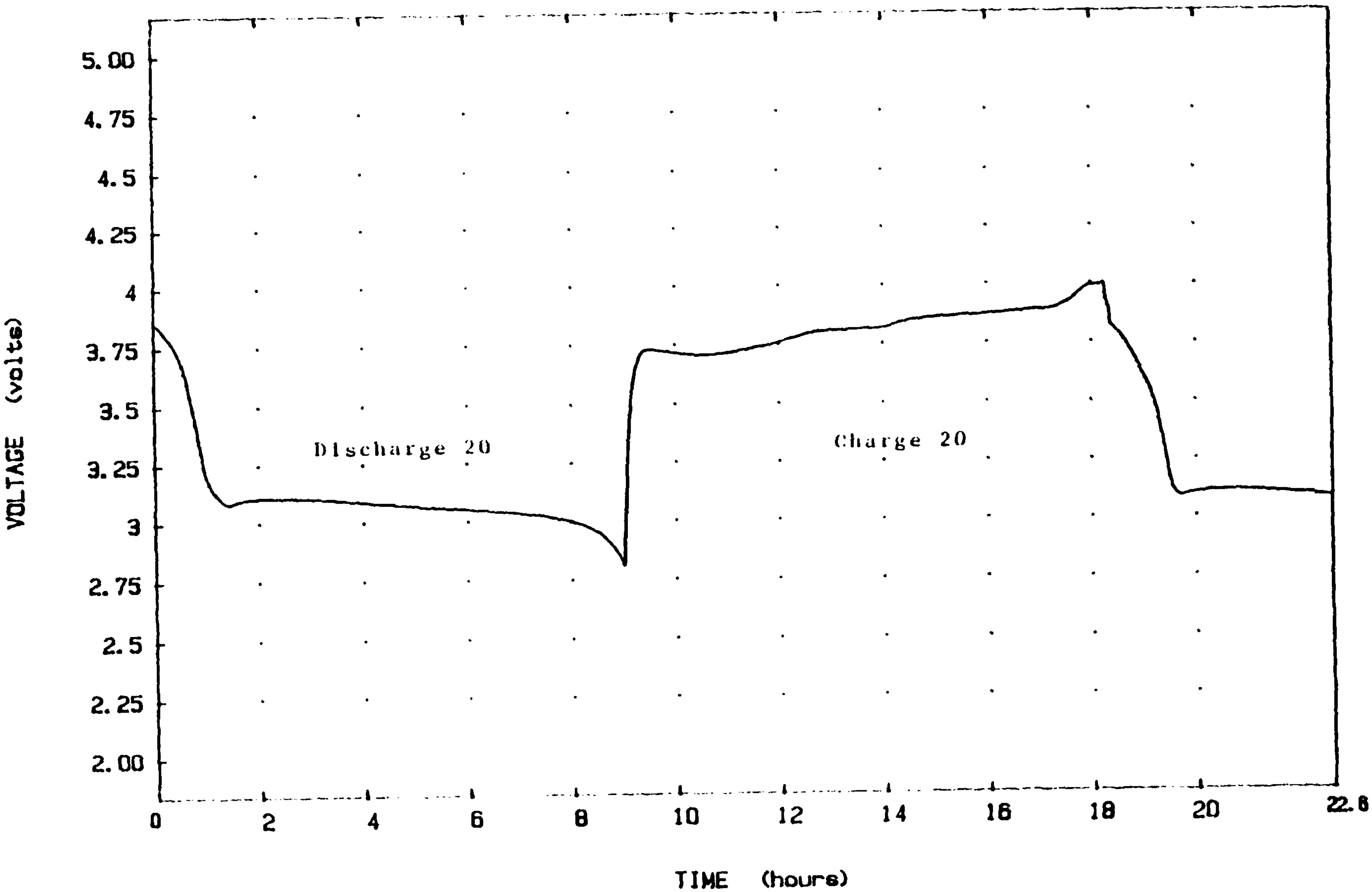

Figure 63: Voltage Profile of Cell DW-1-02, Cycle 20

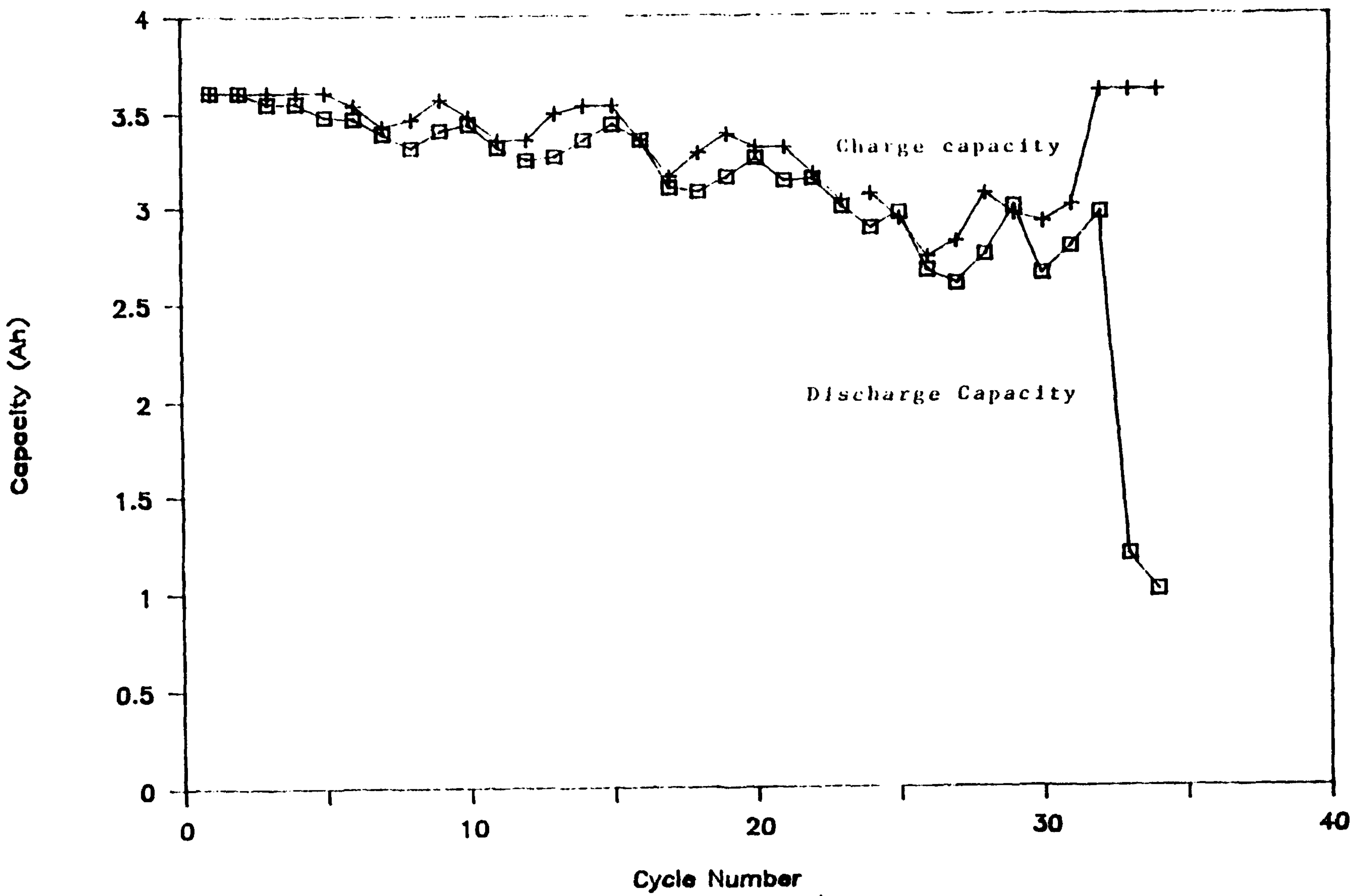

Figure 64: Capacity Retention of Wound Cell DW-1-02

products in primary Li/SO_2 cells. Although the rechargeable system is quite different (there is no acetontrile in the electrolyte solution and the salt is $LiAlCl_4$ rather than LiBr), there may be greater safety associated with the use of aluminum substrates. Also, the nonporous Tefzel insulating sheet covering the inner surface of the case was inadvertently omitted in the first two cells. This will be included in all future cells. The function of this insulator is to hinder dendrite bridging and corrosion involving the positive case and hardware during charge.

Cells 3-9 were contained in C sized steel cans and had an active surface area of $284cm^2$. The cells contained sufficient carbon for approximately 2.5Ah on the first cycle (at 1.4Ah/g) and lithium for a total capacity of about 13.5Ah. The actual stack volume was approximately 22.1ml and the outer cell volume was 34.2ml. The purpose of these tests was to compare performance of aluminum cathode substrates with the earlier nickel substrates and examine the safety performance of cycling. Therefore, the cells were not optimized for electrochemical capacity.

Two of the six cells could not be discharged because of bad weld connection between the aluminum cathode substrate and the nickel tab connected to the cell case. The other four cells, designated DW-1-05 through DW-1-08 were cycled between 2.8V and 4.0V at $1mA/cm^2$. Discharge capacities are shown in Figure 65.

The capacities obtained were all much lower than expected initially. The reason for this was an excessive internal resistance. This can be seen in Figure 66, showing the voltage profile of the first cycles of cell DW-1-05. There is an IR voltage drop of about 350mV initially for cycling at $1mA/cm^2$. This results in low discharge voltage (about 2.9V on average) and low capacity as the cell reaches the

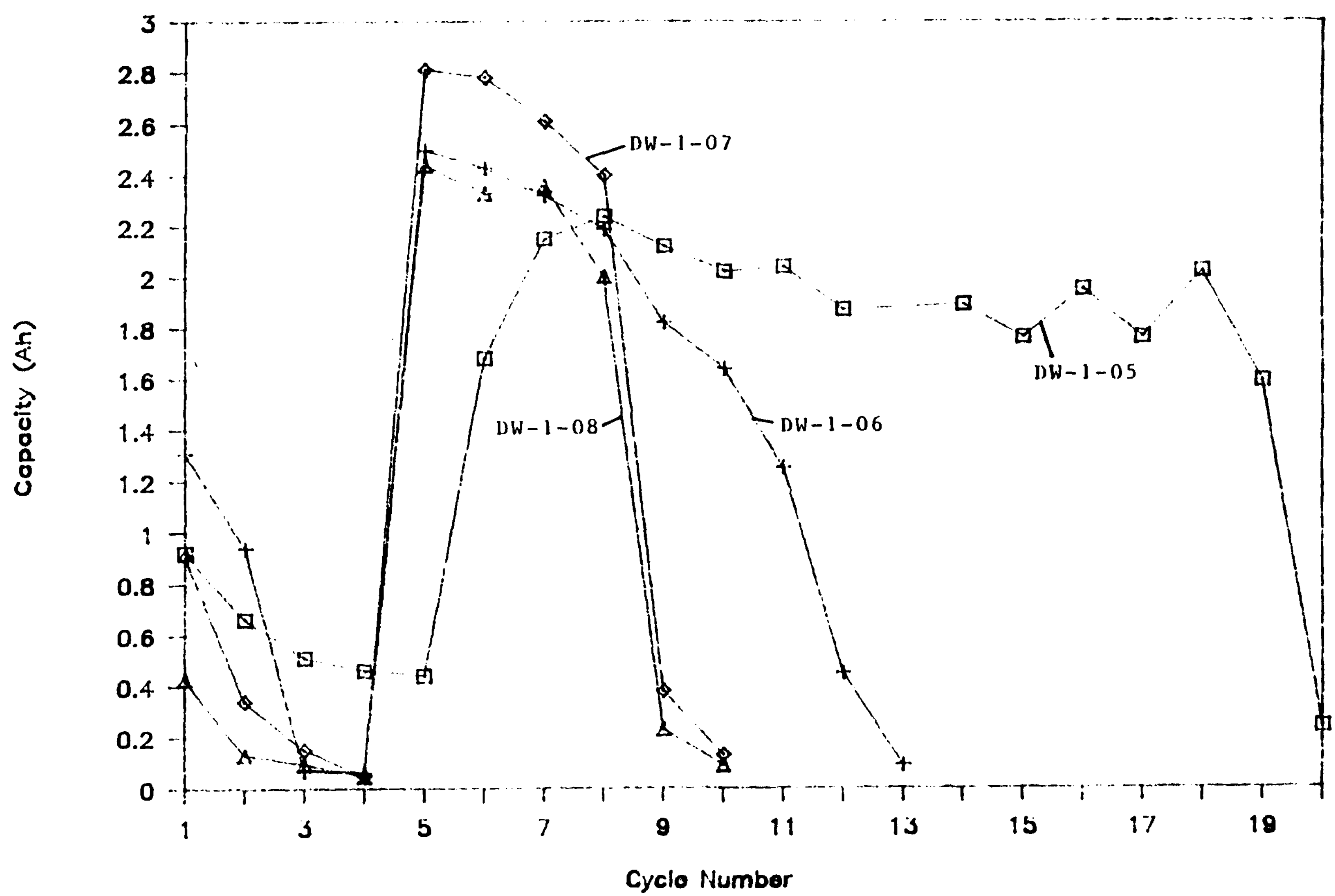

Figure 65:
Discharge Capacities of Cells DW-1-05 through DW-1-08

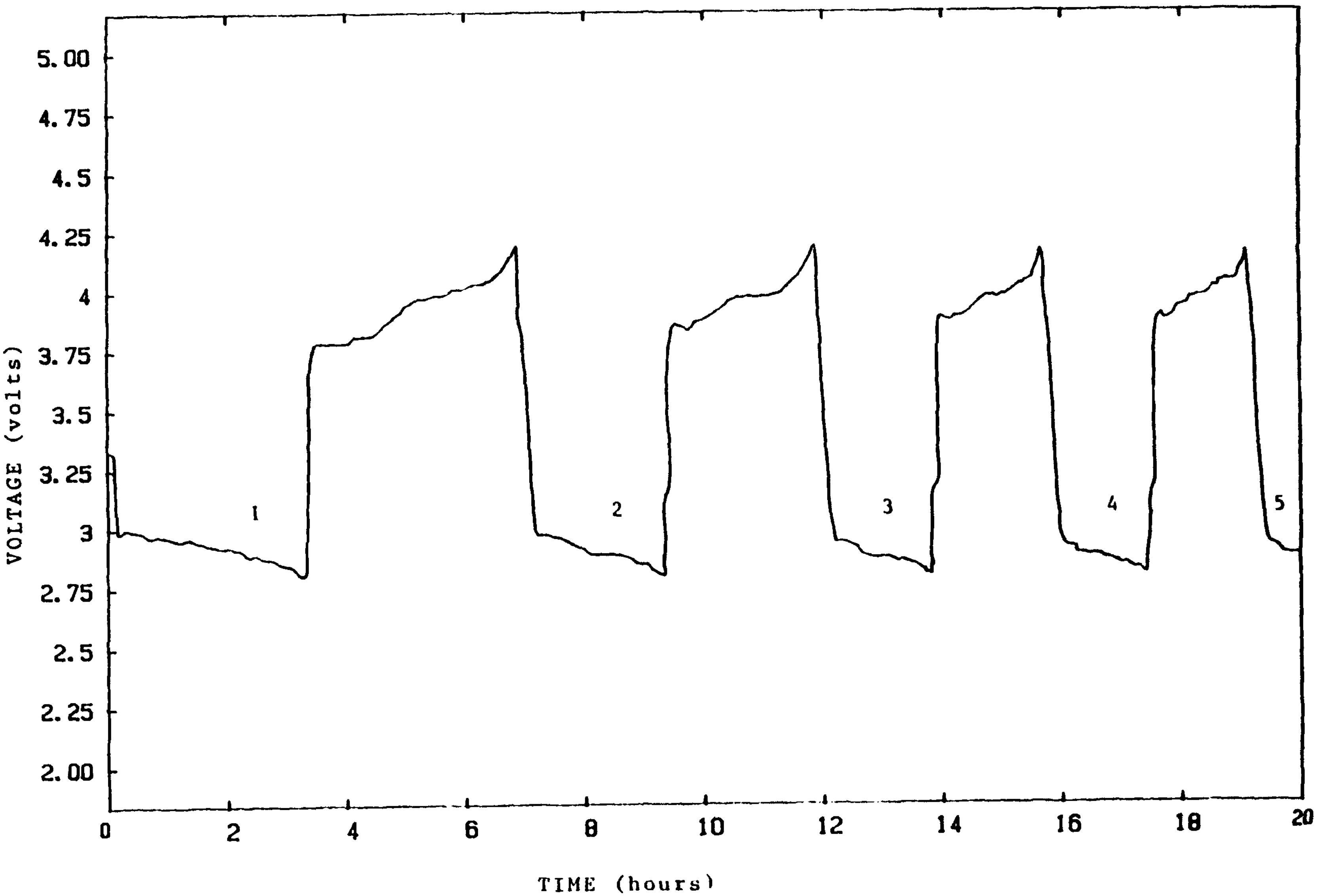

Figure 66:
Voltage Profile of Cell DW-1-05 during Cycles 1-4

discharge voltage cutoff before much of the capacity is removed. After 5 cycles the voltage limits were changed to 2.6V for discharge and 4.2V for charge in order to compensate for the high internal resistance.

This accounts for the jump in discharge capacity observed after the 5th cycle. The voltage profiles of the 6th and 7th cycles for Cell DW-01-05 immediately following the limit changes are shown in Figure 67 and that of the 9th and 10th cycles are shown in Figure 68. The average discharge voltage decreased continually throughout cycle life of the cell indicating that the cell internal impedance actually increased with cycling. During the 15th charge the cell developed dendritic shorts which eventually limited cell life to a few more cycles. This can be seen clearly in Figure 69 which compares the charge and discharge capacities for that cell. The 15th through 18th cycles show nearly twice the charge capacity as discharge capacity as well as voltage fluctuations on charge characteristic of dendrite shorting.

Cells DW-1-06 through 1-08 were treated in a similar manner. These calls failed within 15 cycles as they were unable to charge effectively within the voltage limits. Charge capacity was always less than the discharge capacity. Again, the internal impedance of the cells ultimately limited the cycle life by not permitting efficient cycling within practical voltage limits. It would not be practical for a high rate cell to reduce the current density below $1mA/cm^2$ or to further extend the voltage limits. The aluminum cathode substrate or substrate/lead welds were assumed to be the cause of the excessively high internal impedance.

Resistance Measurements

Resistance measurements were made of substrate/lead

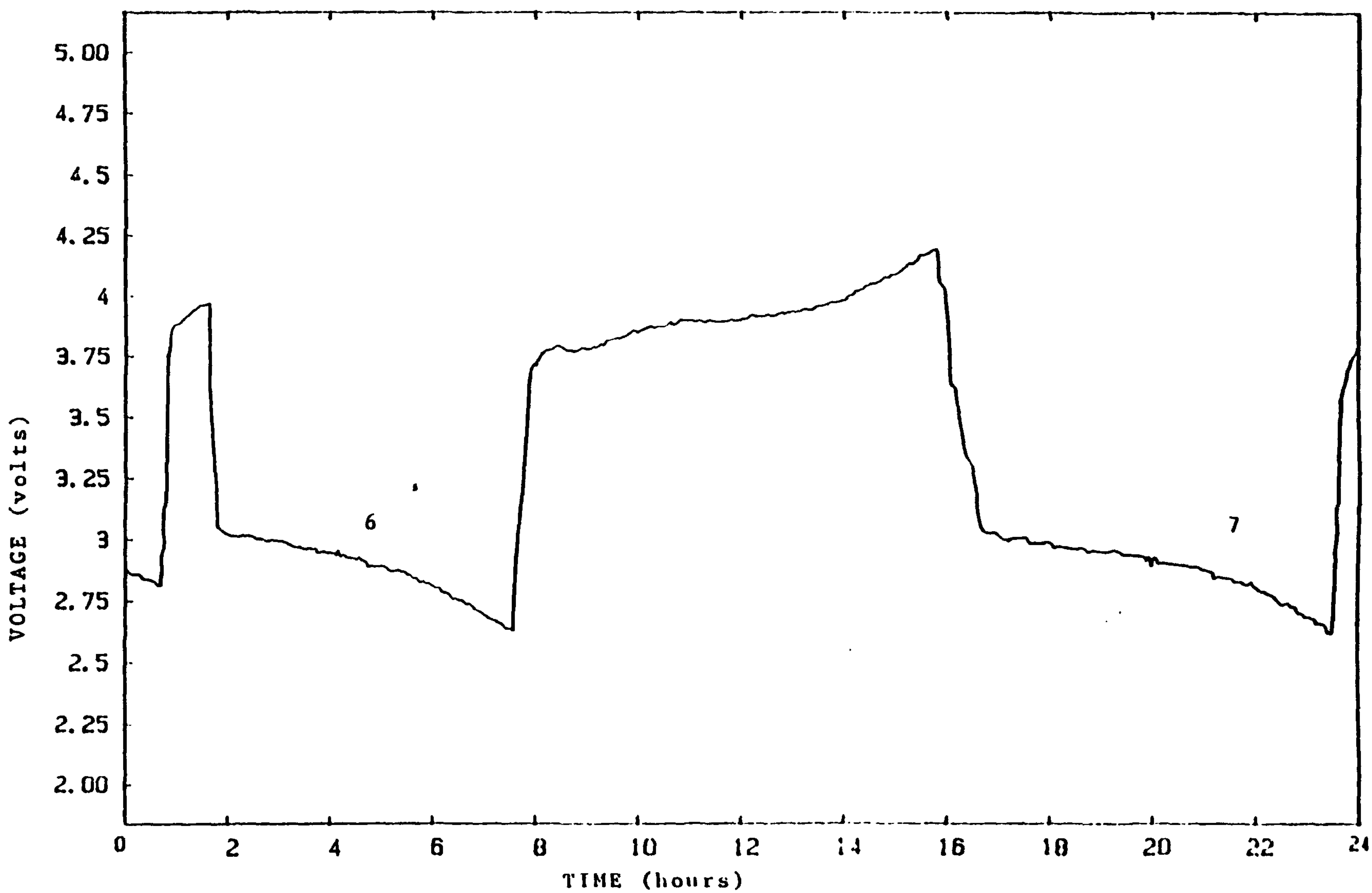

Figure 67:
Voltage Profile of Cell DW-1-05 Immediately Following
Extension of the Voltage Limits

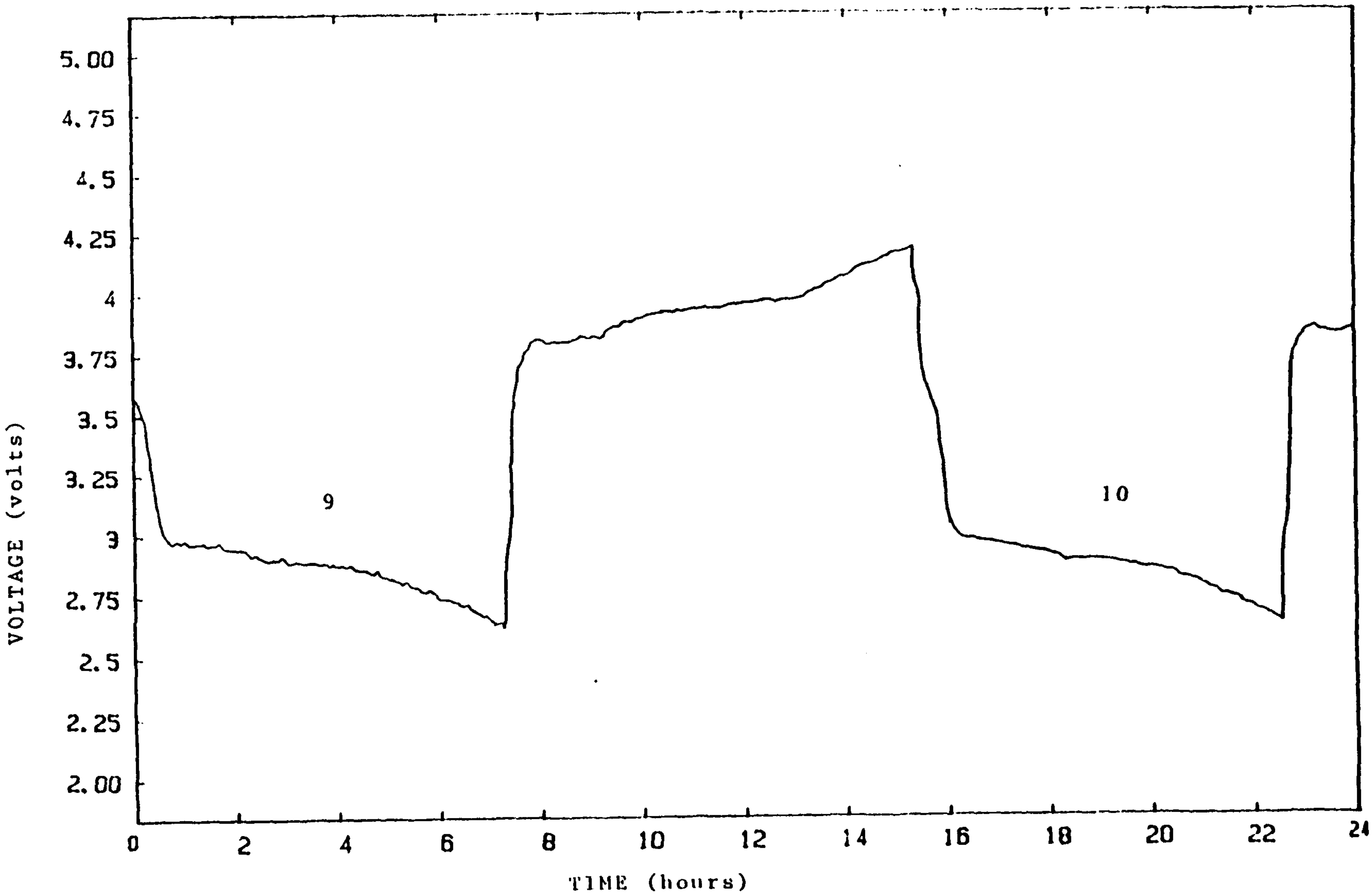

Figure 68
Voltage Profile of Cell DW-1-05 on the 9th and 10th Cycle

assemblies using a variety of materials. The test samples consisted of a two inch square piece of expanded metal substrate with a lead tab 0.25 inch by 0.003 inch welded along one edge of the substrate material. Contact was made to the tab by a copper clip and to the opposite edge of the substrate by a copper strip clamped along the edge. Current was then forced through the assembly and the resistance calculated by the voltage drop between the contact points. Results of the measurements are shown in Table 9.

Table 9: Resistance Measurements

Sample	Tab Material	Substrate Material	Resistance/ohms
1	SS (1 side)	Al	.047
2	SS (2 sides)	Al	.031
3	Ni (2 sides)	Al	.018
4	Ni (1 side)	Ni	.017
5	SS (2 sides)	Al sprayed	.043
6	SS (1 side)	SS	.071

The aluminum substrates were sandwiched between two tabs in some cases. This was not necessary for the stainless or nickel substrates. Sample No. 5 had a carbon/TFE undercoat sprayed onto the aluminum substrate before welding.

The results of the measurements indicate that nickel leads on nickel substrates are the best. Although the aluminum substrates with nickel leads also look good in this test, the earlier cell cycling indicated that in full cells the aluminum/carbon interface is very resistive initially and becomes worse with cycling. These results clearly show that lead/substrate connections are not responsible.

Resistance measurements were also made by passing current from a power supply along various lengths of substrate and measuring the voltage drop between the leads. The calculated resistance was plotted as a function of substrate length and extrapolated to zero length to give lead contact resistance. The lead resistance was then subtracted from the total to give the substrate resistance. For the nickel screen chosen the resistance was 7.5 mΩ/ft. length.

Cells DW-1-09 through DW-1-14 were built in slightly larger cans (BA6590 size) in order to achieve larger surface area and to take advantage of the 300PSIG case vent. Test results are shown in Table 7.

Cells with stacks that fit tightly in their cases were chosen for DOT high temperature testing. The two cells which had the loosest fit were chosen for cycling. These two cells, DW-1-13 and DW-1-14, had relatively thin cathodes with somewhat less carbon than the other cells. Discharge capacities for the two cells are shown in Figure 70. Initial capacity was 2.5 to 3Ah, quite a bit less than the expected 4Ah. It is probable that the capacities were limited by the amount of electrolyte and/or carbon in the cells. The cells were cycled 20 times before being disassembled for analysis. Cell DW-1-13 had a loose lead connection internally which also caused the cell to reach the discharge voltage cutoff prematurely.

DOT Testing

Four cells were tested according to DOT requirements for high altitude shipment and high temperature storage:

- 50,000 feet altitude at 75°F for six hours
- 167°F for 48 hours.

No shock and vibration were performed because of the cell distortion observed at high temperature. The cells were DW-1-09, DW-1-10, DW-1-11 and DW-1-12. All cells completed the

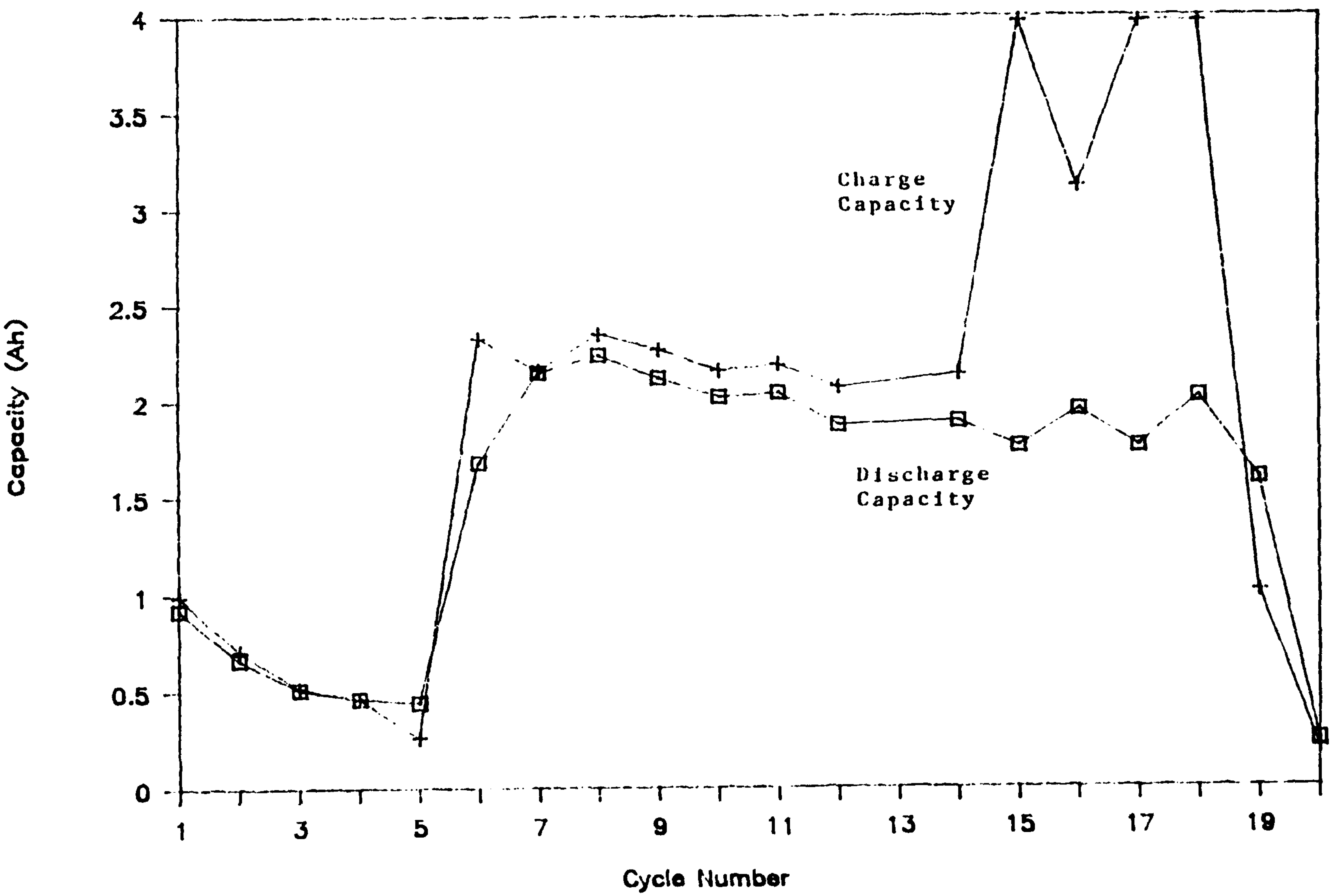

Figure 69
Discharge and Charge Capacities of Cell DW-1-05

altitude storage for six hours without change or incident. During the high temperature storage (167°F for 48 hours), the cells bulged in the case to bottom where the vent was located about 1/16 to 1/8 inch. Cell DW-01-10 developed a slight leak in the case bottom along one leg of the start-pattern pressure relief vent (Figure 71).

Cells DW-01-12 through DW-01-14 achieved 10-20 cycles and were terminated for analysis because of low first cycle capacity (Figure 72). Serial numbers DW-01-15 and DW-01-16 were not used.

Additional cells (DW-01-17 through DW-01-25) were filled with about $1cm^3$ less electrolyte in order to avoid possibly hydrostatic pressure from thermal expansion.

Cells Dw-01-22 through DW-01-25 were passed through high altitude and high temperature storage at 75°C. All four bulged. Cells DW-01-17 through DW-01-22 and Cell DW-01-11 were not tested. Dw-01-25 developed a leak.

Cells DW-01-29 and DW-01-24 were inadvertently charged on the first cycle. These cells vented violently after two and four cycles, respectively, of very short capacity.

Cells DW-01-12 and DW-01-23 achieved poor first cycle capacity and were terminated at a point where venting seemed likely.

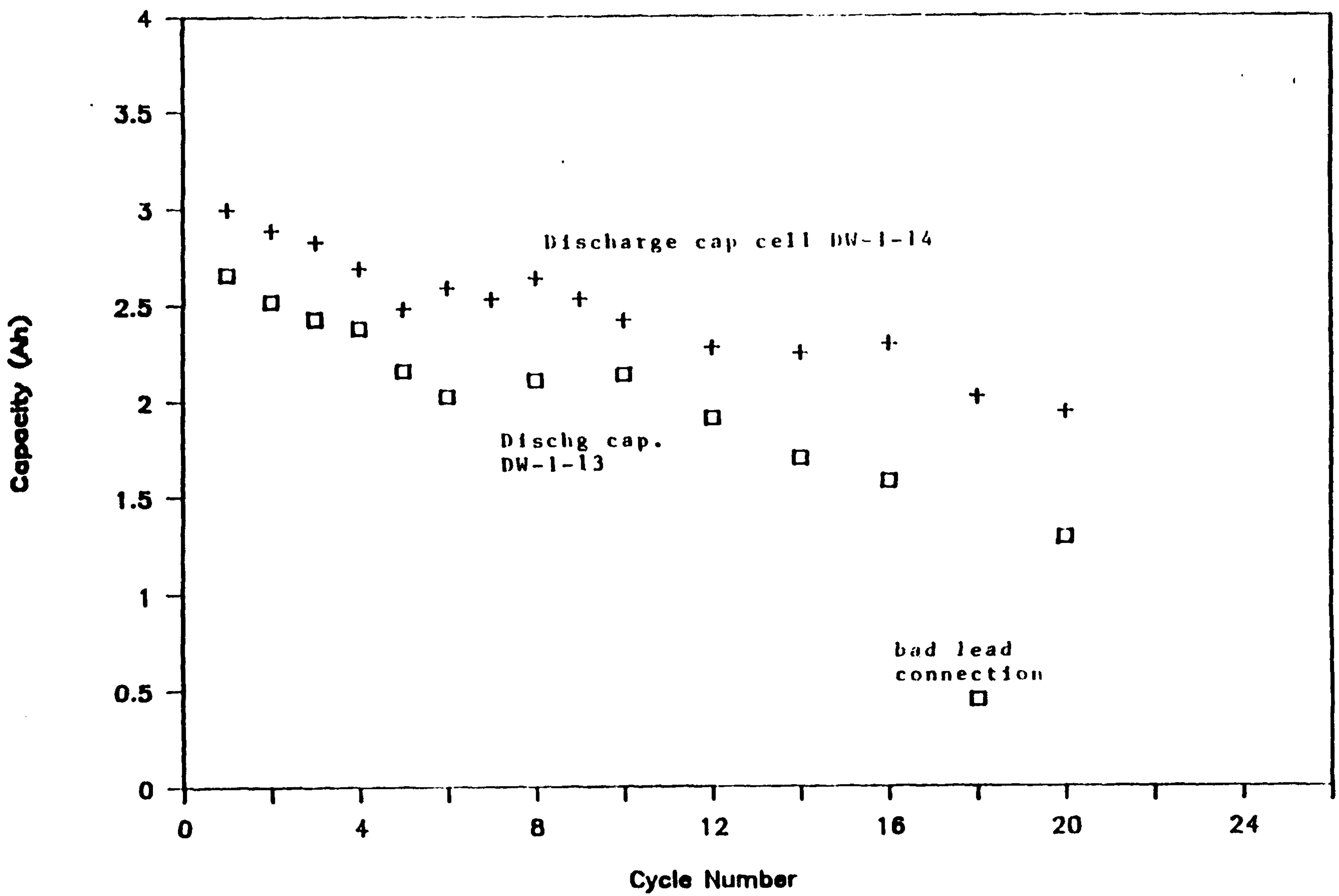

Figure 70 Discharge Capacities of Cells DW-1-13 and DW-1-14

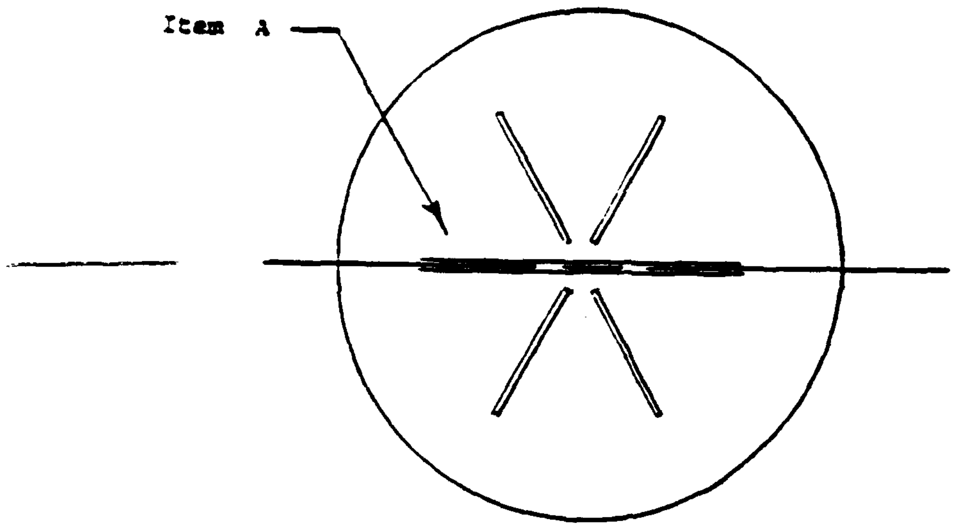

Figure 71 Star Vent Pattern

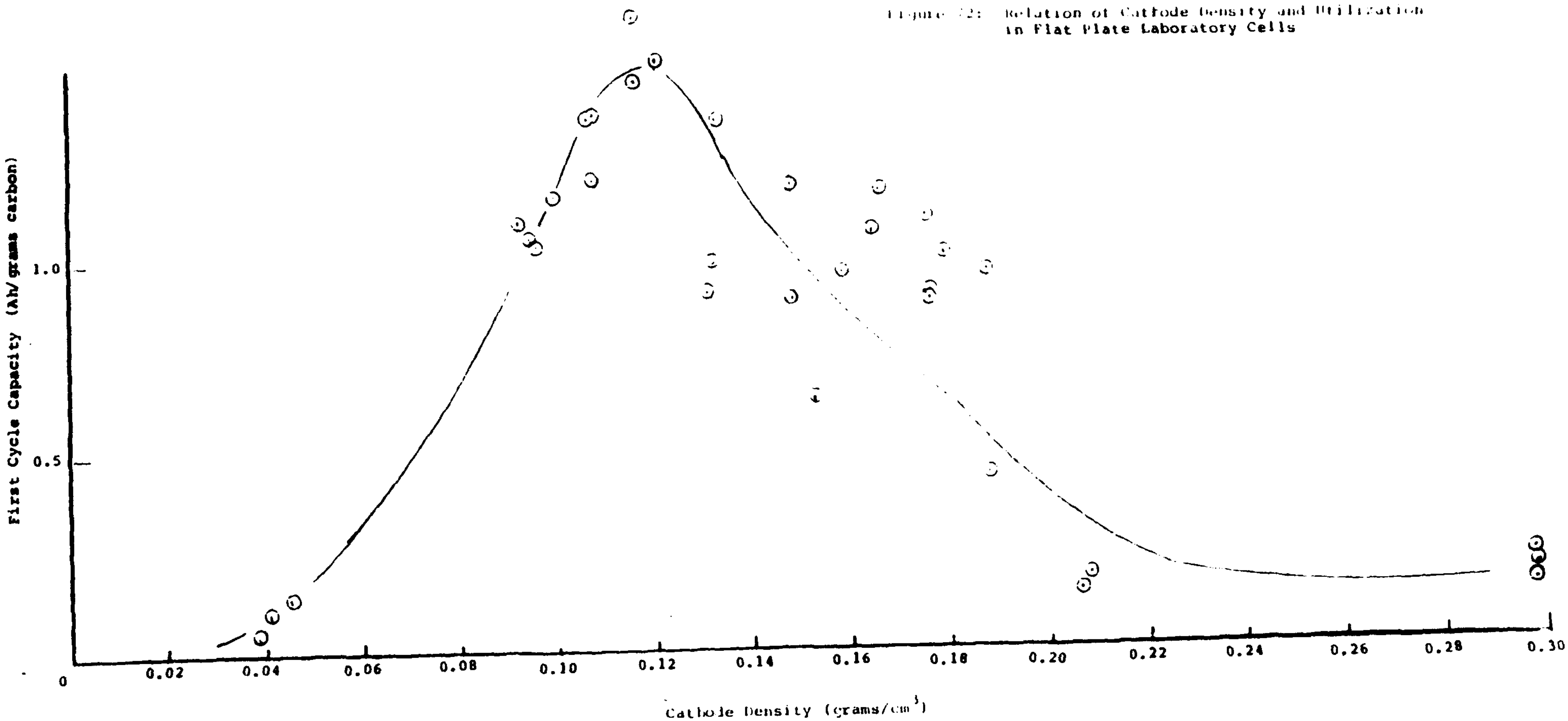

Figure 22: Relation of Cathode Density and Utilization in Flat Plate Laboratory Cells

SUMMARY

Performance of Li/SO_2 rechargeable cells has been improved to the point where 100 cycles can be delivered in low rate cells at cathode utilization in excess of 1.5 Ah/g carbon (0.2 Ah/cm^3 of cathode) on early cycles. The optimal cycling limits are close to 2.8 volts on discharge and 4.0 volts on charge.

Analysis of failed cells and of results for spiral wound cells indicate that safety and performance are sensitive to 1) the design and materials used for stack insulation and inter-electrode separators and 2) control of cathode density and stack compression.

$LiAlCl_4 \cdot 6SO_2$ is a suitable electrolyte composition for good cycling performance allowing for same rate capability down to -30°C. Efficient charging must be done closer to room temperature. Surface analysis of the passivating film on the lithium anode during discharge and charge reveals a complex morphology composed of at least one sulfur-oxygen compound and LiCl. Lithium plating can take place through this film at rates up to $1mA/cm^2$ and discharge of lithium at rates of up to $20mA/cm^2$. On anodes cycled in excess of 100 cycles, the film grows somewhat and begins to envelop parts of the separator and may clog pores in microporous separators.

Upon scaling up from the $25cm^2$ laboratory cells to high rate spiral wound cells, with 265, 361, $675cm^2$ of surface area we were able to achieve discharges of up to 20 cycles but with reduced Amp-hour capacity at the $1mA/cm^2$ rate. We believe the reduced capacity is, at least in part, due to our inability at present to prepare cathodes whose density in these early fully assembled cells was uniformly close to the optimal value of 0.12g/cc throughout the cell.

The Ketjen Black carbon recommended by earlier investigation remains the best material for cycling Li/SO_2 cells. Attempts to use alternate carbon and to modify the carbon surface produced inferior results. Throughout this study many cathodes were tested with a variety of carbon densities. Figure 72 summarizes these results.

Reference cathode measurements indicate that on charge and discharge, the cell polarization is primarily associated with the cathode. At least three other factors must be considered in the improvement of cell voltage and capacity:

1. I.R. losses due to bulk resistivity , interparticle resistance and contact resistance with the nickel substrate.
2. Activation polarization associated with the number and type of active sites at the surface of the carbon.
3. Concentration polarization associated with the different constraints and mobility of ions and intervals in the electrolyte and the quantity of active material available in the pores.

If we examine the relation of cathode utilization (Ah/gram cathode) as a function of cathode density (grams cm^3) for all of the laboratory cells tested, we see a trend which may indicate a fundamental property of the cathode in $LiSO_2$ rechargeable cells. The results shown in Figure 72 show some scatter because we have pooled results with different electrolytes, cathodes and cycling conditions. But there is clearly an optimal density of about 0.12 grams/cm^3. At this density, one can calculate a rough estimate of the quantity of available electrolyte per unit of volume or weight. Assuming a solid density of 2 grams/cm^3 for the cathode and 1.6 grams/cm^3 for the $LiAlCl_4 \cdot 6SO_2$, we arrive at a value of about 1.8Ah of active material per gram of cathode. If we further assume that the active SO_2 complex available for discharge must be completely contained in the cathode pores and that additional space must be present to accommodate the deposition of LiCl, then our achievement of 1.5 - 1.6 Ah/gram cathode is quite respectable.

Overcompression of the cathode decreases pore volume and increases tortuosity while undercompression leads to loss of interparticle contact and increased resistivity.

RECOMMENDATIONS

The future of the Li/SO_2 secondary battery technology rests on a continuing commitment to understand the nature of performance and safety limitations so that appropriate improvements in materials and design can be implemented. This knowledge will further allow us to control the limits of cycling conditions more precisely to achieve safe high energy density performance. Several specific recommendations are in order:

- ✓ Determine the dependence of cathode utilization on cathode density, thickness and expansion.
- ✓ Analyze for accumulation of degradative products in the cell as a function of cycle number.
- ✓ Continue to explore other types and combinations of separator to prevent shorting and plugging.
- ✓ Determine features in cycling behavior which can be used to signal the end of useful life prior to any dangerous set of conditions.
- ✓ Accurately determine the percent loss of active anode per cycle.
- ✓ Measure cell case temperature to monitor the onset and progress of exothermic variations.
- ✓ Determine the uniformity of cycling efficiency across

the surface of large electrodes.

√ Compare efficiency, safety and performance of flat and curved electrode structures.

√ Examine failure modes when cells are first charged..

REFERENCES

1. H.C. Kuo, A.N. Dey, C. Schlaikjer, D. Foster and M.Kalliandidis, Duracell Final Report, Contract No. DOE-DE-AC01-8OER-10191 (1986).

2. A.N. Dey, H.C. Kuo, P. Piliero and M. Kallianidis, J. Electrochem. Soc., 135, 2115 (1988).

3. R.J. Mammone, S. Gilman and M. Binder in "Proceedings of the 32nd Power Sources Symposium," Cherry Hill, NJ, June 9-12, 1986.

4. E. Peled, in "Lithium Batteries" ed., J.P. Gabano, Academic Press, 1983.

5. B. Koslowski, Ph.D. Dissertation, The University of Hanover, 1980.

ELECTRONICS TECHNOLOGY AND DEVICES LABORATORY
MANDATORY DISTRIBUTION LIST
CONTRACT OR IN-HOUSE TECHNICAL REPORTS

8 JUL 91

101 Defense Technical Information Center*
ATTN: DTIC-FDAC
Cameron Station (Bldg 5)
Alexandria, VA 22304-6145

(*Note: Two copies for DTIC will be sent from STINFO Office.)

483 Director
US Army Material Systems Analysis Actv
ATTN: DRXSY-MP
001 Aberdeen Proving Ground, MD 21005

563 Commander, AMC
ATTN: AMCDE-SC
5001 Eisenhower Ave.
001 Alexandria, VA 22333-0001

609 Commander, LABCOM
ATTN: AMSLC-CG, CD, CS (In turn)
2800 Powder Mill Road
001 Adelphi, Md 20783-1145

612 Commander, LABCOM
ATTN: AMSLC-CT
2800 Powder Mill Road
001 Adelphi, MD 20783-1145

680 Commander,
US Army Laboratory Command
Fort Monmouth, NJ 07703-5000
1 - SLCET-DD
2 - SLCET-DT (M. Howard)
1 - SLCET-DR-B
35 - Originating Office

681 Commander, CECOM
R&D Technical Library
Fort Monmouth, NJ 07703-5000
1- ASQNC-ELC-I-T (Tech Library)
3- ASQNC-ELC-IS-L-R (STINFO)

705 Advisory Group on Electron Devices
ATTN: Documents
2011 Crystal Drive, Suite 307
002 Arlington, VA 22202

ELECTRONICS TECHNOLOGY AND DEVICES LABORATORY
SUPPLEMENTAL CONTRACT DISTRIBUTION LIST
(ELECTIVE)

205 Director
Naval Research Laboratory
ATTN: CODE 2627
001 Washington, DC 20375-5000

221 Cdr, PM JTFUSION
ATTN: JTF
1500 Planning Research Drive
001 McLean, VA 22102

301 Rome Air Development Center
ATTN: Documents Library (TILD)
001 Griffiss AFB, NY 13441

437 Deputy for Science & Technology
Office, Asst Sec Army (R&D)
001 Washington, DC 20310

438 HQDA (DAMA-ARZ-D/Dr. F.D. Verderame)
001 Washington, DC 20310

520 Dir, Electronic Warfare/Reconnaissance
Surveillance and Target Acquisition Ctr
ATTN: AMSEL-EW-D
001 Fort Monmouth, NJ 07703-5000

523 Dir, Reconnaissance Surveillance and
Target Acquisition Systems Directorate
ATTN: AMSEL-EW-DR
001 Fort Monmouth, NJ 07703-5000

524 Cdr, Marine Corps Liaison Office
ATTN: AMSEL-LN-MC
001 Fort Monmouth, NJ 07703-5000

564 Dir, US Army Signals Warfare Ctr
ATTN: AMSEL-SW-OS
Vint Hill Farms Station
001 Warrenton, VA 22186-5100

602 Dir, Night Vision & Electro-Optics Ctr
CECOM
ATTN: AMSEL-NV-D
001 Fort Belvoir, VA 22060-5677

603 Cdr, Atmospheric Sciences Lab
LABCOM
ATTN: SLCAS-SY-S
001 White Sands Missile Range, NM 88002

607 Cdr, Harry Diamond Laboratories
ATTN: SLCHD-CO, TD (In turn)
2800 Powder Mill Road
001 Adelphi, MD 20783-1145

ELECTRONICS TECHNOLOGY AND DEVICES LABORATORY
SUPPLEMENTAL CONTRACT DISTRIBUTION LIST
(ELECTIVE)

Duracell Inc.
Duracell Research Center
37 A Street
Needham, MA 02194
ATTN: Dr. A.N. Dey

Eagle-Picher Industries, Inc.
C & Porter Streets
PO Box 47
Joplin, MO 64801
ATTN: Technical Library

Stonehart Associates, Inc.
17 Cottage Road
P.O. Box 1220
Madison, Connecticut 06443
ATTN; Paul Stonehart

EIC Laboratories, Inc.
111 Downey Street
Norwood, MA 02062
ATTN: Technical Library

Electrochimica Corporation
20 Kelly Court
Menlo Park, CA 94025
ATTN: Dr. Morris Eisenberg

Hossain Sohrab Whittaker
Acorn Park ADL, Inc
Cambridge, MA 02140-2390

Honeywell, Inc.
Power Sources Center
104 Rock Road
Harsham, PA 19044
ATTN: Technical Library

Honeywell, Inc.
Sensors and Signal Processing Lab.
10701 Lyndale Avenue South
Bloomington, Minnesota 55420
ATTN: H.V. Venkatasetty

Power Conversion, Inc.
280 Midland Avenue
Saddle Brook, NJ 07662
ATTN: Dr. Thomas Reddy

SAFT America, Inc.
Advanced Battery Systems
107 Beaver Court
Cockeysville, MD 21030
ATTN: Technical Library

Union Carbide Corporation
Section A-2
Battery Products Division
Old Ridgebury Rd.
Danbury, CT 06817
ATTN: Mr. Berger

AT&T Bell Laboratories
600 Mountain Avenue, 7A-317
Murray Hill, NJ 07974
ATTN: Karrie Hanson

Jet Propulsion Laboratory
Mail Stop 277-212
Pasadena, CA 91109
ATTN: Mr. Halpert

Tracor Battery Technology Ctr
1601 Research Blvd
Rockville, MD 20850
ATTN: Dr. Nehemiah Margalit

Gates Energy Products
P.O. Box 114
Gainesville, FL 32602
Attn: Library/T. Brown

Alupower, Inc.
6 Claremont Road
Bernardsville, NJ 07924
ATTN: Dr. Robert P. Hamlen

Catalyst Research
3706 Crondall Lane
Owings Mills, MD 21117
ATTN: Dr. Steven P. Wicelinski

Center for Electrochemical Systems
and Hydrogen Research
238 Wisenbaker ERC
Texas A&M University
College Station, TX 77843
ATTN: A. John Appleby

SRI International
333 Ravenswood Avenue
Menlo Park, CA 94025
ATTN: Digby D. MacDonald

Oxley Research, Inc.
25 Science Park
New Haven, CT 06511
ATTN: Dr. James E. Oxley

Combustion Engineering
1000 Prospect Hill Road
Dept 9351-0501
Windsor, CT 06095-0500
ATTN: David N. Palmer

Lithium Energy Assoc., Inc.
246 Sycamore Street
Watertown, MA 02172
ATTN: Dr. Fred Dampier

Jet Propulsion Laboratory
4800 Oak Grove Drive
Pasadena, CA 91109
ATTN: Technical Library